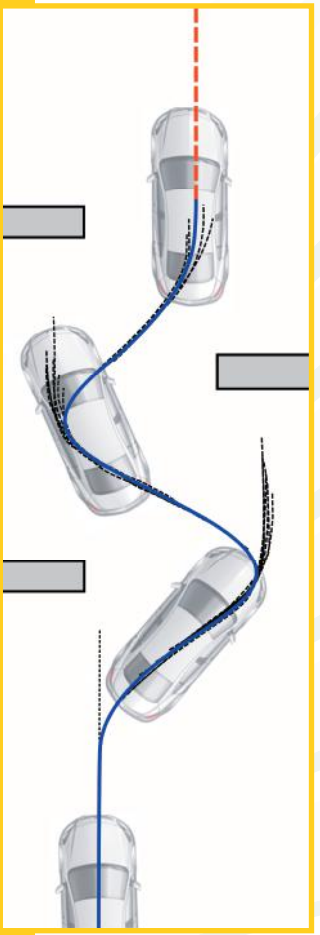

BOLIANG YI

Integrated Planning and Control for Collision Avoidance Systems

KIT Scientific Publishing

Boliang Yi

Integrated Planning and Control for Collision Avoidance Systems

Schriftenreihe
Institut für Mess- und Regelungstechnik,
Karlsruher Institut für Technologie (KIT)

Band 039

Eine Übersicht aller bisher in dieser Schriftenreihe erschienenen Bände finden Sie am Ende des Buchs.

Integrated Planning and Control for Collision Avoidance Systems

by
Boliang Yi

KIT Scientific Publishing

Dissertation, Karlsruher Institut für Technologie
KIT-Fakultät für Maschinenbau

Tag der mündlichen Prüfung: 5. Oktober 2017
Referenten: Prof. Dr.-Ing. Christoph Stiller
Prof. Dr.-Ing. Ulrich Konigorski

Impressum

Scientific Publishing

Karlsruher Institut für Technologie (KIT)
KIT Scientific Publishing
Straße am Forum 2
D-76131 Karlsruhe

www.ksp.kit.edu

Print on Demand 2018 – Gedruckt auf FSC-zertifiziertem Papier

ISSN 1613-4214
ISBN 978-3-7315-0785-7
DOI 10.5445/KSP/1000081452

Integrated Planning and Control for Collision Avoidance Systems

Zur Erlangung des akademischen Grades
Doktor der Ingenieurwissenschaften
der KIT-Fakultät für Maschinenbau
Karlsruher Institut für Technologie (KIT)

genehmigte
Dissertation
von

M.Sc. Boliang Yi

Tag der mündlichen Prüfung:	05. Oktober 2017
Hauptreferent:	Prof. Dr.-Ing. Christoph Stiller
Korreferent:	Prof. Dr.-Ing. Ulrich Konigorski

Abstract

The introduction of driver assistance systems like Anti-lock Braking System and Electronic Stability Control has increased safety of vehicle passengers on public roads. The automotive industry has boosted the development of Advanced Driver Assistance Systems in the last years. Collision avoidance systems like emergency braking assist systems have demonstrated their effectiveness in various studies and thus gained broad acceptance in society. To further increase the effectiveness of collision avoidance systems, the exploitation of the lateral free space by evasive maneuvers is being investigated in this thesis.

Effective avoidance systems drive the need for holistic integrated approaches to cover planning and control in one method. This thesis focuses on methods for integrated trajectory planning and vehicle dynamics control in collision avoidance scenarios by combined evasion and braking. Integrated methods allow for consistent model representation for both planning and control functionality and lead to a reduced number of design parameters in the overall system. This strongly reduces the tuning effort required to adapt both modules to each other and avoids to tune both modules separately. The proposed nonlinear method based on a model predictive approach plans collision-free trajectories taking into account environmental information of obstacles and the available maneuver space. The concept of terminal collision avoidance provides a solution for planning with obstacles detected outside the current prediction horizon.

Application of methods for collision avoidance in real vehicles require algorithms which can be efficiently solved on a real time computation platform. The successive linearization technique is used in this work to linearize nonlinear constraints of the optimization problem and to enable planning in real

vehicles. The concept of robust tube based model predictive control is exploited to consider for stability and constraint satisfaction with linearization errors. The performance and effectiveness of the proposed algorithm is demonstrated in a simulation environment and in a real vehicle application successfully avoiding the collision in characteristic scenarios and showing strong conformance for both environments.

The design concepts investigated in this thesis are promising to accelerate the realization of future design principles and thereby contribute to the overall development of automated driving technologies.

Kurzfassung

Die Einführung erster Fahrassistenzsysteme wie dem Anti-Blockier-System und dem Elektronischen-Stabilitäts-Programm hat erheblich zur Fahrsicherheit auf den Straßen beigetragen. Seitdem wurde in der Automobilindustrie die Entwicklung neuer Fahrassistenzsysteme stark vorangetrieben. Kollisionsvermeidungsysteme wie das Notbremssystem genießen hohe Akzeptanz und haben in Studien eine hohe Effektivität nachgewiesen. Um die Effektivität von Kollisionsvermeidungssystemen weiter auszubauen, wird in dieser Arbeit das Potenzial der Ausnutzung des verfügbaren lateralen Manöverraums durch Kollisionsausweichsysteme untersucht.

Effektive Kollisionsvermeidungssysteme benötigen holistische integrierte Ansätze, um Planung und Regelung in einer einzigen Methode zu vereinen. Der Fokus der Arbeit liegt daher in der Untersuchung von integrierten Planungs- und Regelungsmethoden für Kollisionsvermeidung-Manöver durch Ausweichen und Bremsen. Integrierte Methoden nutzen ein konsistentes physikalisches Model für die Planung und die Regelungsaufgabe, welches zu einer reduzierten Anzahl an Auslegungsparameter im Gesamtsystem führen. Diese Eigenschaft vermeidet die klassische separate Einstellung beider Module und reduziert damit den Anpassungsaufwand im Gesamtsystem. Die untersuchte Methodik basiert auf einem modelprädiktiven Regelungsansatz unter Berücksichtigung eines Fahrdynamikmodells, der erfassten potentiellen Kollisionsobjekte, der vorhandenen Fahrbahnbegrenzung sowie den Fahrdynamik- und Aktor-Limitierungen. Eine Endbeschränkung zur Kollisionsvermeidung ermöglicht die kollisionsfreie Planung mit potentiellen Hindernissen außerhalb des Prädiktionshorizonts.

Die Anwendung von Methoden zur Kollisionsvermeidung im Versuchsfahrzeug erfordert Algorithmen, die auf einer echtzeitfähigen Plattform effizient gelöst werden können. In dieser Arbeit wird daher das Verfahren der sukzessiven Linearisierung eingesetzt, um vorhandene Nichtlinearitäten in den Nebenbedingungen zu linearisieren und damit die Umsetzung der Planung in einem Versuchsfahrzeug zu ermöglichen. Das Konzept der robusten modelprädiktiven Regelung wird genutzt, um die Stabilität sowie die Einhaltung von Beschränkungen unter dem Einfluss von Linearisierungsfehlern zu garantieren. Die Performance und Effektivität der vorgeschlagenen Methoden wurden in einer Simulationsumgebung sowie in einem Versuchsfahrzeug getestet und bewertet. Die Ergebnisse zeigen die erfolgreiche Vermeidung von Kollisionen in allen charackteristischen Szenarien sowie eine hohe Übereinstimmung der Messergebnisse in Simulation und im Versuchsfahrzeug.
Die erarbeiteten Konzepte haben ein großes Potenzial, die Realisierung von zukünftigen Planungsprinzipien zu beschleunigen und damit zu der Entwicklung von automatisiertem Fahren beizutragen.

Acknowledgements

This dissertation is the result of my PhD study at Adam Opel AG, supervised by Prof. Dr.-Ing. Christoph Stiller from Karlsruhe Institute of Technology.
First of all, I would like to thank Prof. Stiller for his scientific advice and guidance during my thesis time. His trendsetting suggestions have been an inspirational source during the PhD time, as well as during the works on the research project. Furthermore, I would like to thank Prof. Konigorski from the Technical University of Darmstadt for serving as co-referent. His advice greatly influenced my research.
The research work was conducted within the framework of the research project UR:BAN - Urbaner Raum: Benutzergerechte Assistenzsysteme und Netzmanagement - funded by the German Federal Ministry of Economics and Energy (BMWi) in the context of the third traffic research program of the German government at Adam Opel AG. Special thanks are dedicated to my industrial supervisors during the PhD time, Frank Bonarens and Nikolas Wagner. Frank combined his extensive engineering experience from manufacturing and project leading skills with his enthusiasm for new technologies to support me as a mentor technically as well as personally during my PhD time. His patient guidance and readiness in all situations encouraged me in difficult circumstances. It is hard to imagine a better industrial supervisor than Frank. Nik enabled me in gaining first work experiences during my PhD time. His activities for the Opel PhD program integrated us well into the organization and represented our interests in all matters. Thanks Frank and Nik for your help over the last years.
I would like to thank my colleagues for the enjoyable collaborations during my time at Opel. I want to especially name Jens Ferdinand, Norbert Simm, Ulrich

Eberle, Steffen Knapp, Bernd Büchs, Harald Berninger, Björn Frank, Oliver Maier, Nikolai Moshchuk, Markus Bauer, Tobias Rückelt, Carsten Büttner, Thomas Streubel, Lena Rittger, Jens Heine, Gerald Schmidt, Stefan Berger, Timo Derichs, Rami Zarife, Jeremias Schucker, David Augustin, Bernhard Wandtner, Sven Hallerbach, Christina Kass, Maximilian Harr, Florian Jomrich and Fabian Fürst. I want to thank Denis Stein for support and help in the layout of this manuscript.

This thesis is based on the support of many students, who participated in the project as well as in the research work. I appreciate having worked with all students during this interesting and challenging time, namely Haoming Wu, Philipp Hoffmann, Christian Pfeiffer, Sebastian Engel, Alexander Schulzke, Holger Stübing, Fernando Gomes Papi, Florian Schindler, Stefan Gottschling, Theodor Rauch, Kay Hansel and Hermann Blondel Ngueko Kameni.

Finally I want to thank my parents. They taught me what is important in life and how to reach my goals. I can count on them when I need advice and in order to gather strength for my next steps. They are my backbone in every important step and shaped me how I am.

Wiesbaden, April 2017 *Boliang Yi*

Contents

Notation and Symbols

General Notation

Scalars	Regular (greek)	a, b, A, B, σ, λ
Vectors	Bold (greek) lower case	$\mathbf{a}$, $\mathbf{b}$, $\mathbf{A}$, $\mathbf{B}$, $\boldsymbol{\sigma}$, $\boldsymbol{\lambda}$
Matrices	Bold upper case	$\mathbf{A}$, $\mathbf{B}$, $\mathbf{C}$
Sets	Bold blackboard upper case	$\mathbb{A}$, $\mathbb{B}$, $\mathbb{C}$

Acronym

ABS	Anti-lock Braking System
ADAS	Advanced Driver Assistance System
COG	Centre Of Gravity
ESC	Electronic Stability Control
EPS	Electronic Power Steering
IEEE	Institute of Electrical and Electronics Engineers
MPC	Model Predictive Control
RRT	Rapidly exploring Random Trees
SAE	Society of Automation Engineers
TCA	Terminal Collision Avoidance

Symbols

a	Slope of sigmoidal trajectory
$a_{(\mathrm{x\,/\,y\,/\,z})}$	Acceleration
$a_{\mathrm{x,cmd}}$	Longitudinal deceleration command

$a_{\mathrm{y,max}}$	Maximum planned lateral acceleration
a_{max}	Deceleration command limit
c	Half of longitudinal maneuver distance in sigmoidal trajectory
$c_{\alpha(\mathrm{f/r})}$	Cornering stiffness
$c_{\alpha(\mathrm{f/r}),0}$	Linearised cornering stiffness
d_{st}	steering damping coefficient
h_{cog}	Height of COG
i	Prediction time step
k	Control time step
l	Wheel base
l_{veh}	Overall length of vehicle
$l(\mathbf{x},\mathbf{u})$	Stage cost
$l_{(\mathrm{f/r})}$	Distance COG to axis
$l_{(\mathrm{f/r}),\mathrm{veh}}$	Distance COG to chassis edge
m	mass
$r_{\mathrm{T}}, r_{\mathrm{a_x}}, q_{\mathrm{y}}, q_{\varphi}, q_{\mathrm{v}}$	Tuning parameters of MPC on state and command signals
s_{obs}	Slack variable
t_{c}	Potential collision time
t_{cmp}	Computation time
t_{pred}	Prediction sampling time
t_{del}	Time constant in longitudinal dynamics
v	Velocity
w	Width of ego vehicle
$w_{\mathrm{obs(l/r)}}$	Obstacle width on corresponding lane
x	Longitudinal position
$x_{\mathrm{obs(l/r)}}$	Longitudinal position of obstacle on corresponding lane
$y_{\mathrm{obs(l/r)}}$	Lateral position of obstacle on corresponding lane

x_E, y_E, t_E	Evasion maneuver distances and time
x_B, t_B	Braking maneuver distance and time
y	Lateral position
y_{Tol}	Tolerance parameter in sigmoidal trajectory
y_{max}	Maximum lateral position
y_L, y_R	Left and right boundary of drivable area
Δv_{red}	Relative velocity reduction
$\alpha_{(f/r)}$	Slip angle
$\alpha_{r,max}$	Maximum rear slip angle
β	Side slip angle
β_{min}, β_{max}	Minimum and maximum side slip angle
δ	Steering angle
μ	Friction coefficient
μ_y	Lateral friction coefficient
$\mu_{y,max}$	Assumed maximum lateral friction coefficient
φ	Yaw angle
$\dot{\varphi}$	Yaw rate
$\dot{\varphi}_{min}, \dot{\varphi}_{max}$	Minimum and Maximum yaw rate
θ	Vector of parametric uncertainties
$B/C/D/E$	Magic formula tire coefficient
D_f	Self alignment parameter
$B_{(l/r)}$	Nearest point of obstacle on vehicle edge
$F_{(x/y/z)(f/r)}$	Force on tire
$F_{(x/y/z)(f/r),max}$	Maximum force on tire
$F_{y(f/r),0}$	Force bias constant
J_{st}	Steering system inertia
J_z	Yaw inertia
M	Maximum lateral maneuver distance in sigmoidal trajectory
N	Number of prediction time steps

R	Curve radius
T	Total assisted torque
T_z	Self alignment torque
T_max	Maximum total assistant torque
T_HW	Driver hand torque
T_OT	Overlay torque
V	Cost function of finite horizon control problem
V_∞	Cost function of infinite horizon control problem
V_f	Terminal cost
$\mathbf{e}$	Error vector
$\mathbf{f}$	State transition function
$\mathbf{k}$	Linear feedback vector
$\mathbf{u}$	Input vector
$\mathbf{u}_\mathrm{min}, \mathbf{u}_\mathrm{max}$	Minimum and maximum input vector
$\mathbf{w}$	Additive uncertainty
$\mathbf{x}$	State vector
$\mathbf{x}^+$	Consecutive state vector
$\mathbf{x}_0$	Initial state vector
$\mathbf{z}$	Nominal state vector
$\mathbf{A}, \mathbf{B}, \mathbf{C}, \mathbf{E}$	State matrices of discrete state space model
$\mathbf{A}_\mathrm{c}, \mathbf{B}_\mathrm{c}, \mathbf{E}_\mathrm{c}$	State matrices of continuous state space model
$\mathbf{P}$	Solution of Ricatti equation
$\mathbf{P}_\mathrm{f}$	Terminal weight
$\mathbf{Q}$	Weight matrix of state vector in cost function
$\mathbf{R}$	Weight matrix of input vector in cost function
$\mathbb{C}$	Collision avoidance set
$\mathbb{C}_\mathrm{q}$	Linearized collision avoidance set
$\mathbb{G}_\mathrm{B}$	Terminal collision avoidance set of a braking maneuver
$\mathbb{G}_\mathrm{E}$	Terminal collision avoidance set of an evasive maneuver

$\mathbb{L}$	Boundary constraint set
$\mathbb{S}$	Stability envelope set
$\mathbb{S}_i$	Set of additive uncertainties for the predicted state *i*
$\mathbb{U}$	Input constraint
$\mathbb{V}$	Nominal input constraint
$\mathbb{V}$	Set of possible state vectors
$\mathbb{V}_q$	Linearized set of possible state vectors
$\mathbb{W}$	Set of possible additive uncertainty vectors
$\mathbb{X}$	State constraint
$\mathbb{X}_f$	Terminal constraint
$\mathbb{X}_{ol}, \mathbb{X}_{or}$	Longitudinal range of left and right obstacle
$\mathbb{Z}$	Nominal state constraint
Θ	Set of vectors for parametric uncertainties

where $_{(x\,/\,y\,/\,z)}$ denotes the vehicle dynamics variable in $_x$ = longitudinal direction/ $_y$ = lateral direction/ $_z$ = vertical direction; $_{(f\,/\,r)}$ denotes the $_f$ = front axis/ $_r$ = rear axis and $_{(l\,/\,r)}$ denotes the $_l$ = left direction/ $_r$ = right direction. Furthermore, $_{traj}$ = trajectory and $_0$ = current value at control time.

1 Introduction

1.1 Motivation

The introduction of driver assistance systems in the 1990's has greatly contributed to increased safety on the road [31][12]. Anti-lock Braking Systems (ABS) and Electronic Stability Control (ESC) assist drivers in controlling their vehicle on slippery roads by stabilzing the vehicle dynamics [75]. According to the natural driver studies in [17] Advanced Driver Assistance Systems (ADAS) have the potential to reduce the impact of negative driver-related factors in pre-crash situations. To further decrease the number of fatalities, car manufacturers have further boosted the development of ADAS technology to help the driver handling difficult situations.

The number of ADAS features has increased tremendously in the last years. In order to classify the systems and get a deeper understanding of the similarities as well as differences the Society of Automotive Engineers (SAE) has clustered the levels of driving automation as documented in the international standard J3016 [64]. The levels of automation provided by the SAE take four main criteria into account. A partially automated system in level 2 intervenes actively into the vehicle dynamics driving task. With level 3, the system being capable to monitor the surroundings of the vehicle takes over the driving task temporarily. The driver is responsible to take back the driving task in a short time frame when adverted by the system. A level 4 highly automated system provides a safe fallback solution during the driving task if needed e.g. by slowing down and swerving to the emergency lane. At level 5 the system is fully automated and has the capability to handle all driving modes. This differentiation of

automation levels provides an orientation for the classification of ADAS systems, but does not contain the complete range of ADAS features [26].
Gasser provides an extension which is based on the classification of the functionalities into three main operation types [24][23][25] . The operation type A consists of informing and warning functions taking only indirect influence on the vehicle control via the driver [25]. Examples of this type are traffic sign recognition or lane departure warning systems. Operation type B comprises continuously automating functions as described in the SAE standard J3016 like adaptive cruise control and traffic-jam-assist systems. Operation type C stands for intervening emergency functions, which take immediate control over the vehicle in near-accident situations that cannot be controlled by the driver. One example of this operation type is the emergency braking system, which can intervene independently of the driver intervention after detection of a critical situation by a sensing system. Recent studies [30][32][34] have shown the effectiveness of emergency braking systems with various system implementations. The study conducted by the Insurance Institute for Highway Safety in [32] showed a significant reduction of accident rates, expressed by lower claim frequency in all crash types of up to 51 % in personal injury claims and 22 % in first party claims.

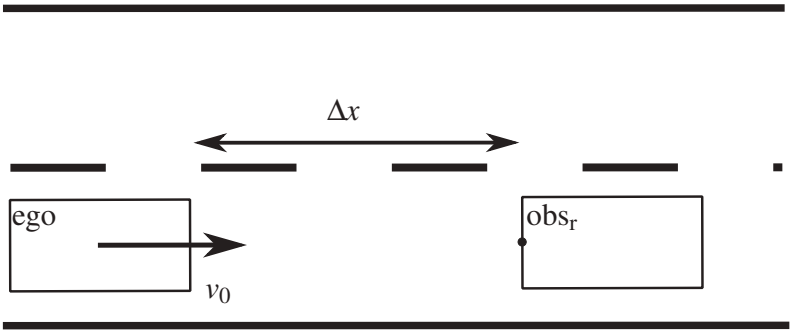

Figure 1.1: Scenario with ego vehicle ego and static obstacle obs_r

To further expand the effectiveness of collision avoidance systems recent studies [53] have investigated the exploitation of the lateral free space by evasive maneuvers.

Figure 1.1 illustrates a scenario with an ego vehicle and a static obstacle obs_r on the right lane. The ego vehicle drives with an initial velocity of v_0 and the rear edge of the static obstacle is located at the distance Δx in front of it. Different strategies of the ego vehicle shall be compared to avoid a collision with the obstacle.

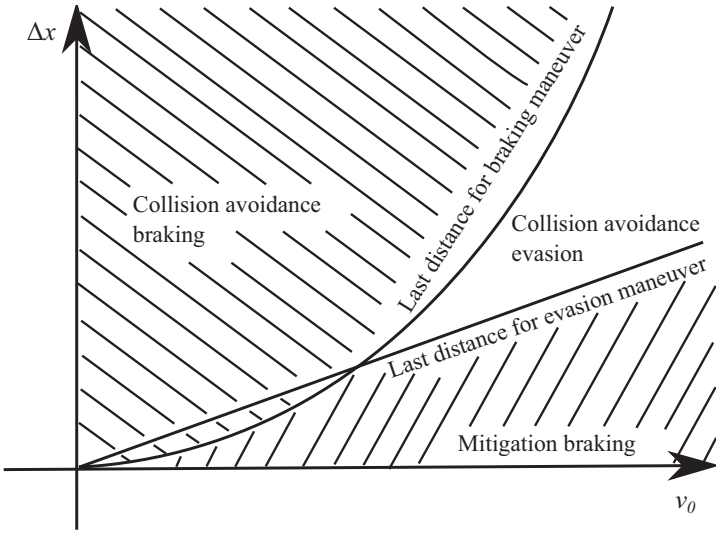

Figure 1.2: Areas of braking, evasion and mitigation braking maneuver in the distance and velocity diagram

The last-distance-to-brake and last-distance-to-evade curves are depicted in Figure 1.2 in the distance-velocity diagram. Areas above the last-distance-to-brake curve represent scenarios where a braking maneuver can avoid the collision, whereas in scenarios above the last-distance-to-evade curve collision-free evasion maneuvers are possible. Scenarios below both curves are maneuvers

where a collision cannot be avoided and mitigation braking must be applied to reduce the collision energy. The figure illustrates that evasive maneuvers are more effective at higher velocity in avoiding the collision in this single obstacle scenario. To assist the driver in critical situations only, collision avoidance systems generally are designed to interact at the latest point in time at which the collision can be avoided by the system.

1.2 Aim of the Thesis

Evasive collision avoidance maneuvers have been introduced in Section 1.1 as a research field providing opportunities for further increasing the positive effect of collision avoidance systems. One of the main challenges of evasive collision avoidance maneuvers is the design of the trajectory planning and the vehicle dynamics control module for this task. The trajectory planning module plans the trajectory to avoid collision with potential obstacles on the road and the vehicle dynamics control module controls the vehicle according to this trajectory. This thesis investigates methods for trajectory planning as well as vehicle dynamics control for collision avoidance systems in urban environments. Key requirements need to be considered to select appropriate concepts and to design the planning and control modules as set down in the following paragraphs.

Guarantee of Collision Freeness
The main goal of collision avoidance systems is to avoid any collision with potential obstacles. Therefore the first requirement for a planning module is to plan collision-free trajectories and ensure safety of the vehicle with a specified safety margin.

Consideration of environmental information
Furthermore, the planning module should be able to take environmental information into account and consider the drivable area given by the road boundaries or the curbstones.

Representation of vehicle dynamics

Design of methods for safety critical maneuvers require a sufficient representation of the required vehicle dynamics for the given task. Planning of maneuvers with an adequate representation of the dynamics can limit the deviation between the planned maneuver and the driven maneuver.

Consideration of Actuator Limitations

Actuators cannot intervene with infinite power. Actuator limitations in braking and steering module constrain the applicable torque and deceleration values due to the design of the electrical and mechanical components.

Computational Complexity

Methods for planning and control of vehicle dynamics maneuvers need to be computationally efficient and realizable by algorithms that can be solved on a real time platform. Sophisticated algorithms that cannot be realized in vehicles cannot contribute to the safety of vehicles on the road. Due to the increase of computational capabilities from year to year the investigation of methods with a high computational burden are still interesting since chances are high that these algorithms can be applied in the near future.

Customization of Performance

Methods for planning and control of vehicle dynamics maneuvers should be able to meet customizable goals like customer experience (e.g. level and type of intervention) and to consider strategies for driver handover. These goals are different for each maneuver and must be defined appropriately to consider the characteristic of the maneuver.

Minimization of Tuning Effort

Customization of maneuver characteristics is usually associated with high tuning efforts. Tuning efforts hinder the methods from being applied to the vehicle

within a short development time. An ideal method should minimize the amount of tuning variables and the tuning effort necessary in the algorithm.
With the main requirements defined above the question adressed in this thesis is formulated as follows.

How can trajectory planning and vehicle dynamics control strategies be designed to

- guarantee collision-freeness with potential obstacles,
- consider complex environmental information,
- represent vehicle dynamics characteristics,
- incorporate actuator limitations,
- enable real time application,
- allow for customization and to reduce tuning effort?

In order to execute successful evasive collision avoidance maneuvers several key challenges need to be overcome. Precise perception of all relevant information in the environment is essential for planning and decision making in critical scenarios. The performance of the perception system is based on the neat cooperation of key technologies such as hardware design of the sensors and algorithmic processing modules such as sensor fusion, object tracking and object classification. In this thesis the environment perception system is assumed to be given and to reflect all relevant information. Design of driver assistance systems need to take the interaction and behaviour of the driver into account. Good system design enables effective cooperation between drivers and systems during the maneuver. This can be achieved by a suitable design of human machine interfaces and hardware as well as software modules. In this thesis, no driver intervention is assumed as is defined for highly automated vehicles [64].

The precise knowledge of the friction coefficient is fundamental for reliable planning of maneuvers in critical situation. At low friction values, the planned maneuver cannot achieve high acceleration dynamics. Therefore, the estimation of the friction coefficient has been investigated in several research works. In this thesis, the friction coefficient is assumed to correspond to the coefficient when driving on dry roads.
Planning and control in driver assistance systems is based on the interaction of high level and low level control systems. Low level control systems control the actuator dynamics to achieve the command input of a high level control system and to compensate for vehicle dynamics instabilities. High level control systems control the vehicle dynamics to achieve a goal in a specified maneuver. This thesis will focus on the design of the high level planning and control system and assume full functionality of the low level control system without additional interventions of ABS and ESC systems.

1.3 Outline

This thesis will focus on concepts and methods for trajectory planning and vehicle dynamics control in evasive collision avoidance systems and is structured as follows:

Chapter 2: Concepts and Methods for Collision Avoidance
Chapter 2 provides an overview of concepts and methods about trajectory planning and vehicle dynamics control suitable for evasive collision avoidance systems. Moreover this chapter will highlight the difference between the classical concepts with separated planning and control modules as well as the integrated planning and control concept discussed in this thesis.

Chapter 3: Fundamentals of Optimal Planning and Control
In Chapter 3 the needed vehicle dynamics models used for the steering and braking system as well as the vehicle dynamics will be introduced. The theoretical

background of Model Predictive Control (MPC) as a finite time constrained optimal control problem as well as robust tube based MPC will be explained. Issues such as stability, robustness and constraint satisfaction are discussed. The applicability of the MPC theory will be shown on the classical trajectory tracking problem in a simulation environment.

Chapter 4: Nonlinear Integrated Planning and Control
A nonlinear model predictive control scheme integrating the vehicle dynamics planning and control together with combined longitudinal and lateral dynamics for collision avoidance maneuvers will be developed in Chapter 4. A nonlinear formulation of the optimization problem with nonlinear constraints for the vehicle dynamic model, the environmental constraints as well as vehicle dynamics limitations will be presented. In addition the collision avoidance system uses the terminal collision avoidance constraint to find a safe trajectory with obstacles outside of the prediction horizon. Characteristic scenarios with single and multiple obstacles will be used to demonstrate the performance of the method in simulation.

Chapter 5: Fast Integrated Planning and Control
The implementation of the nonlinear control problem on a real vehicle in a real time environment is critical due to the high computation time required by the solver. To overcome this issue successive linearization techniques will be presented in Chapter 5 to achieve convex quadratic problems that can be solved using standard optimization solvers. Robust MPC theory is employed to cope with linearization errors and to guarantee stability as well as constraint satisfaction with uncertainties. In addition, simulation and experimental results shall demonstrate the applicability of the algorithm in predefined scenarios.

Chapter 6: Conclusion and Outlook
Chapter 6 concludes this thesis with a summary and gives an outlook for future work.

2 Concepts and Methods for Collision Avoidance

Chapter 2 will first discuss the structure and the components of the classical collision avoidance concept. Furthermore, state of the art methods for the investigated modules, trajectory planning and vehicle dynamics control, will be presented. Subsequently, this section will discuss methods of the integrated planning and control concept in contrast to the classical concept. Finally, the concept and method investigated in this thesis will be motivated, considering the requirements and the key research question formulated in Section 1.2.

2.1 Classical Concept of Collision Avoidance Systems

Figure 2.1 illustrates the classical concept for realizing a collision avoidance system. The environment representation module processes the information of the sensor system and generates an appropriate representation, for example in the form of grids [33][73] or stixels [59][60]. A decision making module then determines the proper action in case of imminent collision risks and triggers the maneuver at the latest point in time unless the driver started to resolve the critical situation. The set of actions may consist of braking, evasion and mitigation maneuvers as discussed in Section 1.1. When the collision can be avoided by an evasive maneuver, the trajectory planning module calculates a drivable collision-free trajectory, considering a safety margin to the obstacles. Further, the vehicle dynamics control module activates the actuators to follow this trajectory. Finally, a handover strategy ensures safe transition to the driver.

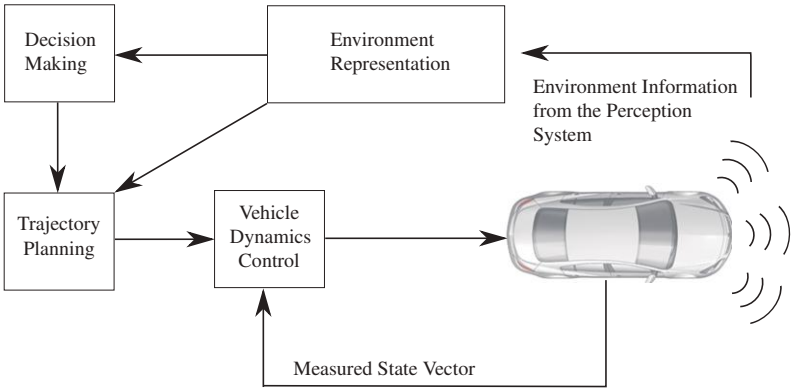

Figure 2.1: Classical concept of collision avoidance systems

The trajectory planning and the vehicle dynamics control module are separated in this classical concept. This implies that the vehicle dynamics control module tracks the trajectory calculated by the planning module and does not consider obstacles explicitly. Furthermore, both modules need to be tuned which requires a lot of tuning efforts.

2.2 Trajectory Planning

Several planning methods have been proposed for evasive maneuvers. Geometrical primitives have been used in many works such as [29][53] [67][68] [71] to calculate trajectories with low computational effort. In the following, properties of geometrical primitives are discussed based on the example of circular shaped and sigmoidal trajectories.

Circular shaped trajectories have been investigated in the context of collision avoidance [29][53][67]. The corresponding equations are composed two circular segments with continuous position and orientation. The discontinuous curvature of the circular shaped trajectory cannot be followed exactly considering actuator limitations of the vehicle.

The build-up time of the dynamics plays an essential role in critical maneuvers. Stählin and Schorn show how the sigmoidal equation can be adapted to consider build-up time of vehicle and different vehicle speeds [68][71]. Planning with geometrical primitives are suitable to handle simple collision avoidance maneuvers or overtaking maneuvers in static scenarios with single obstacles. However, their design does not offer the necessary flexibility to appropriately react under arbitrary environmental conditions with multiple static and dynamic road participants, as discussed in Section 1.2.

Sampling based approaches such as rapidly exploring random trees (RRT) have been proposed by Kuwata [43] and Farinella [21]. These methods sample a map randomly and connect these samples in a tree when their sequential connection is collision-free. The method is able to consider non holonomic constraints such as a vehicle dynamics model and additional environmental information. Although collision-free trajectories can be found with sampling based methods, the solution does not take performance metrics into account. Consequently, the resulting performance metric, in general, is random which does not fulfil the requirement of customization.

Potential field approaches have been investigated by Krogh [42] and Khatib [39]. The basic idea is that environmental obstacles as well as road boundaries shape a gradient field which repel the trajectory of the vehicle. Ideally the vehicle should follow the direction of the negative gradient to prevent collision with other obstacles and keep the vehicle on the center of the lane. Problems arise when overlapping influences of environmental information result in low gradients and local minima such that the potential fields may lead to a collision with an obstacle. Complex environmental information provide qualitative contribution in the potential field approach, however the quantitative contribution of the potential field is difficult to design, in general, to guarantee collision-freeness.

Optimization based methods build on a general framework in which relevant components such as environmental information and vehicle dynamics characteristics as well as desired driving properties can properly be formulated. The components of the framework can be featured with elements of different

complexities that is suitable for the requirements of the considered maneuver. Optimal trajectory planning methods have been proposed by many researchers in different setups [78][79][86] which vary in component complexity as well as in their computational effort.

Simple setups of optimization based methods which rely on a point mass model or kinematic model with a given start and end position can be solved analytically and in real time without the need of complex solver algorithms [78]. However, the applicability is limited since environmental information such as obstacle position or geometry cannot be considered with fast analytic solutions.

In complex scenarios like multiple obstacles and arbitrary road shapes analytical solutions cannot be given explicitly. A solution can be provided by efficient optimization solvers which are available for mathematically standardized formulations. Ziegler [86] designs a quadratic program with a linear model and convex sets for environmental representations. The shown test results verify the performance for autonomous driving as demonstrated in the Bertha Benz drive [87]. However, the applicability of this research work is restricted to simple vehicle models and low environmental complexities.

Nonlinear optimal problems for trajectory planning provide the opportunity to consider complex vehicle dynamics characteristics such as coupling effects between lateral and longitudinal dynamics [28]. Yet no efficient solvers are available for general nonlinear optimization problems which prevents the algorithms from being applied in real time on real vehicles. The trajectory planning methods discussed are evaluated with respect to the requirements formulated according to Section 1.2 in Table 2.1 considering their suitability in collision avoidance tasks.

Table 2.1: Methods of trajectory planning for collision avoidance maneuvers

Planning method	Geometrical	Sampling based	Linear Optimal	Nonlinear Optimal	Potential field
Guaranteed Avoidance	+	+	+	+	-
Environmental Information	-	+	+	+	+
Vehicle Dynamics	-	+	o	+	o
Actuator Limits	-	+	+	+	o
Computational Complexity	+	+	o	-	o
Customization of Performance	-	-	+	+	o

2.3 Vehicle Dynamics Control

Vehicle dynamics control has also been addressed in previous publications. In early investigations by Ackermann [1] robust control methods have been proposed to control a bus on a given path. The method has been demonstrated in a simulation environment. The strength of this approach is the robustness to parameter deviations such as mass changes. A characteristic of robust control methods is its tradeoff betweeen robustness and performance. In [84] the authors have investigated robust control for a collision avoidance application in comparison with other control approaches. It can provide theoretical guarantees for robustness and requires less tuning effort, but it also shows a significant lack of performance for collision avoidance applications.

Linear controllers with feed forward components have been suggested in [37] [41][68]. The feedforward component is calculated based on the sigmoidal design of the trajectory and a simple kinematic single track model. To consider different parameter setups in different speed ranges, Schorn [68] suggests to pair the controller with a gain scheduling approach. Performance in different speed ranges can be achieved by proper tuning in each speed range separately. The controller has been demonstrated in the vehicle for trajectories up to 6 m/s^2.

Longitudinal dynamics control is achieved by calculating the remaining friction capability. Given a suitable trajectory, this approach provides an effective way for collision avoidance control. The tuning effort of linear controllers required for complex systems is enormous as explained in [2][70][76]. In addition actuator limits cannot be considered and the vehicle dynamics characteristics is used only by the feedforward component but not by the feedback component.
Input-output linearization has been considered by Werling [77] and Kranz [40]. The advantage of these approaches is that stability and performance of the control system can be easily analyzed by applying methods from linear control theory on nonlinear systems. Yet, these control methods are not suitable for maneuvers at the limits of the actuators, when executing evasive maneuvers as is required in this thesis.
Katrionik [35] proposes a MPC scheme for combined vehicle dynamics control of the lateral and longitudinal dynamics. The approach considers a single track model with a nonlinear tire model as well as a PT1 characteristic for the longitudinal dynamics. To guarantee vehicle dynamics stability, the maximum tire slip angles are constrained. The performance has been demonstrated in a simulation environment and in a real vehicle. The focus of this thesis is to provide a method for vehicle state estimation and sensor calibration as well as vehicle dynamics control with low cost sensors. Model predictive control is a promising approach for collision avoidance maneuvers due to the explicit consideration of actuator and state limitations. It can handle a rather complex dynamics model and adapt to model errors by repetitive planning of future interventions. An advantage of control algorithms that consider complex models is a reduced tuning effort as the model information can be exploited.
All works mentioned in this section assume a drivable and safe trajectory to be given such that the algorithm achieves good performance by following it. The control methods presented in this section are evaluated in Table 2.2 based on the predefined requirements in Section 1.2.

Table 2.2: Methods of vehicle dynamics control for collision avoidance maneuvers

Control method	Robust Control	Linear Control	Input-Output Linearization	Model Predictive Control
Vehicle Dynamics	o	-	o	+
Actuator Limits	o	-	-	+
Computational Complexity	o	+	+	-
Customization of Performance	-	+	o	+
Tuning Effort	+	-	o	+

2.4 Integrated Planning and Control

State of the art work on trajectory planning and vehicle dynamics control has been presented in previous sections. Due to the separation of both modules high tuning efforts are required to adapt both modules to each other and to cover the functionality in all relevant scenarios, as the planning method generally does not take the control properties into account. On top of that, the missing interaction between the trajectory planning and the control modules implies that the overall system, without an explicit replanning module, is most suitable for static scenarios, but not appropriate for dynamically changing scenarios. By integrating both modules, the interaction between both modules can be realized with reduced tuning effort. Further, the integrated concept allows to handle scenarios with new obstacles entering the environment during the maneuver by adapting the trajectory to updated environmental information in each planning step.
This section reviews collision avoidance methods that integrate the trajectory planning and the vehicle dynamics control module into one single module as shown in Figure 2.2 in contrast to the classical concept shown in Figure 2.1.
Keller and Bauer proposed methods for integrated planning and control combining potential fields and optimal control. Keller [38] has chosen an algorithm with rough discretization for the steering wheel angle and assumed the angle to

stay constant over the complete planning to realize the algorithm in real time. In contrast, Bauer [4] calculated a command sequence for the maneuver based on optimal potential field approach. As described in Section 2.3, potential field approaches cannot guarantee collision-freeness due to local minima and low gradients.

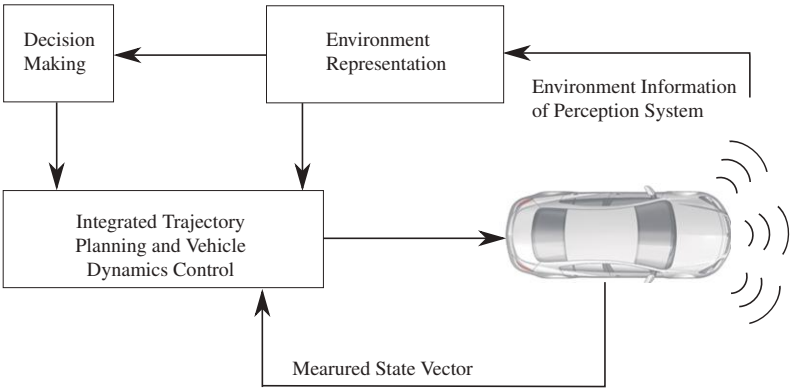

Figure 2.2: Integrated planning and control concept of collision avoidance systems

Erlien [19] investigated an integrated planning and control method with optimal control where inequality constraints are used to avoid collisions with obstacles within the prediction horizon. Similarly to [4] the investigated MPC takes all environmental information into account and further can guarantee collision-free trajectories with obstacles within the horizon. However the method does not consider braking intervention in the optimal control problem and cannot take into account obstacles outside the prediction horizon.

Table 2.3 shows an evaluation of the discussed approaches based on requirements presented in Section 1.2. All methods share the MPC's characteristic of low tuning effort, explicit consideration of actuator limits and vehicle dynamics model information. Further, the mentioned methods plan the maneuver separately for lateral and longitudinal dynamics, which shows deficiencies compared to planning of combined dynamics for the maneuver [67].

Differences arise in handling of obstacles, as potential field based approach cannot guarantee collision-freeness, whereas the work in [19] can provide a guarantee by using hard inequality constraints. However collision avoidance on obstacles that are outside the prediction horizon have not been considered. The method in [38] excells in terms of simplicity such that the computation time is negligible, but the control horizon is not representative for complex scenarios.

2.5 Selection of Methods and Concepts

Methods for trajectory planning, vehicle dynamics control as well as for the integrated planning and control concept have been presented in previous sections. A method that integrates both modules can plan a trajectory in each consecutive step and adapt to new environmental information instead of tracking a fixed trajectory as explained in Section 2.4. Further integration of planning and control functionality simplifies the interaction between both modules, as less parameters need to be tuned and the same vehicle dynamics model is shared. Due to these reasons the integrated planning and control concept will be further exploited in this thesis.

MPC as an optimality based method (Section 2.2 and 2.3) is a method that gives a good base to fulfill all requirements as defined in Section 1.2. In particular nonlinear optimal methods offer a high potential to meet the challenge of evasive collision avoidance systems. The main weakness of this approach is the computational burden required to solve the resulting optimization problem. The methods presented in Section 2.4 are all based on MPC. Among these methods, the method proposed by Erlien[19] can achieve collision avoidance due to inequality constraints, whereas the potential field based approaches cannot guarantee collision-freeness, as discussed in Section 2.2.

Therefore this thesis will investigate the potential of optimality based methods with collision avoidance constraints to solve the research question formulated in Section 1.2. Furthermore, this thesis shall take into account braking interventions in the optimization problem and investigate solutions to avoid collision with obstacles outside of the prediction horizon.

Table 2.3: Methods of integrated vehicle dynamics planning and control for collision avoidance maneuvers

Integrated method	Keller [38]	Bauer [3]	Erlien [19]
Guaranteed Avoidance	-	-	o
Environmental Information	+	+	+
Vehicle Dynamics	o	o	o
Actuator Limits	-	+	+
Computational Complexity	+	o	o
Customization of Performance	o	+	+
Tuning Effort	+	+	+

3 Fundamentals of Optimal Planning and Control

This chapter explains the theoretical background on vehicle dynamics modeling and model predictive control that is required for integrated vehicle dynamics planning and control in the Chapters 4 and 5. Furthermore this chapter will introduce fundamental terminologies, the general optimal framework for trajectory planning and vehicle dynamics control as well as the notation used in this thesis.

3.1 Vehicle Dynamics Modeling

The vehicle dynamics model used in this thesis is composed of the lateral and the longitudinal dynamics as illustrated in Figure 3.1. The lateral dynamics model consists further of the lateral vehicle model, the steering dynamics model and the tire model. The model is complemented by actuator and state limitations.

3.1.1 Lateral Dynamics Model

Lateral Vehicle Model

The vehicle model provides information about the dependancy between basic vehicle dynamics states such as the yaw rate $\dot{\varphi}$, the velocity v, the steering wheel angle δ and the side slip angle β. In this thesis, the single track model by Riekert and Schunck [63] is taken as a starting point and extended in subsequent sections.

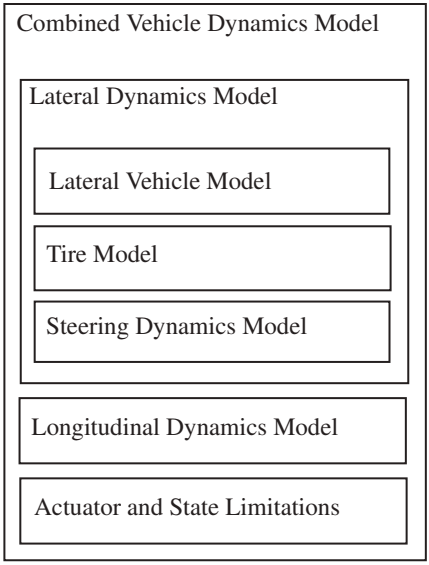

Figure 3.1: Components of the Combined Vehicle Dynamics Model

In Figure 3.2 the single-track model and the real vehicle used in this thesis are illustrated. The single-track model is a simplified approach to represent the lateral vehicle dynamics, which (in its original version) is described by two states corresponding to the yaw rate and the side slip angle. The single-track model models the axes of a vehicle with a single front tire and a single rear tire. The mass m is located at the center of gravity (COG), which is positioned at the distance l_f from the front axis and the distance l_r from the rear axis. The COG moves with the speed v and the side slip angle β to the longitudinal orientation of the vehicle. The vehicle rotates with the inertia J_z and yaw rate $\dot{\varphi}$ around the vertical axis z. The front and rear edge of the vehicle chassis, which need to be taken into account in collision avoidance maneuvers, are located at the longitudinal distances $l_\mathrm{f,veh}$ and $l_\mathrm{r,veh}$ from the COG. δ corresponds to the steering wheel angle, i_L is the steering ratio and α_f as well as α_r are the slip angles of the front and rear wheel. The slip angle is the angle between the tire orientation

and the moving direction of the vehicle [49]. Using the simplification for small angles, the angles can be calculated by

$$\alpha_{\mathrm{f}} = \frac{\delta}{i_{\mathrm{L}}} - \beta - \frac{l_{\mathrm{f}}\dot{\varphi}}{v} \tag{3.1}$$

$$\alpha_{\mathrm{r}} = -\beta + \frac{l_{\mathrm{r}}\dot{\varphi}}{v} \, . \tag{3.2}$$

The lateral and longitudinal tire forces of the front and rear tires are F_{yf}, F_{xf}, F_{yr} and F_{xr} respectively. Setting up the equilibrium of forces for the dynamics of the lateral movement as well as the equilibrium of moments for the yaw dynamics results in

$$m\frac{v^2}{R}cos\beta - F_{\mathrm{yr}} - F_{\mathrm{xf}}sin\delta - F_{\mathrm{yf}}cos\delta = 0 \tag{3.3}$$

$$J_{\mathrm{z}}\ddot{\varphi} - (F_{\mathrm{yf}}cos\delta + F_{\mathrm{xr}}sin\delta)l_{\mathrm{f}} + F_{\mathrm{yr}}l_{\mathrm{r}} = 0 \, . \tag{3.4}$$

In addition, the states of the single track model are extended by the lateral position with the dynamics

$$\dot{y} = v\sin(\varphi + \beta) \, . \tag{3.5}$$

By applying the small angle simplifications and neglecting the effect of longitudinal forces, the nonlinear continuous state transition for the lateral dynamics can be given by

$$\dot{\mathbf{x}}_{\mathrm{lat}} = \mathbf{f}_{\mathrm{lat}}(\mathbf{x}_{\mathrm{lat}}, \mathbf{u}_{\mathrm{lat}}) = \begin{bmatrix} \frac{F_{\mathrm{yf}}+F_{\mathrm{yr}}}{mv} - \dot{\varphi} \\ \frac{F_{\mathrm{yf}}l_{\mathrm{f}}-F_{\mathrm{yr}}l_{\mathrm{r}}}{J_{\mathrm{z}}} \\ \dot{\varphi} \\ v(\varphi+\beta) \end{bmatrix} \tag{3.6}$$

with the state vector $\mathbf{x}_{\mathrm{lat}} = [\beta,\ \dot{\varphi},\ \varphi,\ y]^T$ and the system input $\mathbf{u}_{\mathrm{lat}} = \delta$.

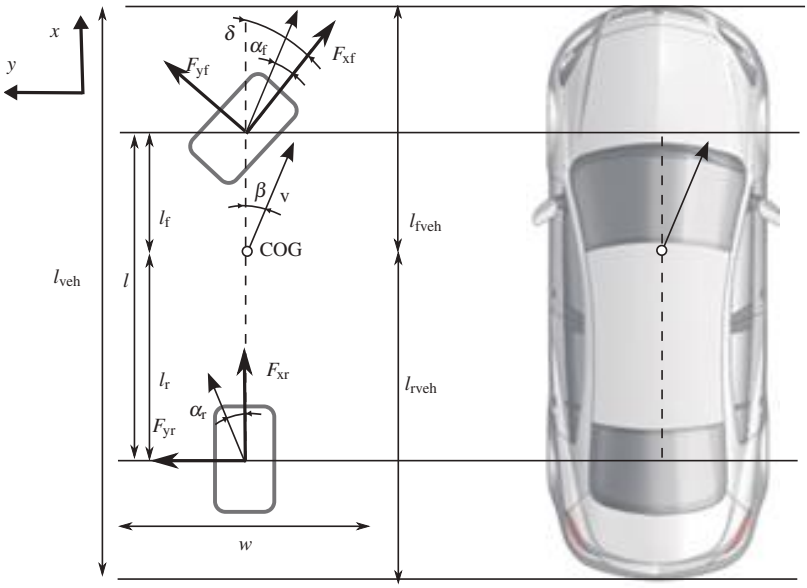

Figure 3.2: Illustration of single-track model and real vehicle

Tire Model

Tires are essential in the execution of vehicle dynamics maneuvers, since they determine the amount of force that can be transmitted to the ground. A basic tire model assumes the tire forces to be linear dependant on the slip angle α with a cornering stiffness c_α given in

$$F_y = c_\alpha \alpha \, . \tag{3.7}$$

In the equation above, the index which reveals the position of the tire is omitted for generalization purpose. Although (3.7) is a good approximation for the tire model at maneuvers with low slip angles, it does not represent the nonlinear tire behaviour of maneuvers with high slip angles[49][56][68]. To improve the model performance, the so called Magic Formula [56] is used to represent the

tire behaviour also for high slip angles. This simple tire model has a limited number of parameters and represents the tire forces at different slip angles α and wheel loads F_z. The structure of the tire model is

$$F_y(\alpha) = F_z \mu_y(\alpha) \tag{3.8}$$

$$\mu_y(\alpha) = D \sin\{C \arctan[B\alpha - E(B\alpha - \arctan(B\alpha))]\} \quad . \tag{3.9}$$

In (3.8) and (3.9), parameter B determines the stiffness, parameter C the shape, parameter D the peak and parameter E the curvature of the function and parameter μ_y the lateral friction coefficient [56].
This thesis neglects coupling effects of the longitudinal and the lateral tire forces. A suitable representation for the friction circle will be presented in Section 3.1.4 to compensate for this weakness.

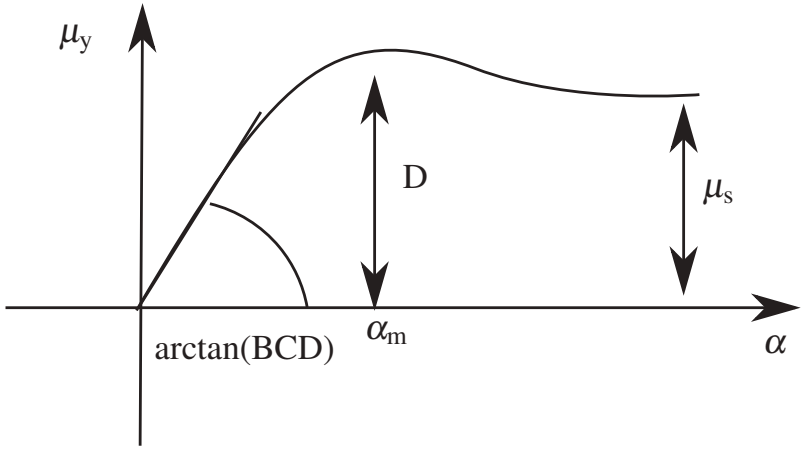

Figure 3.3: Pacejka's tire model [56] for firction coefficient

In Figure 3.3 the function for the friction coefficient is illustrated together with the relevant parameters, where μ_s is the stationary value of the friction coefficient for big slip angles and α_m is the slip angle at the peak of the friction coefficient. The tire parameters in (3.9) can be calculated according to [56] by

$$D = \mu_y(\alpha_m) \tag{3.10}$$

$$C = 1 + \left(1 - \frac{2}{\pi}\arcsin\frac{\mu_s}{D}\right) \tag{3.11}$$

$$B = [\frac{d\mu_y}{d\alpha}|_{\alpha=0}]/CD \tag{3.12}$$

$$E = \frac{B\alpha_m - \tan\{\pi/(2C)\}}{B\alpha_m - \arctan\{B\alpha_m\}}\ . \tag{3.13}$$

The wheel load F_z in equation (3.8) at the front and rear wheel is approximated according to [68] by

$$F_{zf} = m \cdot \left(\frac{l_r}{l} \cdot g + \frac{h_{cog}}{l} \cdot a_x\right) \tag{3.14}$$

$$F_{zr} = m \cdot \left(\frac{l_f}{l} \cdot g - \frac{h_{cog}}{l} \cdot a_x\right) \tag{3.15}$$

with the height of the COG h_{cog}.
To integrate the tire model into the state space equation in Section 3.1.3, the nonlinear tire equation is linearized according to [15] at the operation point given by the slip angle α_f and α_r. The linearized equation for the front and rear tires is then given by

$$F_{yf} = c_{\alpha f,0}\alpha_f + F_{yf,0} \tag{3.16}$$

$$F_{yr} = c_{\alpha r,0}\alpha_r + F_{yr,0} \tag{3.17}$$

and illustrated in Figure 3.4. In the equation above, the tire model is described by the cornering stiffnesses $c_{\alpha f,0}$ and $c_{\alpha r,0}$ as well as the bias values $F_{yf,0}$ and $F_{yr,0}$ for a slip angle α_0.

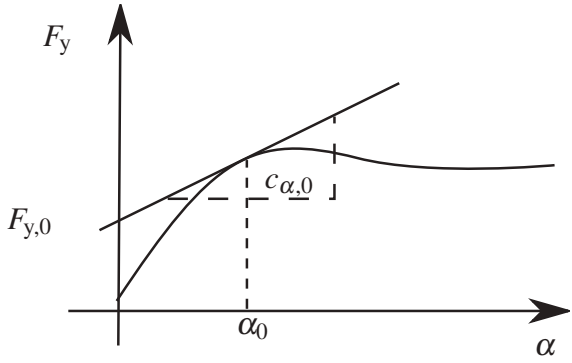

Figure 3.4: Approximation of nonlinear tire todel by a linear equation

Steering model

In order to support the driver during the collision avoidance maneuver, the real vehicles is equipped with an Electrical Power Steering (EPS) system, which can apply a steering torque on the steering system by an electrical motor on the steering rack.

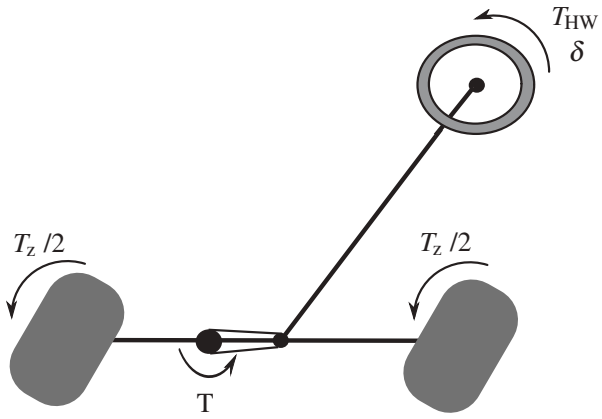

Figure 3.5: Mechanical structure of steering system

Moshchuk [52] provides a simple steering model structure for the mechanical components which will be used in this thesis. As illustrated in Figure 3.5, the electrical motor on the rack amplifies the driver torque T_{HW} by the total assisted torque T and counteracts the self aligning torque of the tires T_{z}. The dynamics equation of the steering system is given by

$$J_{\mathrm{st}}\ddot{\delta} + d_{\mathrm{st}}\dot{\delta} = T + T_{\mathrm{z}} + T_{\mathrm{HW}} \tag{3.18}$$

with the steering inertia J_{st}, the damping parameter d_{st} and the self alignment torque T_{z} which is the torque caused by tire friction on the road. The self alignment torque is modeled linearly by using the front slip angle α_{f} and the self alignment parameter D_{f} with

$$T_{\mathrm{z}} = -2D_{\mathrm{f}}\alpha_{\mathrm{f}} \,. \tag{3.19}$$

In the software of the EPS system, boost curves are implemented to translate the driver torque to an equivalent total assisted torque T on the steering system. The translation ratio is mainly dependant on the driver torque T_{HW} and the vehicle velocity v. In order to command a required total assisted torque T in the real vehicle, the torque T need to be translated into a driver equivalent torque using the boost curve and finally send to the EPS software. As the specific implementation depends on the design of the steering system manufacturer the specific algorithm will not be explained in this section. In the following, this thesis assumes the translation algorithm to be given.

Note that the steering system is modeled based on mechanical components and the boost curves only. The electrical power steering module of a state of the art vehicle is comprised of additional features such as friction compensation, active wheel return and arbitrage modules which may further influence the steering system behaviour during maneuver control. To keep the simplicity of the model, these investigations are not the focus of this thesis. More details may

be retrieved from [83], where the author has investigated the effects of these features for vehicle dynamics control using local linear model trees [54].

3.1.2 Longitudinal Dynamics Model

The electronic brake control module (EBCM) of the real vehicle contains a low level control module, which controls the hydraulic brake pressure in the braking pipe to achieve a desired deceleration command value. Instead of a complex physical model of the brake system, the behaviour of the overall low level control unit is represented by a double integrator with a time delay characteristic. Here, effects of the ABS and the ESC systems are neglected. The vehicle dynamics model for the longitudinal dynamics is given by

$$\dot{\mathbf{x}}_{\mathrm{ln}} = \mathbf{f}_{\mathrm{ln}}(\mathbf{x}_{\mathrm{ln}}, \mathbf{u}_{\mathrm{ln}}) = \begin{bmatrix} v\cos(\varphi+\beta) \\ a_{\mathrm{x}} \\ -\frac{1}{t_{\mathrm{del}}} a_{\mathrm{x}} + \frac{1}{t_{\mathrm{del}}} a_{\mathrm{x,cmd}} \end{bmatrix}. \tag{3.20}$$

Let t_{del} denote the time delay constant and $\mathbf{x}_{\mathrm{ln}} = [x,\ v,\ a_{\mathrm{x}}]^T$ denote the longitudinal state vector of the ego vehicle with the longitudinal position x, the velocity v as well as the longitudinal acceleration a_{x}. The input of the system $\mathbf{u}_{\mathrm{ln}}$, the deceleration command $a_{\mathrm{x,cmd}}$, should be distinguished from the measured acceleration a_{x}, which deviates due to control characteristic of the low level controller.

3.1.3 Combined Vehicle Dynamics Model

This section integrates all presented vehicle dynamics components into one combined vehicle dynamics model. The combined nonlinear vehicle dynamics model is given below. The state vector and the input vector are given by $\mathbf{x} = [\beta,\ \dot{\varphi},\ \varphi,\ y,\ \dot{\delta},\ \delta,\ x,\ v,\ a_{\mathrm{x}}]^T$ and $\mathbf{u} = [T,\ a_{\mathrm{x,cmd}}]^T$.

$$\alpha_{\mathrm{f}} = \frac{\delta}{i_{\mathrm{L}}} - \beta - \frac{l_{\mathrm{f}}\dot{\varphi}}{v}$$

$$\alpha_{\mathrm{r}} = -\beta + \frac{l_{\mathrm{r}}\dot{\varphi}}{v}$$

$$F_{\mathrm{yf}}(\alpha_{\mathrm{f}}) = F_{\mathrm{zf}} D \sin\{C \arctan[B\alpha_{\mathrm{f}} - E(B\alpha_{\mathrm{f}} - \arctan(B\alpha_{\mathrm{f}}))]\}$$

$$F_{\mathrm{yr}}(\alpha_{\mathrm{r}}) = F_{\mathrm{zr}} D \sin\{C \arctan[B\alpha_{\mathrm{r}} - E(B\alpha_{\mathrm{r}} - \arctan(B\alpha_{\mathrm{r}}))]\}$$

$$F_{\mathrm{zf}} = m \cdot \left(\frac{l_{\mathrm{r}}}{l} \cdot g + \frac{h_{\mathrm{cog}}}{l} \cdot a_{\mathrm{x}} \right)$$

$$F_{\mathrm{zr}} = m \cdot \left(\frac{l_{\mathrm{f}}}{l} \cdot g - \frac{h_{\mathrm{cog}}}{l} \cdot a_{\mathrm{x}} \right)$$

$$T_{\mathrm{z}} = -2D_{\mathrm{f}}\alpha_{\mathrm{f}}$$

$$\dot{\mathbf{x}} = \mathbf{f}(\mathbf{x}, \mathbf{u}) = \begin{bmatrix} \frac{F_{\mathrm{yf}} + F_{\mathrm{yr}}}{mv} - \dot{\varphi} \\ \frac{F_{\mathrm{yf}} l_{\mathrm{f}} - F_{\mathrm{yr}} l_{\mathrm{r}}}{J_{\mathrm{z}}} \\ \dot{\varphi} \\ v \sin(\varphi + \beta) \\ \frac{T + T_{\mathrm{z}} + T_{HW} - d_{\mathrm{st}}\dot{\delta}}{J_{\mathrm{st}}} \\ \dot{\delta} \\ v \cos(\varphi + \beta) \\ a_{\mathrm{x}} \\ -\frac{1}{t_{\mathrm{del}}} a_{\mathrm{x}} + \frac{1}{t_{\mathrm{del}}} a_{\mathrm{x,cmd}} \end{bmatrix} \tag{3.21}$$

3.1.4 Actuator and State Limitations

The equation (3.21) describes a detailed model for the vehicle dynamics. The validity of this physical model is limited due to actuator and friction limitations. The EPS unit assists the driver by translating the driver torque T_{HW} with a boost curve to the total assisted torque T. In the frame of this thesis, the torque T will be used to perform the evasive collision avoidance maneuver without intervention of the driver. The limitations of the demanded total assisted torque can be simplified to a maximum steering assist torque $T_{\max}$ with

$$-T_{\max} \leq T \leq T_{\max} \ . \tag{3.22}$$

Furthermore, the EBCM unit introduced in Section 3.1.2 controls the brake pressure in the brake pipe to achieve a given deceleration value. Due to limitations and properties of the actuator, the performance of a braking intervention is limited as well. The maximum deceleration value of the EBCM is $a_{\mathrm{x,cmd,max}} = -9.81\ \mathrm{m}/s^2$ in the chosen real vehicle, such that the limit is given by

$$a_{\mathrm{x,cmd,max}} \leq a_{\mathrm{x,cmd}} \leq 0 \ . \tag{3.23}$$

An acceleration circle represents the combined effect of the friction limitation on each wheel. Figure 3.6 shows the relevant left half of the acceleration circle in the g-g diagram from [5], as only negative acceleration (braking) shall be applied in longitudinal direction during the maneuver. The acceleration circle is given in

$$\sqrt{a_{\mathrm{x}}^2 + a_{\mathrm{y}}^2} \leq a_{\max} \ . \tag{3.24}$$

The lateral acceleration is not represented in the vehicle dynamics states, but can be calculated according to [49] by

$$a_{\mathrm{y}} = v(\dot{\varphi} + \dot{\beta}) \ . \tag{3.25}$$

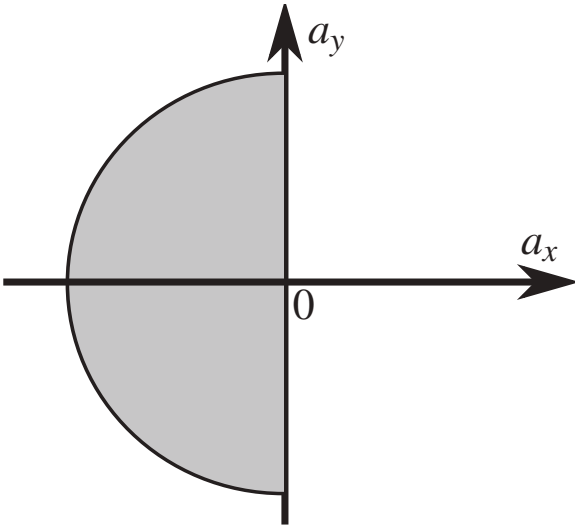

Figure 3.6: Acceleration circle in g-g diagram with shaded area for maneuver dynamics with combined braking and steering [6]

3.1.5 Model Validation

In this section, relevant parameters of the real vehicle, an Opel Insignia, are given based on the vehicle dynamics model presented in previous section. The basic model parameters are listed in Table 3.1.

Subsequently, the model is evaluated using test drives by executing an evasive maneuver in the real vehicle on the proving ground. Modelled signals are generated using the model structure and parameters as presented in this chapter with commanded steering torque T and deceleration $a_{\mathrm{x,cmd}}$ as input.

Figure 3.7 illustrates a comparison of the modelled signals with the measured signals for the positions x and y, the accelerations a_{x} and a_{y}, the steering wheel angle δ, the velocity v, the yaw rate $\dot{\varphi}$ and the yaw angle φ. The maneuver is performed at approximately 50 km/h, a typical urban velocity.

During the maneuver lateral accelerations of up to 6 m/s^2 are achieved, which corresponds to maximum values of evasive collision avoidance maneuvers [68].

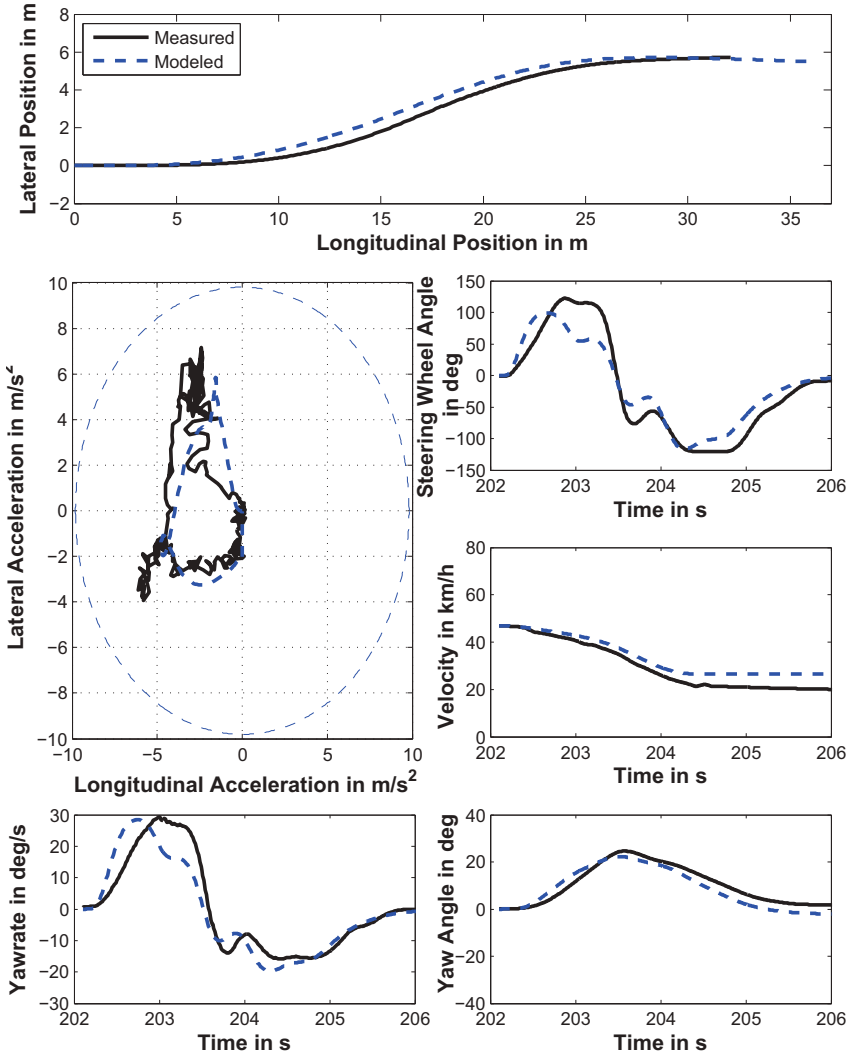

Figure 3.7: Model Validation on a maneuver with 50 km/h and lateral acceleration up to 6 m/s^2

The signal curves in Figure 3.7 show the main curve characteristics, such that the combined vehicle dynamics model can represent the considered maneuvers. Table 3.2 shows the model deviations when commanded signals in a test drive are applied to the vehicle dynamics model in open loop simulation. The model deviations can be attributed to deviations in model structure, parameter uncertainties and environmental changes. Because of these effects, this model can not be used in open loop simulation for localization tasks without feedback information. In a closed loop setup, effect of uncertainties and deviations can be reduced due to replanning.

Table 3.1: Measured and estimated parameters of the vehicle dynamics model in Section 3.1.3

Parameter	Symbol	Value	Unit
Vehicle mass	m	2050	kg
Wheel base	l	2.74	m
Track width	w	1.585	m
Distance to front axis	l_f	1.227	m
Distance to ground	h_cog	0.548	m
Inertia of Vehicle	J_z	3500	kgm^2
Tire parameters	$B/C/D/E$	19.56/0.44/ 2.05/-0.70	1/rad /(none)/ (none)/(none)
Steering inertia	J_st	0.57	kgm^2
Steering ratio	i_L	16	(none)
Steering damping	d_st	2.54	Nms/rad
Steering self alignment torque	D_f	460	Nm/rad

Figure 3.8: Opel Insignia Sports Tourer

Table 3.2: Model deviation for test drive in Figure 3.7 in open loop

Maximum lateral deviation	0.7 m
Maximum longitudinal deviation	7.2 m
Maximum acceleration deviation	1.3 m/s^2

3.2 Model Predictive Control

Optimality based methods like model predictive control (MPC) have gained growing application in a broad range of industrial fields. Since its first successfull application in 1978 by Richalet [62], the method has been applied in various industrial applications like: fluid catalytic cracking, batch reactors, regenerators loadings, pressure controls, temperature control etc. [16][22][45][47][55][65]. Due to increased computation power and faster optimization algorithms in recent years, MPC can now be applied on highly dynamical problems and systems such as adaptive cruise control [50], DC/DC converters[7], traction control [9] or autonomous vehicle steering [51].

The basic principle of MPC is to solve a finite horizon optimal control problem online starting from an initial state of a given discretized plant model [61]. The result of the method is a finite input vector sequence, where the first input vector is applied. The advantage compared to other control methods is its ability to consider input and state constraints as well as model equations over a prediction horizon [10].
This section explains the theoretical background of the nominal and the robust MPC by giving a brief extract of the work in [61].

3.2.1 Nominal Model Predictive Control

The ideal regulating problem that the nominal MPC tries to solve is to find a solution for the following optimization problem:

$$\begin{aligned} \min\ & V_\infty = \sum_{i=0}^{\infty} l(\mathbf{x}(i,k),\mathbf{u}(i,k)) \\ \text{s.t. }\ & \mathbf{x}(i+1,k) = f(\mathbf{x}(i,k),\mathbf{u}(i,k)),\ \ \mathbf{x}(0,k) = \mathbf{x}_0 \\ & \mathbf{u}(i,k) \in \mathbb{U},\ \ \mathbf{x}(i,k) \in \mathbb{X} \end{aligned} \tag{3.26}$$

The control problem above has been designed in [61] to steer the state to the origin under consideration of the state transition equation $\mathbf{x}(i+1,k) = f(\mathbf{x}(i,k),\mathbf{u}(i,k))$, the initial state $\mathbf{x}_0$, the input constraint set $\mathbb{U}$ and the state constraint set $\mathbb{X}$. In the considered problem, $\mathbf{x}(i,k)$ and $\mathbf{u}(i,k)$ are the discrete state and input vector. Here i is the index for the prediction step and k is the index for the control time step. If the target state is not the origin, modifications [61] can be made to use the generalized optimization problem in (3.26). The input constraint set $\mathbb{U}$ and state constraint set $\mathbb{X}$ are exploited to consider for limitations of actuators and requirements of the control problem. The cost function V_∞ in (3.26) consists of stage costs $l(\mathbf{x},\mathbf{u})$ for predictive time steps of an infinite time horizon. The consideration of an infinite horizon has advantages in terms of closed loop properties compared to the consideration of a

finite horizon [61]. Yet, the considered horizon is infinite and the cost function is not necessarily a convex function of $\mathbf{u}$ which makes the problem hard to solve numerically for generalized settings of optimization problems.
In [61] this infinite time optimal control problem is replaced by two sub-problems, one representing a finite horizon optimal control problem and one describing an infinite horizon optimal control problem [61]. The equations of the resulting quasi-infinite control problem are given by

$$\begin{aligned} \min\ & V = \sum_{i=0}^{N-1} l(\mathbf{x}(i,k),\mathbf{u}(i,k)) + V_{\mathrm{f}}(\mathbf{x}(N)) \\ \text{s.t.}\ & \mathbf{x}(i+1,k) = \mathbf{f}(\mathbf{x}(i,k),\mathbf{u}(i,k)) \\ & \mathbf{u}(i,k) \in \mathbb{U},\ \ \mathbf{x}(i,k) \in \mathbb{X},\ \ \forall i = 0,\cdots,N \\ & \mathbf{x}(N,k) \in \mathbb{X}_{\mathrm{f}}\ . \end{aligned} \tag{3.27}$$

with the terminal set $\mathbb{X}_{\mathrm{f}}$ and the terminal penalty V_{f}. The solution calculated with the finite time interval control problem should be equivalent to the infinite time optimal control problem by forcing the terminal state of the finite horizon to enter the terminal set $\mathbb{X}_{\mathrm{f}}$. Within the terminal set, the method should be able to guarantee stability and recursive feasibility with a linear feedback vector $\mathbf{k}$ and the terminal weight $\mathbf{P}_{\mathrm{f}}$, such that

$$V_{\mathrm{f}}(\mathbf{x}) = \mathbf{x}^T \mathbf{P}_{\mathrm{f}} \mathbf{x} \tag{3.28}$$

$$\mathbf{k} = -\mathbf{R}^{-1}\mathbf{B}\mathbf{P}_{\mathrm{f}}\ . \tag{3.29}$$

Here $\mathbf{B}$ is the input matrix of the state space model and $\mathbf{R}$ is the input weight of the control problem.
Rawling [61] shows that an arbitrary optimization problem does not necessarily have a solution. In order to guarantee the existence of a solution according to the extreme value theorem of Weierstrass in [36], the cost function needs to be continuous and the set constraints should be compact. This leads to the following assumptions for the existence of a solution according to [61].

Assumption 1: *(Continuity of system and cost)*
The functions $\mathbf{f}: \mathbb{X} \times \mathbb{U} \to \mathbb{R}^n, l: \mathbb{X} \times \mathbb{U} \to \mathbb{R}_{\geq 0}$ *and* $V_f: \mathbb{X}_f \to \mathbb{R}_{\geq 0}$ *are continuous and satisfy* $\mathbf{f}(\vec{0},\vec{0}) = 0, l(\vec{0},\vec{0}) = 0$ *as well as* $V_f(\vec{0},\vec{0}) = 0$

The notation used should be understood as follows, $\mathbf{f}: \mathbb{X} \times \mathbb{U} \to \mathbb{R}^n$ describes a function **f**, which maps a state vector given in the admissible state constraint set $\mathbb{X}$ and the input vector in the input constraint set $\mathbb{U}$ to a vector of real numbers of dimension *n* and $\mathbb{R}_{\geq 0}$ is the set of positive real numbers.

Assumption 2: *(Properties of constraint sets)*
The sets $\mathbb{X}$ *and* $\mathbb{X}_f$ *are closed,* $\mathbb{X}_f$ *is a subset of* $\mathbb{X}$ *and* $\mathbb{U}$ *is compact; each set contains the origin.*

Proposition 1: *(Existence of a solution to an optimal control problem)*
Suppose assumptions 1 and 2 hold. Then
a. The function V is continuous in $\mathbb{X}$ *and* $\mathbb{U}$.
b. For each $\mathbf{x} \in \mathbb{X}$ *a solution to the problem in (3.27) exists.*

To ensure asymptotic stability of the MPC controller, the Lyapunov theorem is deployed. This implies that the origin is asymptotically stable with a region of attraction $\mathbb{X}$ for the autonomous system $\mathbf{x}^+ = \mathbf{f}(\mathbf{x})$ if there exists a Lyapunov function V, a positive definite invariant set $\mathbb{X}$, two $\mathscr{K}_\infty$ functions $\gamma_1(\cdot)$ and $\gamma_2(\cdot)$, and a positive definite function $\gamma_3(\cdot)$ satisfying

$$V(\mathbf{x}) \geq \gamma_1(|\mathbf{x}|) \tag{3.30}$$

$$V(\mathbf{x}) \leq \gamma_2(|\mathbf{x}|) \tag{3.31}$$

$$V(f(\mathbf{x})) \leq V(\mathbf{x}) - \gamma_3(|\mathbf{x}|) \tag{3.32}$$

for all $\mathbf{x} \in \mathbb{X}$. The properties of the functions and sets are defined below.

Definition 1: *(Properties of functions and sets)*
a. A function γ *is a* $\mathscr{K}_\infty$ *function, if* $\gamma: \mathbb{R} \to \mathbb{R}_{\geq 0}$ *is continuous, strictly increasing, satisfies* $\gamma(0) = 0$ *and is unbounded.*

b. A function γ is a positive definite function, if it is continuous and positive everywhere except at the origin.
c. A set $\mathbb{X}$ is positive invariant for the system $\mathbf{x}^+ = \mathbf{f}(\mathbf{x})$ if $\mathbf{x} \in \mathbb{X}$ implies $\mathbf{f}(\mathbf{x}) \in \mathbb{X}$.
d. A set $\mathbb{X}$ is a region of attraction for the system $\mathbf{x}^+ = \mathbf{f}(\mathbf{x})$, if the states in the set $\mathbb{X}$ evolve to zero, $|\mathbf{x}(k)|_{\mathbb{X}} \to 0$, as $k \to \inf$.

A standard approach is to consider the value function of the infinite horizon optimal control problem as a Lyapunov function. For the quasi-infinite optimal control problem this implies several design concepts that need to be satisfied to guarantee asymptotic stability according to the Lyapunov theorem.

Assumption 3: *(Basic stability assumptions)*

$$\min_{u \in \mathbb{U}} \{V_f(\mathbf{f}(\mathbf{x},\mathbf{u}) + l(\mathbf{x},\mathbf{u})) | \mathbf{f}(\mathbf{x},\mathbf{u}) \in \mathbb{X}_f\} \leq V_f(\mathbf{x}), \quad \forall \mathbf{x} \in \mathbb{X}_f$$

Assumption 4: *(Implied invariance) assumptions*
The set $\mathbb{X}_f$ is control invariant for the system $\mathbf{x}^+ = \mathbf{f}(\mathbf{x},\mathbf{u})$

Further to guarantee (3.30) and (3.31), bounds need to be considered for the stage cost and the terminal cost.

Assumption 5: *(Bounds on stage and terminal cost)*
The stage cost l and the terminal cost V_f satisfy

$$l(\mathbf{x},\mathbf{u}) \geq \gamma_l(|\mathbf{x}|) \; \forall \mathbf{x} \in \mathscr{X}_N, \forall \mathbf{u} \in \mathbb{U} \tag{3.33}$$

$$V_f(\mathbf{x}) \leq \gamma_2(|\mathbf{x}|) \; \forall \mathbf{x} \in \mathbb{X}_f \tag{3.34}$$

in which γ_l and γ_2 are $\mathscr{K}_\infty$ functions.

It can be derived that (3.33) guarantees (3.30) for the Lyapunov function if $\mathbb{X}_\mathrm{f}$ contains the origin in its interior [61]. The conditions defined above thus guarantee Lyapunov stability [61] summarized in the following proposition. The terminal set $\mathbb{X}_\mathrm{f}$ can be chosen to be the maximal control invariant set, which

corresponds to the inclusion of the set $\mathscr{W} \subseteq \{\mathbf{x} \in \mathbb{X} | \mathbf{k}\mathbf{x} \in \mathbb{U}\}$ and the invariant set in which $\mathbf{x} \in \mathbb{X}$ implies $\mathbf{f}(\mathbf{x}) \in \mathbb{X}$.

Proposition 2: *(Optimal value function properties)*
Suppose that Assumptions 1, 2, 3, 4 and 5 are satisfied. Then there exist $\mathscr{K}_\infty$ functions $\gamma_1(\cdot)$ and $\gamma_2(\cdot)$ such that $V(\cdot)$ has the following properties

$$V(\mathbf{x}) \geq \gamma_1(|\mathbf{x}|) \quad \forall \mathbf{x} \in \mathbb{X}$$
$$V(\mathbf{x}) \leq \gamma_2(|\mathbf{x}|) \quad \forall \mathbf{x} \in \mathbb{X}_f$$
$$V(f(\mathbf{x},\mathbf{u})) \leq V(\mathbf{x}) - \gamma_3(|\mathbf{x}|) \quad \forall \mathbf{x} \in \mathbb{X}$$

Finally the stability of the MPC can be ensured by Theorem 1.

Theorem 1: *(MPC stability)*
Suppose that Assumptions 1, 2, 3, 4 and 5 are satisfied and that $\mathbb{X}_f$ contains the origin in its interior. Then the origin is asymptotically stable with a region of attraction $\mathbb{X}$ for the system $\mathbf{x}^+ = \mathbf{f}(\mathbf{x},\mathbf{u})$.

For proofs and detailed explanations for this section please refer to [61]. This section presented requirements formulated for linear time invariant (LTI) systems. Consider that the assumptions and propositions formulated above can be equivalently used to design for control of linear time varying (LTV) systems, as is presented in Chapter 5.

3.2.2 Robust Model Predictive Control

The robust design of controllers is important in the presence of uncertainties causing a deviation between predicted behaviour based on the nominal system and actual behavior. Two different types of uncertainties have been adressed in [61]: additive and parametric uncertainties. Parametric uncertainties can directly represent effects of parameters in sophisticated models, such as mass or inertia, whereas additive uncertainties can be easily considered mathematically as a further summand in the equation and can be converted from the parametric uncertainties.

Consider the linear system with parametric uncertainties in the vector θ in

$$\mathbf{x}^+ = \mathbf{f}(\mathbf{x},\mathbf{u},\theta) = \mathbf{A}(\theta)\mathbf{x} + \mathbf{B}(\theta)\mathbf{u} \tag{3.35}$$

where $\theta \in \Theta$ and Θ being the uncertainty set.
This system with parametric uncertainties can be reformulated in a form with additive uncertainties

$$\mathbf{x}^+ = \mathbf{f}(\mathbf{x},\mathbf{u},\theta) = \mathbf{A}\mathbf{x} + \mathbf{B}\mathbf{u} + \mathbf{w} \tag{3.36}$$
$$\mathbf{w} \in \mathbb{W},\ \ \mathbb{W} := \{(\mathbf{A}(\theta) - \mathbf{A})\mathbf{x} + (\mathbf{B}(\theta) - \mathbf{B})\mathbf{u} | \theta \in \Theta, (\mathbf{x},\mathbf{u}) \in \mathbb{X} \times \mathbb{U}\},$$

where the matrices $\mathbf{A}$ and $\mathbf{B}$ are the nominal state space matrices defined at nominal parameters in θ_0.
To treat the additive uncertainties, [48] and [61] proposed tube based MPC as a computationally efficient method for this task. The feedback policy proposed by tube based MPC is

$$\mathbf{u} = \mathbf{v} + \mathbf{k}(\mathbf{x} - \mathbf{z}) \tag{3.37}$$

Here $\mathbf{v}$ and $\mathbf{z}$ are the input and state vector of a nominal system given by

$$\mathbf{z}^+ = \mathbf{A}\mathbf{z} + \mathbf{B}\mathbf{v}, \tag{3.38}$$

$\mathbf{k}$ is a linear feedback vector calculated offline to stabilize the system and minimize the deviation between the actual state $\mathbf{x}$ and the nominal state $\mathbf{z}$. The feedback policy of the tube based MPC in (3.37) is composed of two components. The open loop control $\mathbf{v}$ controls the nominal system in (3.38) whereas the feedback control with linear feedback vector $\mathbf{k}$ minimizes the deviation between the nominal system states and the actual system states.
With the control policy given, the overall system dynamics is

$$\mathbf{x}^+ = \mathbf{A}\mathbf{x} + \mathbf{B}\mathbf{v} + \mathbf{B}\mathbf{k}\mathbf{e} + \mathbf{w} \tag{3.39}$$

where $\mathbf{e}$ is the error between the actual state $\mathbf{x}$ and the nominal state $\mathbf{z}$ with

$$\mathbf{e} = \mathbf{x} - \mathbf{z} \tag{3.40}$$

and the error dynamics

$$\mathbf{e}^{+} = \mathbf{A}_{\mathrm{k}}\mathbf{e} + \mathbf{w} \tag{3.41}$$

$$\mathbf{A}_{\mathrm{k}} = \mathbf{A} + \mathbf{B}\mathbf{k}\ . \tag{3.42}$$

The error can be calculated with the closed loop state matrix $\mathbf{A}_{\mathrm{k}}$ using

$$\mathbf{e}(i) = \mathbf{A}_{\mathrm{k}}^{i}\mathbf{e}_0 + \sum_{j=0}^{i-1} \mathbf{A}_{\mathrm{k}}^{j}\mathbf{w}(j) \tag{3.43}$$

with $\mathbf{e}(i) \in \mathbb{S}_{\mathrm{i}}$ where $\mathbb{S}_{\mathrm{i}}$ is composed of the uncertainties and state transition matrices up to the prediction time step i.

$$\mathbb{S}_{\mathrm{i}} = \sum_{j=0}^{i-1} \mathbf{A}_{\mathrm{k}}^{j}\mathbb{W} = \mathbb{W} \oplus \mathbf{A}_{\mathrm{k}}\mathbb{W} \oplus \ldots \oplus \mathbf{A}_{\mathrm{k}}^{i-1}\mathbb{W} \tag{3.44}$$

Control with tube based MPC can be viewed as control of tubes rather than control of trajectories. The feedback policy enables control under uncertainty and can be explained by controlling a tube around the nominal trajectory, in which each trajectory in this tube corresponds to a particular realization of the uncertainty.

To satisfy the constraints $\mathbb{X}$ and $\mathbb{U}$ in the real system, suitable tightened constraint sets $\mathbb{Z}$ and $\mathbb{V}$ need to be considered for the open loop control with the nominal system formulated by

$$\begin{aligned}
&\mathbf{z}(i,k) \in \mathbb{Z} := \mathbb{X} \ominus \mathbb{S} \\
&\mathbf{v}(i,k) \in \mathbb{V} := \mathbb{U} \ominus \mathbf{k}\mathbb{S} \\
&\mathbf{x}(0,k) \in \{\mathbf{z}(0,k)\} \;\; \mathbf{e}(i,k) \in \mathbb{S}_\mathrm{i} \\
&\mathbf{z}(N,k) \in \mathbb{Z}_\mathrm{f} \;\; \mathbb{Z}_\mathrm{f} \subseteq \mathbb{Z}
\end{aligned}$$

where the set operations are defined by

Definition 2: *(Set algebra)*
(a) Set addition $\mathbb{A} \oplus \mathbb{B} := \{\mathbf{a}+\mathbf{b} | \mathbf{a} \in \mathbb{A}, b \in \mathbb{B}\}$.
(b) Set substraction $\mathbb{A} \ominus \mathbb{B} := \{\mathbf{x} \in \mathbb{R}^n | \{\mathbf{x}\} \oplus \mathbb{B} \subseteq \mathbb{A}\}$.
(c) Set multiplication: Let $\mathbf{K} \in \mathbb{R}^{m \times n}$. *Then* $\mathbf{K}\mathbb{A} := \{\mathbf{K}\mathbf{a} | \mathbf{a} \in \mathbb{A}\}$.

The tightened constraints guarantee satisfaction of constraints for $\mathbf{x}$ and $\mathbf{u}$ with the feedback control law in presence of uncertainties. Calculation of the set $\mathbb{Z}$ and $\mathbb{V}$ is in general a difficult task. [61] shows how the set can be calculated with minimal computational burden achieving a tradeoff between conservatism and simplicity.
Let the state constraints be given by

$$\mathbb{X} := \{\mathbf{x} \in \mathbb{R}^n | \mathbf{c}_\mathrm{j}\mathbf{x} \leq d_\mathrm{j}\}$$

with the number of the constraint given by the index j then the tightened state constraints corresponding to the nominal states are given by

$$\mathbb{Z} := \{\mathbf{z} \in \mathbb{R}^n | \mathbf{c}_\mathrm{j}\mathbf{z}(i,k) \leq d_\mathrm{j} - \max\{\mathbf{c}_\mathrm{j}\mathbf{e}(i) | \mathbf{e}(i) \in S_\mathrm{i}\}\}$$

where the maximum error in the set S_i with respect to the vector $\mathbf{c}_\mathrm{j}$ is calculated for each constraint equation separately. Similarly, if the input constraint of the actual input is given by

$$\mathbb{U} := \{\mathbf{u} \in \mathbb{R}^m | \mathbf{a}_\mathrm{j}\mathbf{u} \leq b_\mathrm{j}\}$$

the tightened input constraint can be calculated by

$$\mathbb{V} := \{\mathbf{v} \in \mathbb{R}^m | \mathbf{a}_\mathrm{j}\mathbf{v} \leq b - \max\{\mathbf{a}_\mathrm{j}\mathbf{k} \sum_{i=0}^{N-1} \mathbf{A}_\mathrm{k}^i \mathbf{w} | \mathbf{w} \in \mathbb{W}\}\} \quad .$$

To guarantee stability of the tube based controller, the definitions and theorems stated in Chapter 3 need to be reformulated in consideration of the uncertainty. The basic stability assumption with uncertainties can be reformulated as below.

Assumption 6: *(Basic stability assumption; robust case)*
(a) For all $\mathbf{x} \in \mathbb{X}_f$

$$\min_{\mathbf{u}\in\mathbb{U}} \max_{\mathbf{w}\in\mathbb{W}} [\Delta V_f + l](\mathbf{x}, \mathbf{u}, \mathbf{w}) \leq 0$$

with $\Delta V_f(\mathbf{x}, \mathbf{u}, \mathbf{w}) = V_f(\mathbf{f}(\mathbf{x}, \mathbf{u}, \mathbf{w})) - V_f(\mathbf{x}, \mathbf{u}, \mathbf{w})$
(b) $\mathbb{X}_f \subseteq \mathbb{X}$

Assumption 6 requires the reduction of the loss function under any uncertainty $\mathbf{w} \in \mathbb{W}$, which makes the loss function a local Lyapunov function in $\mathbb{X}_\mathrm{f}$. This implies properties for the terminal set which are equivalent to Assumption 4 for the nominal MPC in Chapter 3.

Assumption 7: *(Implied stability assumption; robust case)*
The set $\mathbb{X}_f$ *is robust control invariant for* $\mathbf{x}^+ = \mathbf{f}(\mathbf{x}, \mathbf{u}, \mathbf{w}), \mathbf{w} \in \mathbb{W}$

The term robust control invariant is defined by

Definition 3: *(Robust control invariance)*
A set $\mathbb{X} \subseteq \mathbb{R}^n$ *is robust control invariant for* $\mathbf{x}^+ = \mathbf{f}(\mathbf{x}, \mathbf{u}, \mathbf{w}), \mathbf{w} \in \mathbb{W}$ *if, for every* $\mathbf{x} \in \mathbb{X}$*, there exists a* $\mathbf{u} \in \mathbb{U}$ *such that* $\mathbf{f}(\mathbf{x}, \mathbf{u}, \mathbf{w}) \in \mathbb{X}$

Satisfaction of the Assumptions 1, 2, 5, 6 and 7 with bounded disturbances ensures asymptotic stability to a robust control invariant set discussed in [61]. Finally, limitation on the uncertainty set need to be formulated as unlimited disturbances cannot be compensated and stability as well as constraint satisfaction can not be guaranteed. The characteristic of the uncertainty is described in the following assumptions.

Assumption 8: *(Restricted disturbance for constraint satisfaction)*
$S \subseteq \mathbb{X}, \mathbf{k}S \subseteq \mathbb{U}$.

Assumption 9: *(Compact convex disturbance set)*
The compact convex set $\mathbb{W}$ *contains the origin in its interior.*

The Assumptions 8 and 9 underline that the compensation of uncertainty is limited by the input and the state constraint. If the effect of the uncertainties reaches the input limits, the performance and stability of the system can no longer be guaranteed. In this thesis, the Assumptions 8 and 9 are assumed to be satisfied, such that the uncertainty can be compensated by the control.
Similarly to Section 3.2.1 the assumptions and propositions formulated above can be equivalently used to design for control of linear time varying systems, as is used in Chapter 5.

3.3 Model Predictive Tracking

In the last sections, the theoretical background of the MPC necessary for guaranteeing the existence and the stability of the solution have been briefly presented. In this section these results will be applied to the simple control problem

of trajectory tracking for a vehicle. Similar approaches have been presented in works like [35][15][20][6]. The structure of the MPC in the classical control concept is presented in Figure 3.9. The MPC for the tracking problem makes use of a preplanned trajectory and the state vector information of the plant vehicle. The core of the MPC method is the optimization algorithm, which comprehends several modules such as the vehicle dynamics model, the cost function, the state and input constraints as well as the terminal cost. After solving the MPC optimization problem the first input vector is applied to the actors of the vehicle.

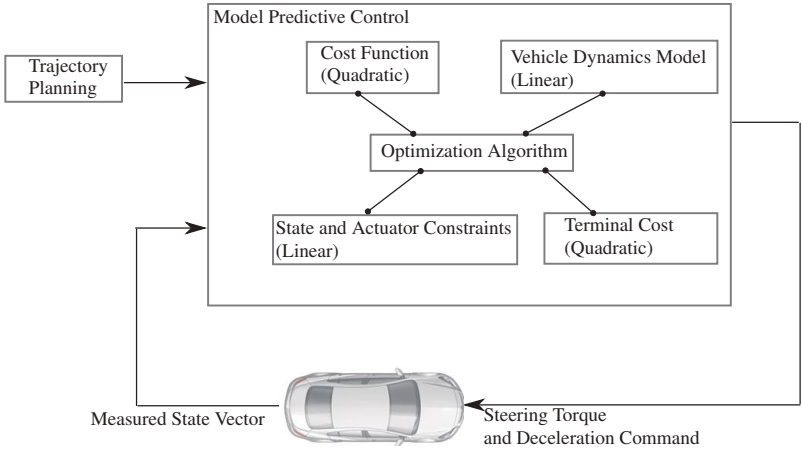

Figure 3.9: MPC structure in Classical Control Concept

3.3.1 Trajectory Planning

The trajectory planning method exploited in this chapter for the lateral dynamics is the sigmoidal trajectory presented by Stählin [71] and Schorn [68].
The equation of the sigmoidal trajectory is

$$y(x) = \frac{M}{1 + e^{-a(x-c)}} \tag{3.45}$$

where M is the lateral maneuver distance, c is half of the longitudinal maneuver distance and a is the slope at the middle of the maneuver. Since the sigmoidal reaches its both ends in positive and negative infinity only, y_{Tol} is introduced, such that $y(0) = y_{\text{Tol}}$ and $y(2c) = M - y_{\text{Tol}}$. The parameters of the sigmoidal trajectory are illustrated in Figure 3.10. Given a maximum lateral acceleration $a_{\text{y,max}}$, the lateral maneuver distance M and the tolerance constant y_{Tol}, the remaining parameters c and a have been derived in [71] to

$$c = \frac{1}{a_{\text{y}}} ln(\frac{M - y_{\text{Tol}}}{y_{\text{Tol}}})$$

$$a = \frac{(p+1)^2 \sqrt{-pM(a_{\text{y,max}} pM - v^2 p^2 + v^2) a_{\text{y,max}}}}{pM(a_{\text{y,max}} pM - v^2 p^2 + v^2)}$$

with the parameters

$$p = \sqrt{2} \frac{s_2}{\sqrt{s_1}} \left(6v^2 + 2a_{\text{y,max}} M + \frac{4a_{\text{y,max}}^2 M^2}{3v^2} \right) + \frac{2a_{\text{y,max}} M}{3v^2} + 1$$

$$s_1 = 9v^4 + 3a_{\text{y,max}} Mv^2 + 2a_{\text{y,max}}^2 M^2$$

$$s_2 = \cos\left(\frac{1}{3} \arctan\left(\frac{3v^2 \sqrt{num}}{den} \right) \right)$$

$$num = 81v^8 + 27v^4 a_{\text{y,max}}^2 M^2 + 4a_{\text{y,max}}^3 M^3 + 3a_{\text{y,max}}^4 M^4$$

$$den = 27v^6 + 9v^2 a_{\text{y,max}}^2 M^2 + 4a_{\text{y,max}}^3 M^3 + 27v^4 a_{\text{y,max}} M \ .$$

The trajectory for the longitudinal dynamics is generated using the approach of [35]. Katriniok distinguishes between several maneuver phases and plans different constant deceleration values for different phases. Similarly to [35], the trajectory in this section is created by planning a constant deceleration of -5 m/s^2 from t = 0 s to 0.8 s and -1.5 m/s^2 from t = 0.8 s to 1.3 s. From t = 1.3 s to 2.2 s no braking is planned. Finally for t > 2.2 s, a braking maneuver of -8 m/s^2 is planned until standstill.

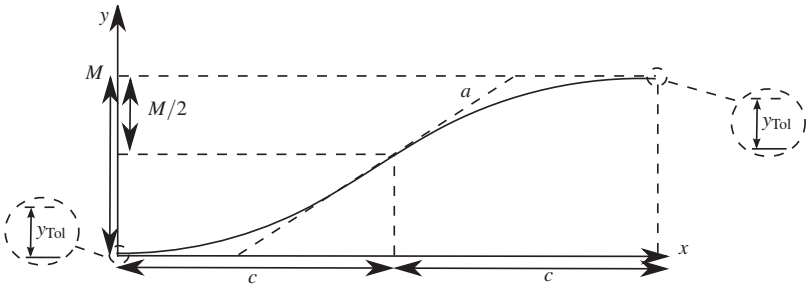

Figure 3.10: Sigmoidal Trajectory [71]

3.3.2 Vehicle Dynamics Model

The state transition model represents the system characteristics in the considered control process, i.e. the combined braking and steering dynamics behaviour of the vehicle in the collision avoidance maneuver. Though the combined vehicle dynamics model can represent the model behaviour for these maneuvers, a control algorithm based on the nonlinear model in (3.21) cannot be implemented in the real vehicle due to computational limitations. In the equation below the affine state space matrices with the system matrix $\mathbf{A}_c$, the input matrix $\mathbf{B}_c$ and the bias vector $\mathbf{E}_c$ are calculated by taking the derivates with respect to the state and the input vector of (3.21) respectively at the operation point (measured state) $\mathbf{x}_0$ and the last input vector $\mathbf{u}_0$.

$$\mathbf{A}_c = \frac{\partial \mathbf{f}(\mathbf{x}_0, \mathbf{u}_0)}{\partial \mathbf{x}} \tag{3.46}$$

$$\mathbf{B}_c = \frac{\partial \mathbf{f}(\mathbf{x}_0, \mathbf{u}_0)}{\partial \mathbf{u}} \tag{3.47}$$

$$\mathbf{E}_c = \mathbf{f}(\mathbf{x}_0, \mathbf{u}_0) - \mathbf{A}_c \mathbf{x}_0 - \mathbf{B}_c \mathbf{u}_0 \ . \tag{3.48}$$

The affine continuous state space model and the corresponding matrices are given by

$$\dot{\mathbf{x}} = \mathbf{A}_c \cdot \mathbf{x} + \mathbf{B}_c \cdot \mathbf{u} + \mathbf{E}_c \tag{3.49}$$

with

$$\mathbf{A}_\mathrm{c} = \begin{bmatrix} A_{11} & A_{12} & 0 & 0 & 0 & \frac{c_{\alpha_{\mathrm{f},0}}}{m v_0 i_\mathrm{L}} & 0 & A_{18} & 0 \\ A_{21} & A_{22} & 0 & 0 & 0 & A_{26} & 0 & A_{28} & 0 \\ 0 & 1 & 0 & 0 & 0 & 0 & 0 & 0 & 0 \\ v_0 & 0 & v_0 & 0 & 0 & 0 & 0 & 0 & 0 \\ \frac{2D_\mathrm{f}}{J_\mathrm{st}} & \frac{2l_f D_\mathrm{f}}{v_0 J_\mathrm{st}} & 0 & 0 & -\frac{-d_\mathrm{st}}{J_\mathrm{st}} & \frac{-2D_\mathrm{f}}{i_\mathrm{L} J_\mathrm{st}} & 0 & A_{58} & 0 \\ 0 & 0 & 0 & 0 & 1 & 0 & 0 & 0 & 0 \\ 0 & 0 & 0 & 0 & 0 & 0 & 1 & 0 & 0 \\ 0 & 0 & 0 & 0 & 0 & 0 & 0 & 1 & 0 \\ 0 & 0 & 0 & 0 & 0 & 0 & 0 & 0 & -\frac{1}{t_\mathrm{del}} \end{bmatrix};$$

$$\mathbf{B}_\mathrm{c} = \begin{bmatrix} 0 & 0 \\ 0 & 0 \\ 0 & 0 \\ 0 & 0 \\ \frac{1}{J_\mathrm{st}} & 0 \\ 0 & 0 \\ 0 & 0 \\ 0 & 0 \\ 0 & \frac{1}{t_\mathrm{del}} \end{bmatrix}; \mathbf{E}_\mathrm{c} = \begin{bmatrix} \frac{F_{\mathrm{yf},0} + F_{\mathrm{yr},0}}{m v_0} - A_{18} v_0 \\ \frac{F_{\mathrm{yf},0} l_\mathrm{f} + F_{\mathrm{yr},0} l_\mathrm{r}}{J_\mathrm{z}} - A_{28} v_0 \\ 0 \\ 0 \\ -A_{58} v_0 \\ 0 \\ 0 \\ 0 \\ 0 \end{bmatrix};$$

$$A_{11} = -\frac{c_{\alpha_{\mathrm{f},0}} + c_{\alpha_{\mathrm{r},0}}}{m v_0}; A_{12} = \frac{c_{\alpha_{\mathrm{r},0}} l_\mathrm{r} - c_{\alpha_{\mathrm{f},0}} l_\mathrm{f}}{m v_0^2} - 1;$$
$$A_{18} = \frac{c_{\alpha_{\mathrm{f},0}} + c_{\alpha_{\mathrm{r},0}}}{m v_0^2}\beta_0 - 2\frac{c_{\alpha_{\mathrm{r},0}} l_\mathrm{r} - c_{\alpha_{\mathrm{f},0}} l_f}{m v_0^3}\dot{\varphi}_0 - \frac{c_{\alpha_{\mathrm{f},0}}}{i_\mathrm{L} m v_0^2}\delta_0;$$
$$A_{21} = \frac{c_{\alpha_{\mathrm{r},0}} l_\mathrm{r} - c_{\alpha_{\mathrm{f},0}} l_\mathrm{f}}{J_\mathrm{z}}; A_{22} = -\frac{c_{\alpha_{\mathrm{r},0}} l_\mathrm{r}^2 + c_{\alpha_{\mathrm{f},0}} l_f^2}{J_\mathrm{z} v_0};$$
$$A_{26} = -\frac{c_{\alpha_{\mathrm{r},0}} l_\mathrm{r}^2 + c_{\alpha_{\mathrm{f},0}} l_\mathrm{f}^2}{J_\mathrm{z} v_0}; A_{28} = \frac{c_{\alpha_{\mathrm{f},0}} l_\mathrm{f}^2 + c_{\alpha_{\mathrm{r},0}} l_\mathrm{r}^2}{J_\mathrm{z} v_0^2}\dot{\varphi}_0;$$
$$A_{58} = \frac{-2 l_f D_\mathrm{f}}{J_\mathrm{st} v_0^2}\dot{\varphi}_0;$$

Here v_0, δ_0, $\dot{\varphi}_0$ and β_0 denote the measured velocity, steering wheel angle, yaw rate as well as the side slip angle and $c_{\alpha_{\mathrm{f},0}}$, $c_{\alpha_{\mathrm{r},0}}$, $F_{\mathrm{yf},0}$ and $F_{\mathrm{yr},0}$ denote parameters of the linearized tire model in (3.16). In the model predictive control design, the discretized state space equation

$$\mathbf{x}_{k+1} = \mathbf{A}\mathbf{x}_k + \mathbf{B}\mathbf{u}_k + \mathbf{E} \tag{3.50}$$

is used. The state vector is given by $\mathbf{x}^T = [\beta, \dot{\varphi}, \varphi, y, \dot{\delta}, \delta, x, v, a_\mathrm{x}]$ and the input vector by $\mathbf{u}^T = [T, a_{\mathrm{x,cmd}}]$. The state transition equation is continuous for the state and the input vector, so that it satisfies Assumption 1. Note that the affine state space equation in (3.50) needs to be reformulated in section 3.3.5 to calculate the penalty matrix based on a linear state space model.

3.3.3 Cost Function

A central component of MPC methods is the selection of a suitable cost function, which follows the design goal of the control problem. In this section we choose the cost function to minimize the deviation of the vehicle states from a preplanned trajectory. The trajectory shall be followed explicitly for the lateral position, the velocity as well as the yaw angle of the vehicle dynamics state. Furthermore, we need to consider weights for the control signals, the steering

torque and the commanded deceleration, to avoid permanent planning of maneuvers at the actuator limits. The cost function is given by

$$\begin{aligned} J = &\sum_{i=0}^{N-1} q_y(y(i,k) - y_{\text{traj}}(i,k))^2 + q_\varphi(\varphi(i,k) - \varphi_{\text{traj}}(i,k))^2 \\ &+ q_v(v(i,k) - v_{\text{traj}}(i,k))^2 + r_{\text{T}} T^2(i,k) + r_{\text{a}_\text{x}} a_{x,cmd}^2(i,k) \\ &= (\mathbf{x}(i,k) - \mathbf{y}_{\text{traj}}(i,k))^T \mathbf{Q}(\mathbf{x}(i,k) - \mathbf{y}_{\text{traj}}(i,k)) + \mathbf{u}(i,k)' \mathbf{R} \mathbf{u}(i,k) \end{aligned} \tag{3.51}$$

$$\text{with } \mathbf{Q} = \begin{bmatrix} 0 & 0 & 0 & 0 & 0 & 0 & 0 & 0 & 0 \\ 0 & 0 & 0 & 0 & 0 & 0 & 0 & 0 & 0 \\ 0 & 0 & q_\varphi & 0 & 0 & 0 & 0 & 0 & 0 \\ 0 & 0 & 0 & q_y & 0 & 0 & 0 & 0 & 0 \\ 0 & 0 & 0 & 0 & 0 & 0 & 0 & 0 & 0 \\ 0 & 0 & 0 & 0 & 0 & 0 & 0 & 0 & 0 \\ 0 & 0 & 0 & 0 & 0 & 0 & 0 & 0 & 0 \\ 0 & 0 & 0 & 0 & 0 & 0 & 0 & q_{\text{v}} & 0 \\ 0 & 0 & 0 & 0 & 0 & 0 & 0 & 0 & 0 \end{bmatrix} \quad \mathbf{R} = \begin{bmatrix} r_{\text{T}} & 0 \\ 0 & r_{\text{a}_\text{x}} \end{bmatrix}$$

The chosen cost function is continuous for the state as well as the input vector and the matrices $\mathbf{P}$ and $\mathbf{Q}$ are chosen to be symmetric positive semidefinite such that the Assumptions 1, 3 and 5 are satisfied. The trajectory vector $\mathbf{y}_{\text{traj}}$ is composed of the trajectory values for the yaw angle q_φ, the lateral position q_y and the velocity q_v with

$$\mathbf{y}_{\text{traj}}(i,k) = [0, 0, \varphi_{\text{traj}}(i,k), y_{\text{traj}}(i,k), 0, 0, 0, v_{\text{traj}}(i,k), 0]^T.$$

3.3.4 Constraints

One of the main advantages of model predictive control is the ability to consider state and input constraints in the control design. In this section, constraints are used to ensure stability when controlling the vehicle at high yaw rate φ and side slip angle β as well as to consider actuator limitations for the input vector $\mathbf{u}$.

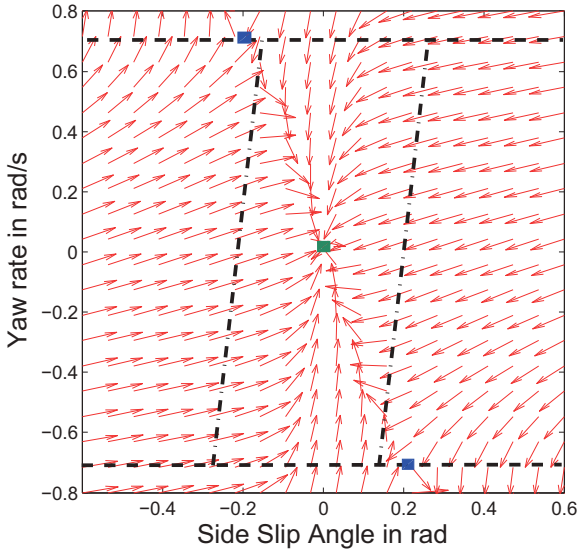

Figure 3.11: Phase plane map for v =50km/h and δ =3 °

Stable Handling Envelopes

Stable handling envelopes can guarantee for vehicle dynamics stability when integrated in MPC methods for maneuvers with high yaw rate and side slip angle. This was addressed by Beal [6] by presenting an invariant set in a phase plane, spanned by the yaw rate and the side slip angle axis. Beal shows that the limit of instability in the phase plane map for a vehicle dynamics model with nonlinear tires and different steering wheel angle as well as velocity values can be considered by a maximum yaw rate and a maximum side slip angle limit.

A phase plane map is exemplarily shown in Figure 3.11 for a single track model with constant velocity and steering wheel angle. The figure illustrates the snapshot dynamics of the model at different states (arrows), the stable equilibrium point (marked point near the origin), to which states in the stable set evolve to, and the unstable equilibrium points (marked points at +0.7 rad/s and -0.7 rad/s), which separates the stable states from the unstable states. The unstable states are characterized by states moving away from the origin. Beal [5] explains that the stable equilibrium points move to higher yaw rate values with increasing steering wheel angle, whereas the unstable equilibrium points move to lower slip angles at constant yaw rate value with increasing steering wheel angle. The yaw rate value of the unstable equilibrium point is

$$\dot{\varphi}_{max} = \begin{cases} \frac{F_{\mathrm{yr,max}}(1+\frac{l_r}{l_f})}{mv} \text{ for } F_{\mathrm{yf,max}} < \frac{l_\mathrm{r}}{l_\mathrm{f}} F_{\mathrm{yr,max}} \\ \frac{F_{\mathrm{yf,max}}(1+\frac{l_\mathrm{f}}{l_\mathrm{r}})}{mv} \text{ for } F_{\mathrm{yf,max}} < \frac{l_\mathrm{r}}{l_\mathrm{f}} F_{\mathrm{yr,max}} \end{cases} . \tag{3.52}$$

for different maximum lateral forces. These forces are dependent on the tire parameter, slip angle and load of each axis. The conditional equation can be rewritten with (3.14) in terms of the longitudinal acceleration.

$$\begin{aligned} & F_{\mathrm{yf,max}} - \frac{l_\mathrm{r}}{l_\mathrm{f}} F_{\mathrm{yr,max}} \\ &= \mu_{\mathrm{y,max}} m (\frac{l_\mathrm{r}}{l} g + \frac{h_\mathrm{cog}}{l} a_\mathrm{x}) - \frac{l_\mathrm{r}}{l_\mathrm{f}} \mu_{\mathrm{y,max}} m (\frac{l_\mathrm{f}}{l} g - \frac{h_\mathrm{cog}}{l} a_\mathrm{x}) \\ &= \mu_{\mathrm{y,max}} m (\frac{h_\mathrm{cog}}{l} + \frac{l_\mathrm{r}}{l_\mathrm{f}} \frac{h_\mathrm{cog}}{l}) a_\mathrm{x} \\ &= \mu_{\mathrm{y,max}} m \frac{h_\mathrm{cog}}{l_\mathrm{f}} a_\mathrm{x} \end{aligned}$$

For the considered maneuver the longitudinal acceleration a_x is negative for the duration of the maneuver, so that the second case in (3.52) applies.
The limit for the maximum yaw rate can thus be calculated by

$$\begin{aligned}\dot{\varphi}_\mathrm{max} &= \frac{F_\mathrm{yf,max}(1+\frac{l_\mathrm{f}}{l_\mathrm{r}})}{mv} \\ &= \frac{\mu_\mathrm{y,max} m(\frac{l_\mathrm{r}}{l}g + \frac{h_\mathrm{cog}}{l}a_\mathrm{x})(1+\frac{l_\mathrm{f}}{l_\mathrm{r}})}{mv} \\ &= \frac{\mu_\mathrm{y,max}(g+\frac{h_\mathrm{cog}}{l_\mathrm{r} r}a_\mathrm{x})}{v} \quad .\end{aligned}$$

The maximum side slip angle β_max is

$$\beta_\mathrm{max} = -\alpha_\mathrm{r,max} + \frac{l_\mathrm{r}\dot{\varphi}}{v} \tag{3.53}$$

with $\alpha_\mathrm{r,max}$ being the maximum allowed slip angle for the rear tire. The stablility envelope can then be given by

$$-\dot{\varphi}_\mathrm{max} \leq \dot{\varphi} \leq \dot{\varphi}_\mathrm{max} \tag{3.54}$$

$$-\beta_\mathrm{max} \leq \beta \leq \beta_\mathrm{max} \ . \tag{3.55}$$

The admissible set for the stability is therefore

$$\mathbb{S} = \{\mathbf{x} \in \mathbb{R}^9 \mid \dot{\varphi} \in [-\dot{\varphi}_\mathrm{max}, \dot{\varphi}_\mathrm{max}], \beta \in [-\beta_\mathrm{max}, \beta_\mathrm{max}]\} \ . \tag{3.56}$$

For the case that the maximum lateral force on the front and rear tires are achieved simultaneously and a maximum slip angle of $\alpha_\mathrm{r,max} = 12^\circ$ should not be exceeded, the maximum yaw rate and side slip angle limits are illustrated in Figure 3.11. In this chapter the state constraint set $\mathbb{X}$ comprises of the set $\mathbb{S}$ only, such that $\mathbb{X} = \mathbb{S}$ holds.

Actuator Limitations

The input vector $\mathbf{u}$ is limited by an admissible actuator range, i.e. the maximum and minimum possible steering wheel torque and the maximum longitudinal deceleration command.

The set of admissible actuator limits is thus given by

$$\mathbb{U} = \{\mathbf{u} \in \mathbb{R}^2 \,|T \in [-T_{\max}, T_{\max}], a_{\mathrm{x,cmd}} \in [a_{\mathrm{x,cmd,max}}, 0]\} \quad . \tag{3.57}$$

Note that the set $\mathbb{U}$ is compact and $\mathbb{X}$ is closed which satisfies Assumption 2.

3.3.5 Terminal Cost

As explained in Section 3.2.1 the quasi-infinite optimal control problem is composed of two sub-problems, the finite optimal control problem and the infinite optimal control problem. The infinite control problem is designed to guarantee stability for consecutive control step $i > N$. Therefore a penalty matrix $\mathbf{P}_{\mathrm{f}}$ needs to be calculated to stabilize the system for the time steps $i > N$ in a wide range of vehicle dynamics. To calculate the penalty matrix the affine state space equation in (3.50) will be rewritten into the linear state space equation

$$\begin{bmatrix} \mathbf{x}_{k+1} \\ 1 \end{bmatrix} = \begin{bmatrix} \mathbf{A} & \mathbf{E} \\ 0 & 1 \end{bmatrix} \begin{bmatrix} \mathbf{x}_k \\ 1 \end{bmatrix} + \begin{bmatrix} \mathbf{B} \\ 0 \end{bmatrix} \mathbf{u}_k \tag{3.58}$$

Based on this linear state space model, the theory of linear quadratic control and Lyapunov inequality [11] will be exploited with

$$\begin{bmatrix} \mathbf{A}(\theta) & \mathbf{E}(\theta) \\ 0 & 1 \end{bmatrix}^T \mathbf{P}_{\mathrm{f}} \begin{bmatrix} \mathbf{A}(\theta) & \mathbf{E}(\theta) \\ 0 & 1 \end{bmatrix} - \mathbf{P}_{\mathrm{f}} \leq \begin{bmatrix} -\mathbf{Q} & 0 \\ 0 & 0 \end{bmatrix} \tag{3.59}$$

Here $\mathbf{A}(\theta)$ denotes the dependance of the state space matrix from the parameter vector $\theta \in \Theta$ with

$$\begin{aligned}\Theta := \{\theta \in \mathbb{R}^3 | v \in [v_{\min}, v_{\max}], \alpha_{\mathrm{r}} \in [-\alpha_{\mathrm{r,max}}, \alpha_{\mathrm{r,max}}], \\ \alpha_{\mathrm{f}} \in [-\alpha_{\mathrm{f,max}}, \alpha_{\mathrm{f,max}}]\}\end{aligned} \tag{3.60}$$

The parameter set Θ considers the change of velocity and slip angles for a wide range of vehicle dynamics maneuvers. The matrix $\mathbf{P}_{\mathrm{f}}$ is calculated offline with solvers for linear matrix inequalities [11][44] with the parameter vector $\theta \in \Theta$.

3.3.6 MPC Formulation

The overall MPC method proposed in this chapter is

$$\begin{aligned}\min_{\mathbf{u}} J = \sum_{i=0}^{N-1} & (\mathbf{x}(i,k) - \mathbf{y}_{\mathrm{traj}}(i,k))' \mathbf{Q} (\mathbf{x}(i,k) - \mathbf{y}_{\mathrm{traj}}(i,k)) \\ & + \mathbf{u}(i,k)' \mathbf{R} \mathbf{u}(i,k) \\ & + [\mathbf{x}^T(N,k) - \mathbf{y}_{\mathrm{traj}}^T(N,k)\ 1]^T \mathbf{P}_{\mathrm{f}} [\mathbf{x}^T(N,k) - \mathbf{y}_{\mathrm{traj}}^T(N,k)\ 1]^T \\ & \mathbf{x}(i+1,k) = \mathbf{A}\mathbf{x}(i,k) + \mathbf{B}\mathbf{u}(i,k) + \mathbf{E},\ \forall i = 0, \cdots N \\ & \mathbf{u} \in \mathbb{U},\ \mathbf{x} \in \mathbb{X}\,.\end{aligned} \tag{3.61}$$

The components of the proposed tracking method satisfy the Assumptions 1, 2, 3, 4 and 5. Theorem 1 can thus provide stability guarantee for the presented control algorithm. Figure 3.12 illustrates the performance of this simple tracking method on a scenario with a static obstacle. The sigmoidal trajectory and the MPC are set up with the parameters given in Table 3.3. The top picture illustrates the position of the planned trajectory (thick dashed line) and the driven trajectory of the COG (thick solid line) as well as of the four vehicle corners (thin dashed lines line). The method shows lateral deviations of approximately $y_{\mathrm{dev}} = 0.65$m which results from an aggressive parameterization of the trajectory planner. The maneuver is triggered at $x = 4$m. At ① the maximum

steering torque and the maximum deceleration command values are applied. The counter steering phase starts at ② where the deceleration command is reduced to zero. In the stabilization phase at ③ maximum deceleration command is applied to reduce the vehicle velocity. The deviation between the planned trajectory and the driven trajectory indicates that proper tuning of the geometrical parameters in the planning method on the control characteristic is very important to ensure collision avoidance in the maneuver. Furthermore, both steering torque and deceleration command are not planned according to the most recent obstacle position but according to the curvature of the trajectory which is fixed during maneuver execution.

Table 3.3: Parameter setup for trajectory planning and vehicle dynamics control module

Parameter	Symbol	Value	Unit
Lateral maneuver distance	M	2.1	m
Tolerance Value	y_{Tol}	0.01	m
Maximum lateral acceleration	$a_{\mathrm{y,max}}$	9.81	$\mathrm{m/s^2}$
Penalty value on lateral position	q_{y}	1000	$\mathrm{1/m^2}$
Penalty value on yaw angle	q_{φ}	10	$\mathrm{1/rad^2}$
Penalty value on velocity	q_{v}	50	$\mathrm{s^2/m^2}$
Penalty value on steering torque	r_{T}	0.01	$\mathrm{1/Nm^2}$
Penalty value on deceleration	$r_{\mathrm{a_x}}$	0.01	$\mathrm{s^4/m^2}$
Maximum steering assist torque	T_{max}	50	Nm
Maximum rear slip angle	$\alpha_{\mathrm{r,max}}$	12	°
Maximum lateral friction	$\mu_{\mathrm{y,max}}$	1	(none)
Maximum deceleration value	$a_{\mathrm{x,cmd,max}}$	-9.81	$\mathrm{m/s^2}$

In Chapter 4 and 5, methods for the integrated planning and control concept will be investigated, where the obstacle is considered by the method directly and no tuning effort is needed between the planning and the control module.

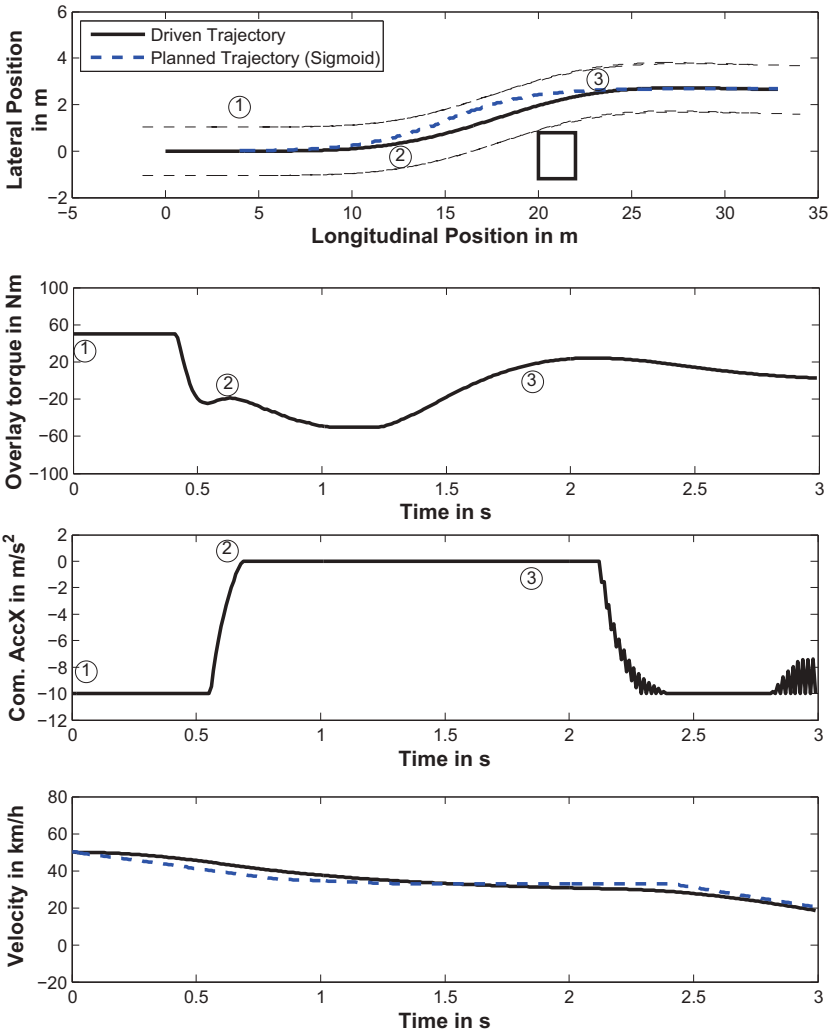

Figure 3.12: Tracking on predefined trajectory in single obstacle scenario

4 Nonlinear Integrated Planning and Control

The classical planning and control concept based on a trajectory, calculated with geometrical primitives, and a MPC approach as described in Section 3.3 is suitable to avoid a collision in simple scenarios, but cannot consider environmental information in complex scenarios with multiple obstacles and road boundaries. The integrated planning and control concept according to Section 2.4 can overcome the weaknesses of the classical concept. This chapter describes a nonlinear integrated planning and control method based on a nonlinear MPC structure. Preliminary work of this chapter has been published at the IEEE Intelligent Vehicles Symposium 2016 [83].

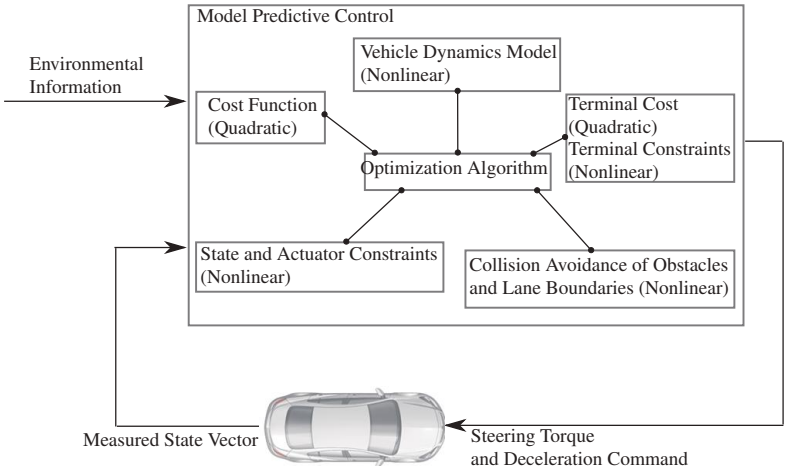

Figure 4.1: MPC structure of Nonlinear Integrated Planning and Control Method

The structure of the integrated planning and control method is illustrated in Figure 4.1. Instead of the preplanned trajectory as part of the classical concept, environmental information such as road boundaries and obstacle information serve as direct input for the proposed method. This information is used in the collision avoidance constraint to predict collision-free trajectories. The state and actuator constraints, the terminal cost as well as the vehicle dynamics model are taken from Chapter 3.
The remainder of this chapter is structured as follows. Section 4.1 introduces design goals for the desired planning characteristic of the proposed method. The cost function and the collision avoidance constraints required to consider the design goals and the environmental information are explained in Sections 4.2 and 4.3. The problem of obstacles outside of the prediction horizon is discussed and the terminal collision avoidance constraint is formulated for specific scenarios in Section 4.4. In Section 4.5, soft constraints are introduced to ensure smooth calculation of the result. The overall nonlinear MPC formulation is summarized in Section 4.6. The performance of the integrated method in a simulation environment is demonstrated in Section 4.7.

4.1 Design Goals

Key requirements to design the trajectory planning and the vehicle dynamics control module have been introduced in Section 1.2. By selecting the integrated planning and control concept based on the MPC method with collision avoidance constraints, several requirements can be fulfilled with reasonable effort as will be explained in this chapter. After establishing a proper implementation in this chapter to fulfill all given requirements independent on computational load, Chapter 5 will serve to deduce a time efficient method.
The optimization goal will be designed through a cost function as will be shown in the next section. The cost function enables the customization of the collision avoidance maneuver performance. This customization defines the characteristic

of optimality and determines how the performance of the method shall be later evaluated in the simulation environment and in the real vehicle.
The design goals for collision avoidance maneuvers impact constraints and cost function. Design goals like guaranteed collision-freeness, consideration of environmental information, representation of vehicle dynamics and actuator limitations directly lead to the formulation of constraints. The performance of the optimization algorithm is thus indirectly influenced by those design goals. Two design goals have been chosen to be directly considered in the cost function. This concept can be easily modified with respect to performance by changing the states being considered in the cost function.
An emergency maneuver in urban environments should always be designed to reduce the velocity until the critical situation is dissolved. This supports the item of uncertain information as discussed in Section 1.2, leading to a reduced potential collision energy in the case that obstacles did not move dynamically as predicted. By reducing the velocity during the evasive maneuver, the prerequisite to do the best for avoiding the collision with an obstacle not detected early enough is given.
Similarly the planning and control method should aim to reduce the final yaw angle of the maneuver. By following this design goal, larger yaw angles not needed for the maneuvver are reduced. A potential threat of the maneuvering vehicle to other road participants like oncoming traffic can also be reduced by considering the yaw angle in the cost function. This indirectly supports the minimization of the lateral displacement. Furthermore, both criteria support better coorporation with the driver after being exposed to an emergency maneuver.
The key requirements and the design goals shape the properties of the integrated planning and control method investigated in this thesis. By selection of the concept and method based on the key requirements already build the fundament to cope with the objectives of evasion maneuvers. In addition, the described design goals shall further shape the desired driving characteristics of the planned maneuver and will be used to develop the required metrics in Section 4.7.1.

4.2 Cost Function

While the cost function for the trajectory tracking method in Section 3.3 serves to reduce deviations to a preplanned trajectory, the function for the integrated planning and control method directly considers the design goals from Section 4.1, i.e. it is designed to reduce the velocity and the final yaw angle deviation to the orientation of the road boundaries. In scenarios with straight lanes the yaw angle deviation can be substituted by the yaw angle. In addition, command signals are weighted in the cost function to prevent the method from permanent planning of interventions at the limits of the actuators. In addition to the desired control characteristic in (4.1), the cost function needs to be appended with a terminal cost V_f which can ensure stability of the control characteristic. The cost function is thus given by

$$J = \sum_{i=1}^{N-1} \mathbf{x}(i)^T \mathbf{Q}\mathbf{x}(i) + \mathbf{u}(i)^T \mathbf{R}\mathbf{u}(i) + [\mathbf{x}(N)^T \; 1]\mathbf{P}_\mathrm{f}[\mathbf{x}(N)^T \; 1]^T \tag{4.1}$$

$$\mathbf{Q} = \begin{bmatrix} 0 & 0 & 0 & 0 & 0 & 0 & 0 & 0 & 0 \\ 0 & 0 & 0 & 0 & 0 & 0 & 0 & 0 & 0 \\ 0 & 0 & q_\varphi & 0 & 0 & 0 & 0 & 0 & 0 \\ 0 & 0 & 0 & 0 & 0 & 0 & 0 & 0 & 0 \\ 0 & 0 & 0 & 0 & 0 & 0 & 0 & 0 & 0 \\ 0 & 0 & 0 & 0 & 0 & 0 & 0 & 0 & 0 \\ 0 & 0 & 0 & 0 & 0 & 0 & 0 & 0 & 0 \\ 0 & 0 & 0 & 0 & 0 & 0 & 0 & q_\mathrm{v} & 0 \\ 0 & 0 & 0 & 0 & 0 & 0 & 0 & 0 & 0 \end{bmatrix} \quad \mathbf{R} = \begin{bmatrix} r_\mathrm{T} & 0 \\ 0 & r_{\mathrm{a_x}} \end{bmatrix}$$

The chosen cost function is continuous for the state vector $\mathbf{x}$ as well as the command vector $\mathbf{u}$ and the matrices $\mathbf{Q}$ as well as $\mathbf{R}$ are chosen to be symmetric positive semi-definite to satisfy Assumptions 1, 3 and 5 from Section 3.2.1. The penalty matrix $\mathbf{P}_\mathrm{f}$ is calculated to stabilize the system with (3.59). Note that the

MPC theory, explained in Section 3.2, designed methods to steer the whole state vector **x** to the origin (zero), whereas the proposed method is designed to steer individual states (velocity and yaw angle) to zero.

4.3 Obstacles and Road Boundaries

To explain the design of the proposed constraints in this section, consider a scenario with two straight lanes and a static obstacle on the right lane with the width w_{obsr} and the length l_{obsr}. Further the relative position from the obstacle rear edge to the origin is x_{obsr} and y_{obsr}. All road participants like pedestrians, cyclists or vehicles are enframed by a rectangle.
The proposed planning and control method considers potential collision obstacles and lane boundary information to plan a collision-free trajectory during the maneuver without exceeding of road boundaries.
The planned trajectory is calculated in relative position to the ego vehicle's COG at current time step i = 0. Figure 4.2 illustrates the scenario with the ego vehicle and the obstacle at current time step i = 0 (solid lines) and the predicted ego vehicle for a time step *i* (dotted lines). The longitudinal and lateral position of the front left, front right, rear left and rear right corners of the ego vehicle are marked in the figure and can be denoted by $(x_{\text{fl}}, y_{\text{fl}})$, $(x_{\text{fr}}, y_{\text{fr}})$, $(x_{\text{rl}}, y_{\text{rl}})$ and $(x_{\text{rr}}, y_{\text{rr}})$. In this scenario the ego vehicle shall swerve to the left to avoid the collision. The evasion direction is predetermined by a higher order decision making module (e.g. [8]). Let B_{r} be defined as the intersection point of the right edge of the ego vehicle rectangle at time step i with the elongated rear edge of the obstacle vehicle.
The lateral position of the point B_{r} for the time step i, y_{Br}, is then calculated based on the lateral position y of the COG and the yaw angle φ at time step i in

$$y_{\text{Br}} = y - \frac{w}{2\cos\varphi} + \Delta x \tan\varphi \quad . \tag{4.2}$$

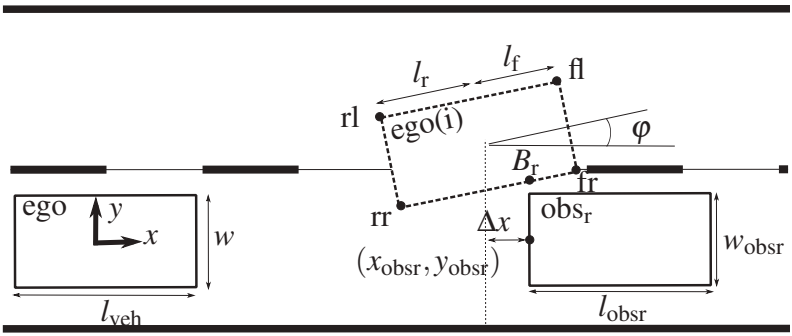

Figure 4.2: Illustration of collision avoidance constraints for an evasive collision avoidance maneuver to the left

The collision avoidance constraint can be expressed as

$$\begin{aligned} y_{\text{Br}} &\geq y_{\text{obsr}} + w_{\text{obsr}}/2 \\ \forall (x_{\text{fr}} > x_{\text{obsr}}) &\cap (x_{\text{rr}} < x_{\text{obsr}} + l_{\text{obsr}}) \end{aligned} \tag{4.3}$$

for an evasive maneuver to the left. In the equation above, the constraint is only active when the dimension of the vehicle overlaps with the dimension of the obstacle. The longitudinal positions x_{fr} and x_{rr} are calculated with

$$\begin{aligned} x_{\text{fr}} &= x + l_{\text{f,veh}} \cos(\varphi) + \frac{w}{2} \sin(\varphi) \quad \text{and} \\ x_{\text{rr}} &= x - l_{\text{r,veh}} \cos(\varphi) + \frac{w}{2} \sin(\varphi). \end{aligned} \tag{4.4}$$

Similarly the constraint for a collision avoidance maneuver to the right as shown in Figure 4.3 can be treated analogously with an obstacle obs_{l} with the width w_{obsl}, the length l_{obsl} as well as the the distances x_{obsl} and y_{obsl}.
The set for the vehicle dynamics states to ensure collision avoidance is given by

$$\begin{aligned} \mathbb{C} = \{\mathbf{x} \in \mathbb{R}^9 |\ & y_{\text{Br}} \geq y_{\text{obsr}} + w_{obsr}/2, \forall x \in \mathbb{X}_{\text{or}}, \\ & y_{\text{Bl}} \leq y_{\text{obsl}} - w_{\text{obsl}}/2, \forall x \in \mathbb{X}_{\text{ol}}\} \end{aligned} \tag{4.5}$$

$$
\begin{aligned}
\text{with} \quad & \mathbb{X}_{\text{or}} := \{x \in \mathbb{R} | (x_{\text{fr}} > x_{\text{obsr}}) \cap (x_{\text{rr}} < x_{\text{obsr}} + l_{\text{obsr}})\} \\
& \mathbb{X}_{\text{ol}} := \{x \in \mathbb{R} | (x_{\text{fl}} > x_{\text{obsl}}) \cap (x_{\text{rl}} < x_{\text{obsl}} + l_{\text{obsl}})\} \\
& y_{\text{Bl}} = y + \frac{w}{2\cos\varphi} + \Delta x \tan\varphi \\
& x_{\text{fl}} = x + l_{\text{f,veh}} \cos(\varphi) - \frac{w}{2}\sin(\varphi) \\
& x_{\text{rl}} = x - l_{\text{r,veh}} \cos(\varphi) - \frac{w}{2}\sin(\varphi).
\end{aligned}
$$

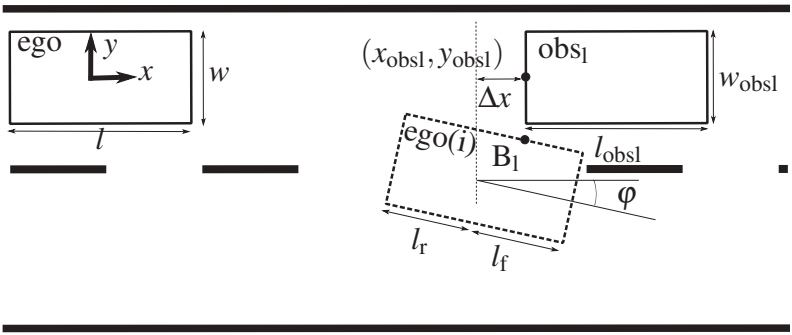

Figure 4.3: Illustration of collision avoidance constraints for an evasive collision avoidance maneuver to the right

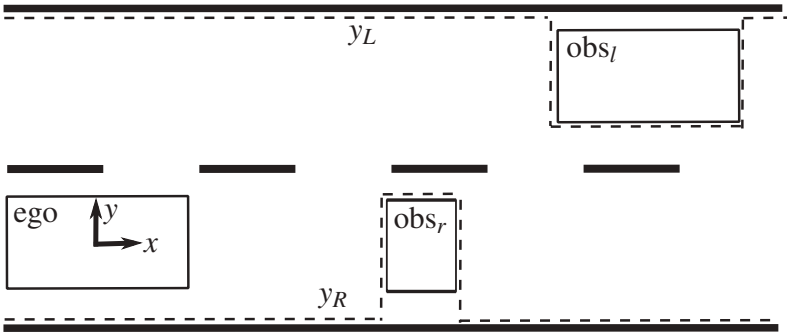

Figure 4.4: Illustration of boundary lines y_R and y_L to consider for road boundaries and restrictions due to obstacles

Furthermore, constraints for the planning method will be presented to consider position restrictions such as road boundaries and curb stones. Let the boundaries on the left and on the right side be given by y_{L} and y_{R} as shown in Figure 4.4.
To keep all corners of the vehicle within these boundaries, the following constraints shall be considered

$$\begin{aligned} \min(y_{\mathrm{fr}}, y_{\mathrm{rr}}) &\geq y_{\mathrm{R}}(x) \\ \max(y_{\mathrm{fl}}, y_{\mathrm{rl}}) &\leq y_{\mathrm{L}}(x) \\ \text{with } y_{\mathrm{fr}} &= y + l_{\mathrm{f,veh}} \sin(\varphi) - \frac{w}{2}\cos(\varphi) \\ y_{\mathrm{rr}} &= y - l_{\mathrm{f,veh}} \sin(\varphi) - \frac{w}{2}\cos(\varphi) \\ y_{\mathrm{fl}} &= y + l_{\mathrm{f,veh}} \sin(\varphi) + \frac{w}{2}\cos(\varphi) \\ y_{\mathrm{rl}} &= y - l_{\mathrm{r,veh}} \sin(\varphi) + \frac{w}{2}\cos(\varphi) \end{aligned} \tag{4.6}$$

The corresponding set to consider the road boundaries is defined in

$$\mathbb{L} = \{\mathbf{x} \in \mathbb{R}^9 |\ \min(y_{\mathrm{fr}}, y_{\mathrm{rr}}) \geq y_{\mathrm{R}}(x),\ \max(y_{\mathrm{fl}}, y_{\mathrm{rl}}) \leq y_{\mathrm{L}}(x)\}. \tag{4.7}$$

The constraints in the set $\mathbb{C}$ and $\mathbb{L}$ are closed such that Assumption 2 is satisfied.

4.4 Terminal Collision Avoidance

One aspect that has not been adressed in prior works, according to the knowledge of the author, is the guarantee of collision avoidance for obstacles outside of the prediction horizon. In practice, the length of the prediction horizon and the number of prediction steps are selected as a trade off between high coverage of relevant obstacles and low computational burden of the resulting optimization problem. Problematic scenarios can be found when the prediction horizon is not long enough by design to consider all relevant obstacles that have been detected. To enable planning of collision-free trajectories in these scenarios,

terminal collision avoidance constraint (TCA) introduced in this section can be exploited. The terminal collision avoidance constraints are implemented on the terminal prediction step of the prediction horizon to enable planning of safe trajectories with a simple point mass model [67].
First consider a scenario as illustrated in Figure 4.5 where the ego vehicle needs to perform an evasive maneuver to avoid collision with obs_r followed by a braking maneuver in order to avoid collision with vehicle obstacles in the traffic jam at a distance of x_{Tjam}.

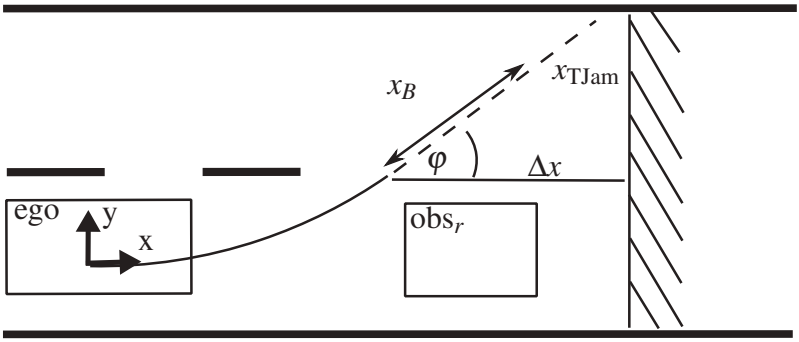

Figure 4.5: Illustration of terminal collision avoidance constraint for a braking maneuver

Figure 4.5 illustrates the predicted trajectory to avoid collision with the first obstacle, but due to the length of the prediction horizon and the chosen control parameters it may not be able to avoid collision with vehicle obstacles in the traffic jam. The terminal collision avoidance constraint in this section requires the vehicle dynamics state at the last prediction step to comply with collision avoidance requirements based on a point mass model.
Let the equation for the maneuver distance of a braking maneuver from [67] be given by

$$x_\text{B} = -\frac{v_0^2}{2a_\text{x}} \tag{4.8}$$

where v_0 is the initial velocity and a_x is the required longitudinal acceleration value, then the terminal collision avoidance constraint in this section requires the vehicle dynamics state for the last prediction step to satisfy

$$\begin{aligned} &\Delta x(N)/\cos\varphi(N) \geq x_\mathrm{B}(N) \\ \equiv\ &(x_\mathrm{Tjam} - x(N)) \geq \frac{v(N)^2\cos(\varphi(N))}{2a_\mathrm{x}(N)}. \end{aligned} \tag{4.9}$$

where $x(N), v(N), \varphi(N)$ and $a_\mathrm{x}(N)$ correspond to predicted vehicle dynamics states and $\Delta x(N) = x_\mathrm{Tjam} - x(N)$ is the remaining longitudinal distance to the traffic jam at the last prediction step of the prediction horizon N. To avoid division by zero in the equation for the optimization problem, $a_\mathrm{x}(N)$ is substituted by $\min(a_\mathrm{x}, -0.1)$ which has marginal influence on the overall performance.
Further, consider Scenario 2 with two obstacles in Figure 4.6 and assume again the short prediction horizon for this scenario by design. The algorithm is not able to consider an avoidance maneuver with the second obstacle already at maneuver start without any additional constraints.

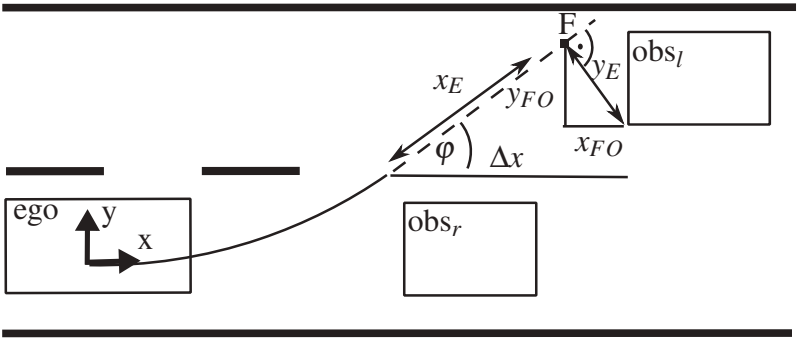

Figure 4.6: Illustration of terminal collision avoidance constraint for an evasion maneuver

Subsequently the terminal collision avoidance constraint for evasive maneuver will be developed.

Let the required maneuver distance for an evasive maneuver according to [67] be given as

$$x_{\mathrm{E}} = v_0 \sqrt{\frac{2y_{\mathrm{E}}}{a_{\mathrm{y}}}} \tag{4.10}$$

where y_E is the lateral maneuver distance and a_{y} is the assumed lateral acceleration, then the terminal collision avoidance constraint for evasive maneuver requires the maneuver distance to be smaller than the available longitudinal distance in the equation

$$\begin{aligned} & \Delta x(N) \geq x_{\mathrm{E}}(N) \\ \equiv\ & (x_{\mathrm{obsl}} - x(N)) \geq v(N) \sqrt{\frac{2y_{\mathrm{E}}(N)}{a_{\mathrm{y}}(N))}} \ . \end{aligned} \tag{4.11}$$

The required lateral maneuver distance in the orientation of the last prediction step y_{E} illustrated in Figure 4.6 is calculated with

$$y_{\mathrm{E}} = \sqrt{x_{\mathrm{FO}}^2 + y_{\mathrm{FO}}^2} \tag{4.12}$$

$$x_{\mathrm{FO}} = x_{\mathrm{obsl}} - x_{\mathrm{F}} \tag{4.13}$$

$$y_{\mathrm{FO}} = y_{\mathrm{F}} - y_{obsl} - w_{\mathrm{obsl}}/2 \ . \tag{4.14}$$

Here point F is located on the straight line starting at the position of the last predicted time step N with the orientation of the corresponding yaw angle with the nearest distance to the critical corner G at obs_{l} (see Figure 4.6). The exact position can be determined by calculating the crossing point of the two lines

$$\begin{aligned} & y_1(x) = y(N) + \tan(\varphi(N))(x - x(N)) \quad \text{and} \\ & y_2(x) = y_{\mathrm{obsl}} - w_{\mathrm{obsl}}/2 - \tan(\varphi(N))(x - x_{\mathrm{obsl}}). \end{aligned} \tag{4.15}$$

The coordinates of the point F can then be calculated by

$$y_F = (y(N) + \tan(\varphi(N))(x_{obsl} - x(N)) + y_{obsl} - w_{obsl}/2)/2$$
$$x_F = (y_F - y(N))/\tan\varphi(N) + x(N)$$

Similarly to the terminal constraint for a subsequent braking maneuver, $a_y(N)$ is substituted by $\min(a_y(N), -0.1)$ in (4.11) to avoid division by zero in. The sets of the terminal collision avoidance constraints for a braking and an evasive maneuver are

$$\mathbb{G}_B := \{\mathbf{x} \in \mathbb{R}^9 | (x_{obsl} - x(N,k)) \geq \frac{v(N)^2 \cos^2(\varphi(N,k))}{2a_x(N,k)}\} \tag{4.16}$$

and

$$\mathbb{G}_E := \{\mathbf{x} \in \mathbb{R}^9 | (x_{obsl} - x(N)) \geq v(N)\sqrt{\frac{2y_E(N)}{a_y(N))}}\}. \tag{4.17}$$

4.5 Soft Constraints

The introduction of soft constraints using slack variables is important for the practical application of the method with many numerical solvers. To ensure satisfaction of the collision avoidance constraints with numerical smoothness of the results according to [19], slack variables s_{obs} are added to the sets in $\mathbb{C}, \mathbb{L}, \mathbb{G}_B$ and $\mathbb{G}_E$ such that the modified sets are

$$\begin{aligned}\mathbb{C} := \{\mathbf{x} \in \mathbb{R}^9 |\ & y_{Br} + s_{obs} \geq y_{obsr} + w_{obsr}/2, \forall x \in \mathbb{X}_{or}, \\ & y_{Bl} + w_{obsl}/2 \leq y_{obsl} + s_{obs}, \forall x \in \mathbb{X}_{ol}\}, \\ \mathbb{L} := \{\mathbf{x} \in \mathbb{R}^9 \mid & \min(y_{fr}, y_{rr}) + s_{obs} \geq y_R(x)\ , \\ & \max(y_{fl}, y_{rl}) \leq y_L(x) + s_{obs}\},\end{aligned}$$

$$\mathbb{G}_{\mathrm{B}} := \{\mathbf{x} \in \mathbb{R}^9 | (x_{\mathrm{tjam}} - x(N,k)) + s_{\mathrm{obs}} \geq \frac{v(N)^2 \cos^2(\varphi(N,k))}{2a_{\mathrm{x}}(N,k)}\} \text{ and}$$

$$\mathbb{G}_{\mathrm{E}} := \{\mathbf{x} \in \mathbb{R}^9 | (x_{\mathrm{obsl}} - x(N)) + s_{\mathrm{obs}} \geq v(N)\sqrt{\frac{2y_{\mathrm{E}}(N)}{a_{\mathrm{y}}(N)}}\} .$$

To minimize these slack values, the variables are considered by a modified cost function J_{s} and the cost function J defined in (4.1) in Section 4.2.

$$J_{\mathrm{s}} = J + Q_{\mathrm{s}} s_{\mathrm{obs}}(i)^2 \tag{4.18}$$

The introduction of soft constraints may endanger the calculation of collision-free trajectories. The already introduced safety margins help to cope with minor constraint violations. The safety integrity with the soft constraints can be further ensured by an additional module double checking the trajectory after the optimization step prior to any activation of the planned maneuver.

4.6 MPC Formulation

The overall nonlinear optimization problem in this chapter is a nonconvex optimization problem and is formulated below.

$$\begin{aligned}
\min_{\mathbf{u}} \; & J_{\mathrm{s}} = \sum_{i=1}^{N} \mathbf{x}(i,k)^T \mathbf{Q}\mathbf{x}(i,k) + \mathbf{u}(i,k)^T \mathbf{R}\mathbf{u}(i,k) + \cdots \\
& \qquad [\mathbf{x}(N,k)^T \; 1]\mathbf{P}_{\mathrm{f}}[\mathbf{x}^T(N,k)1]^T + Q_{\mathrm{s}} s_{\mathrm{obs}}(i,k)^2 \\
\text{s.t.} \; & \mathbf{x}(i+1,k) = \mathbf{x}(i,k) + t_{\mathrm{pred}}\mathbf{f}(\mathbf{x}(i,k), \mathbf{u}(i,k)) \\
& \mathbf{u}(i,k) \in \mathbb{U} \\
& \mathbf{x}(i,k) \in \mathbb{X} \\
& \mathbb{X} = \mathbb{S} \cap \mathbb{V} \cap \mathbb{C} \cap \mathbb{L} \;\; i = 1, \cdots, N \\
& \mathbf{k}\mathbf{x}(N,k) \in \mathbb{U} \\
& \mathbf{x}(N,k) \in \mathbb{G}_{B/E} \;\; \text{if TCA is applied}
\end{aligned} \tag{4.19}$$

Here t_{pred} is the discretization time between predicted time steps and $\mathbb{V}$ is the set described in

$$\mathbb{V} = \{\mathbf{x} \in \mathbb{R}^9 \mid v \geq 0,\ \sqrt{{a_{\text{x}}}^2 + a_{\text{y}}^2} \leq \mu g,\ a_{\text{x}} \leq 0\} \ . \tag{4.20}$$

The set $\mathbb{V}$ is closed, such that Assumption 2 is satisfied.

4.7 Simulation Results

After explaining the modules of the integrated trajectory planning and vehicle dynamics control method, the performance of the proposed method will be presented in a simulation environment with the vehicle dynamics model as presented in Section 3.1. The integrated trajectory planning and vehicle dynamics control method has been implemented in MATLAB Simulink on a computer with 8 GB RAM and Intel CORE i5 processor with 2.90 GHz.
First this section will present the considered metrics and scenarios to evaluate the integrated planning and control method for collision avoidance maneuvers. Finally the performance of the proposed method on the predefined metrics and scnearios will be shown in the simulation environment.

4.7.1 Metrics

The metrics defined in this section are derived from the design goals of Section 4.1. The first metric relates to the amount of **velocity reduction** at the longitudinal position of the potential collision. The relative velocity reduction is calculated by

$$\Delta v_{\text{red}} = \frac{v_0 - v(t_{\text{c}})}{v_0} \ . \tag{4.21}$$

Here v_0 is the initial velocity of the ego vehicle at the start of the manuver intervention, whereas $v(t_{\text{c}})$ is the velocity at the potential collision time - the point in time when the front edge of the vehicle bypasses the rear edge of the obstacle.

The second metric considers the **final yaw angle** φ_{fnl} of the vehicle at the end of the maneuver. According to Section 4.1, the vehicle shall reorientate the vehicle at the end of an ideal maneuver.
The third metric is the **computation time** t_{cmp} of the implemented algorithm per control step. The method presented in this chapter does not focus on the reduction of computation time. Therefore the computation time metric will not be used for evaluation in this chapter but shall be calculated prior to further modification in Chapter 5.

4.7.2 Scenarios

In this section typical scenarios in urban environments are presented to evaluate the performance of the proposed planning and control concept. The scenarios consider a straight road with two lanes. The overall width is 7 m with 3.5 m for each lane. All road participants like pedestrians, cyclists or vehicles are enframed by a rectangle. The ego vehicle with the width $w = 2$ m and the length $l_{\mathrm{veh}} = 3.5$ m moves with the velocity $v_0 = 50$ km/h on the right lane. In the presented scenarios, the collision avoidance maneuvers will not start immediately but triggered after $x = 4$ m which corresponds to the latest point in time.

Scenario 1: Single Obstacle
In Scenario 1, the static obstacle with the width $w_{\mathrm{obsr}} = 2$ m and the length $l_{\mathrm{obsr}} = 3.5$ m, which represent a static vehicle, is located on the center of the right lane. The corresponding scenario is given in Figure 4.7.
Let the origin of the reference system be located at the COG of the ego vehicle, then the relative position of the obstacle rear edge to the origin shall be ($x_{\mathrm{obsr}} = 20$ m, $y_{\mathrm{obsr}} = 0$ m).

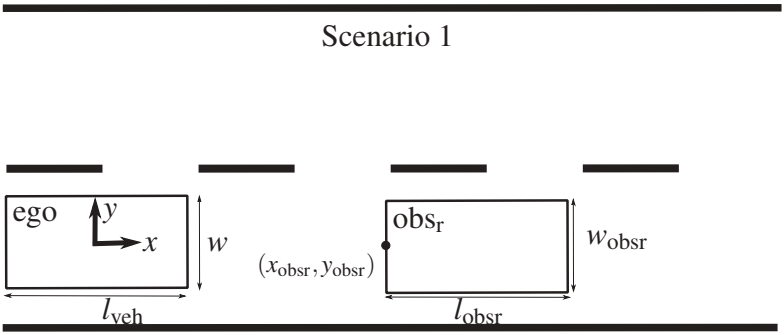

Figure 4.7: Scenario 1 with one static obstacle

Scenario 2: Multiple Obstacles

The second use case considers multiple obstacles representing another typical situation in urban environments. The first obstacle with the width $w_{obsr} = 2$ m and the length $l_{obsr} = 1$ m, representing a pedestrian or a cyclist, is located on the center of the right lane similarly to Scenario 1. The second obstacle (obs_l) is located on the left lane with the relative distances $x_{obsl} = 24$ m and $y_{obsl} = 4.5$ m to the COG of the ego vehicle and with the width $w_{obsl} = 2$ m and length $l_{obsl} = 3.5$ m. The gap between both obstacles is chosen such that it can be passed through by the ego vehicle without a collision. The scenario is shown in Figure 4.8.

Scenario 3: Single Obstacle with Traffic Jam

The last scenario shown in Figure 4.9 considers a single obstacle obs_r, with the width $w_{obsr} = 2$ m and the length $l_{obsr} = 3.5$ m on the right lane, and a traffic jam at the distance $x_{TJam} = 28$ m illustrated by a wall, such that the system needs to apply a braking maneuver after the first evasive maneuver in order to avoid a collision.

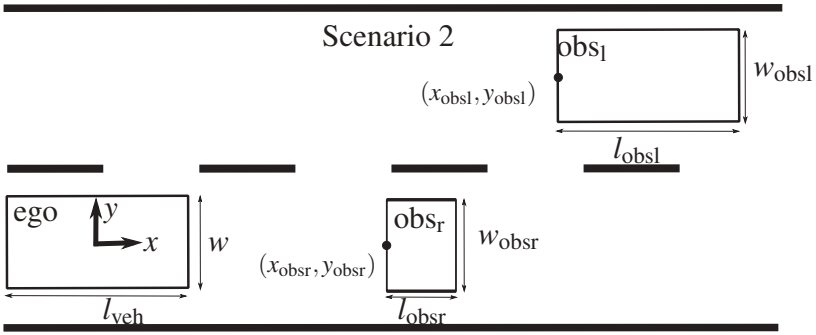

Figure 4.8: Scenario 2 with two static obstacles on both lanes

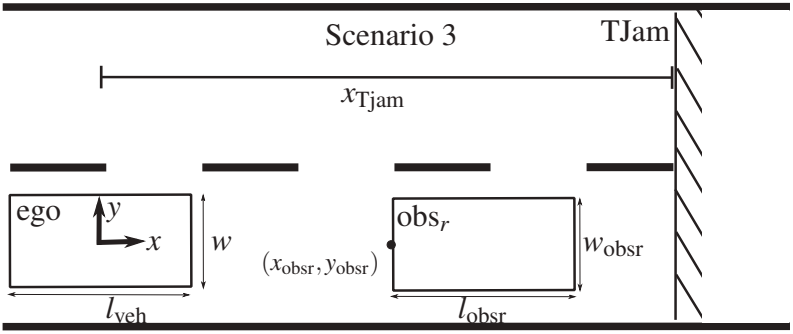

Figure 4.9: Scenario 3 with single obstacle and end of a traffic jam / wall

4.7.3 Typical Scenarios

The performance of the proposed method for the Scenarios 1 and 2 (Section 4.7.2) shall be demonstrated in this section.

The focus of this section is to discuss the maneuver performance with three different parameter setups for the proposed method. Parameter setup 1 for the proposed nonlinear MPC is shown in Table 4.1.

Table 4.1: Parameter setup 1 for the Nonlinear Integrated Planning and Control Method

Parameter	Symbol	Value	Unit
Prediction horizon length	N	15	(none)
Prediction horizon step size	dt_{pred}	0.14	s
Controller time step size	dt_{ctrl}	0.03	s
Penalty of slack variable	q_{s}	$3{\cdot}10^{6}$	$1/\text{m}^2$
Penalty of yaw angle	q_{φ}	$3{\cdot}10^{3}$	$1/\text{rad}^2$
Penalty of velocity	q_{v}	10	s^2/m^2
Penalty of steering torque command	r_{T}	10^{-1}	$1/\text{Nm}^2$
Penalty of deceleration command	r_{a_x}	10^{-1}	s^4/m^2
Limit for steering system	T_{max}	50	Nm
Limit for braking system	$a_{\text{x,cmd,max}}$	-9.81	m/s^2

Figure 4.10 shows the result for the single obstacle scenario. In the top picture, the driven trajectories of the vehicle with the COG (solid lines) and its four corners (front right, front left, rear right and rear left in dashed lines) are illustrated in the plane, spanned by the axes for the lateral and longitudinal position. The figure shows how the vehicle avoids a collision with the obstacle and brakes the vehicle to a standstill.

At maneuver start ①, the algorithm commands the maximum steering torque and maximum deceleration to avoid the collision. This may seem to violate the restrictions of the friction circle but due to the time delay characteristic of the vehicle dynamics model the friction limits can not be reached instantly. Subsequently at ②, the algorithm introduces the counter steering phase. When the ego vehicle with its front edge is passing the rear edge of the obstacle ③, the algorithm again commands a high steering torque value in the stabilization phase and prevents further rotation towards the obstacle. At ④, the algorithm stops the steering and the braking intervention and due to the characteristic of the longitudinal model the vehicle is decelerated to a standstill.

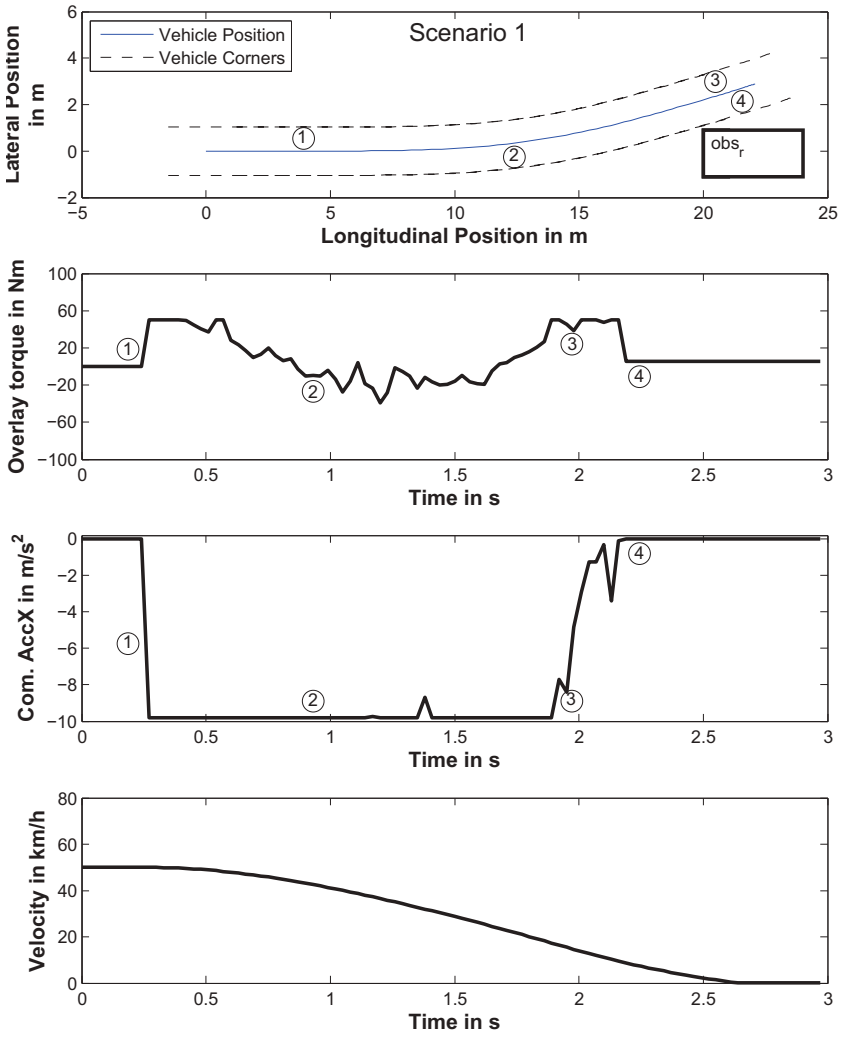

Figure 4.10: Simulation results of the nonlinear integrated trajectory planning and vehicle dynamics control method with parameter setup 1 in Scenario 1

To explain the main influence of different parameters on the maneuver performance, parameter setup 2 in Table 4.2 will be used. The parameter setup 2 is designed with a higher penalty on the yaw angle and a lower penalty on the velocity, which represents higher emphasis on the reorientation of the vehicle.

Table 4.2: Parameter setup 2 for Nonlinear Integrated Planning and Control Method

Parameter	Symbol	Value	Unit
Prediction horizon length	N	15	(none)
Prediction horizon step size	dt_{pred}	0.14	s
Controller time step size	dt_{ctrl}	0.03	s
Penalty of slack variable	q_{s}	$3{\cdot}10^{7}$	$1/\text{m}^2$
Penalty of yaw angle	q_{φ}	10^{4}	$1/\text{rad}^2$
Penalty of velocity	q_{v}	1	s^2/m^2
Penalty of steering torque command	r_{T}	10^{-1}	$1/\text{Nm}^2$
Penalty of deceleration command	r_{a_x}	10^{-1}	s^4/m^2
Limit of steering system	T_{max}	50	Nm
Limit of braking system	$a_{\text{x,cmd,max}}$	-9.81	m/s^2

Figure 4.11 shows the performance of the algorithm in the same scenario. Similarly to Figure 4.10 the maneuver is characterized by several time marks. A difference in the control characteristic can be found in the counter steering phase, between ② and ③, where the deceleration command is reduced to zero for a longer time period. This reduction of deceleration command ensures faster yaw angle reduction and avoids standstill of the vehicle without reorientation during this time period which can be explained by the high penalty on the yaw angle and the lower penalty on the velocity. The figure illustrates that zero velocity and yaw angle at the end of the maneuver at ④ is achieved.

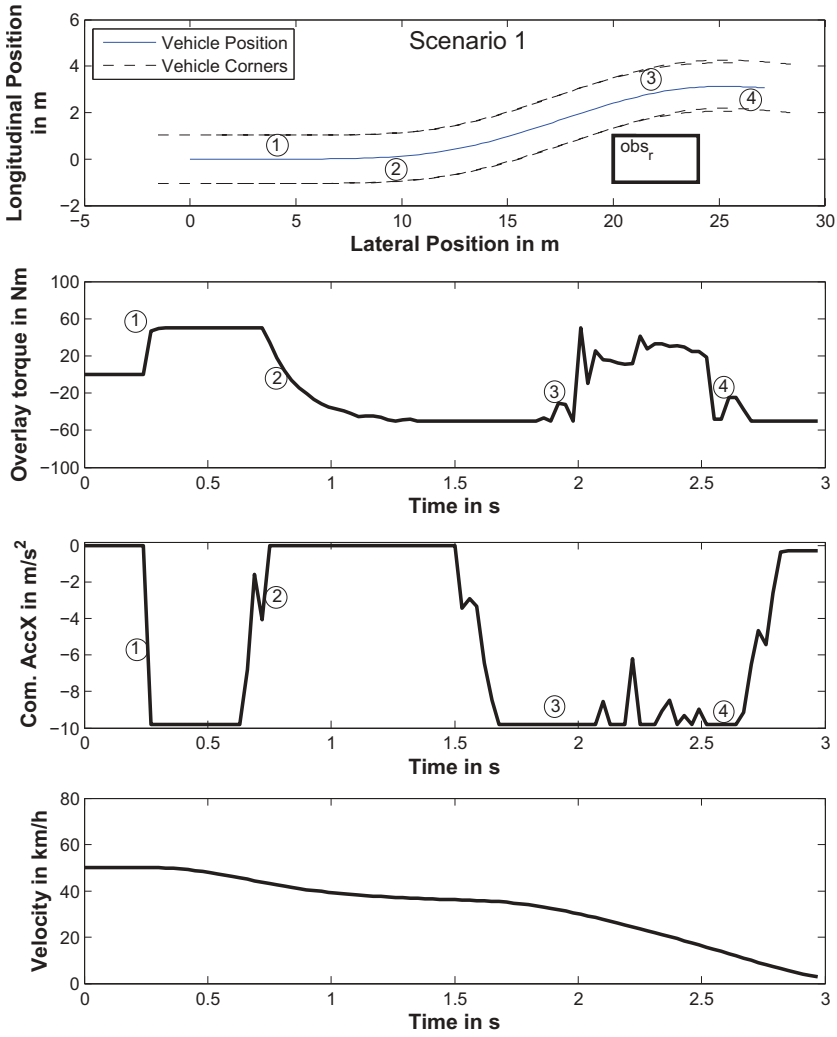

Figure 4.11: Simulation results of the nonlinear integrated trajectory planning and vehicle dynamics control method with parameter setup 2 in Scenario 1

In a last variation, the parameter setup 3 in Table 4.3 is used. This setup is very different compared to the setups 1 and 2. The step size of the prediction horizon is reduced by half, such that the algorithm has a shorter prediction horizon. The sampling time of the algorithm is increased to 100 ms which corresponds to a lower sampling frequency. The penalty on the velocity is decreased to zero and the penalty of both the command values are increased to high values.
Figure 4.12 shows the performance of the method with the parameter setup 3. Similarly to the previous figures, high steering torque and deceleration commands are applied at ①. However, the high command values are reduced after a short time and the counter steering phase is introduced at ② with a small deceleration command which can be attributed to high penalty on the command values. After passing the obstacle edge the command values are reduced continuously to zero.

Table 4.3: Parameter setup 3 for the Nonlinear Integrated Planning and Control Method

Parameter	Symbol	Value	Unit
Prediction horizon length	N	15	(none)
Prediction horizon step size	dt_{pred}	0.07	s
Controller time step size	dt_{ctrl}	0.1	s
Penalty of slack variable	q_{s}	$3{\cdot}10^{7}$	$1/\text{m}^2$
Penalty of yaw angle	q_{φ}	10^{4}	$1/\text{rad}^2$
Penalty of velocity	q_{v}	0	s^2/m^2
Penalty of steering torque command	r_{T}	10^{0}	$1/\text{Nm}^2$
Penalty of deceleration command	r_{a_x}	10^{1}	s^4/m^2
Limit of steering system	T_{max}	50	Nm
Limit of braking system	$a_{\text{x,cmd,max}}$	-9.81	m/s^2

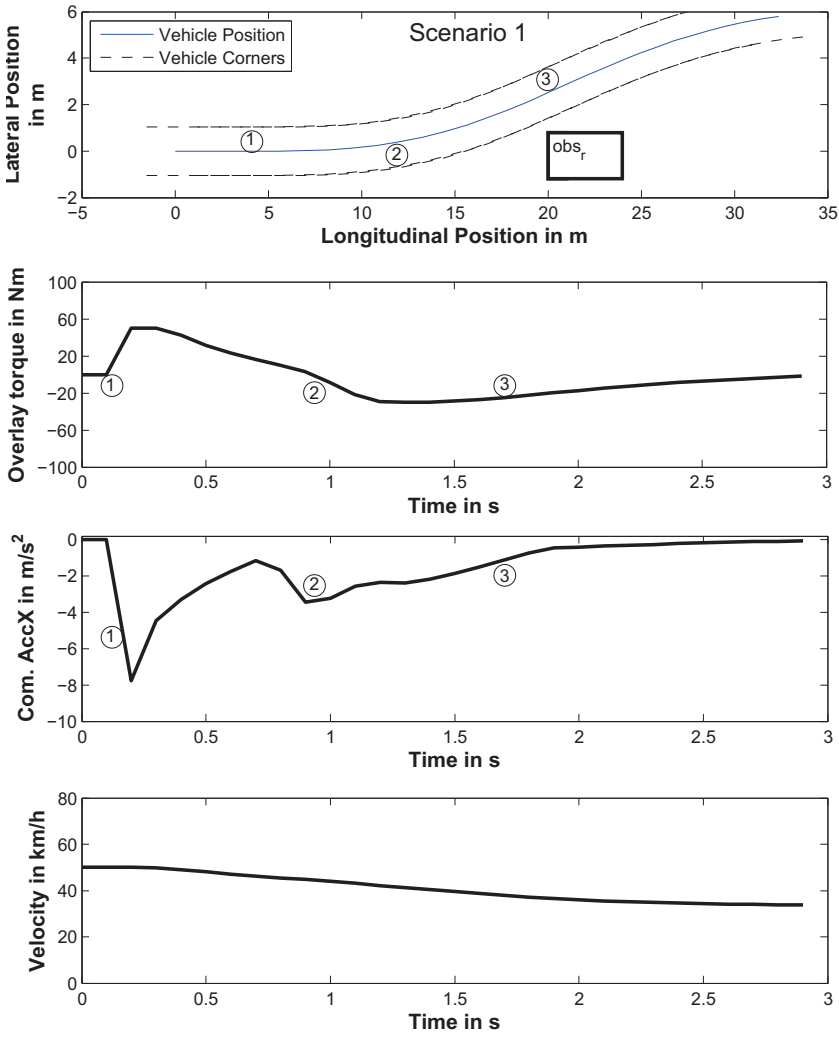

Figure 4.12: Simulation results of the nonlinear integrated trajectory planning and vehicle dynamics control method with parameter setup 3 in Scenario 1

The figure demonstrates that the vehicle avoids the collision with the obstacle and has a velocity of 35 km/h at the end of the maneuver. Overall, the algorithm applied low command values during the maneuver so that it does not brake the velocity to a standstill and reorientate the vehicle to zero yaw angle. This performance can as well be explained by high penalties on the command steering torque and deceleration command as well as zero penalty on the velocity in parameter setup 3.

The results with the three different parameter setups in Scenario 1 illustrate the influence of the key parameters on the maneuver performance. With parameter setup 1, the evasive collision avoidance maneuver applies nearly full braking throughout the evasive maneuver. The vehicle avoids a collision with the obstacle but does not reorientate the vehicle to a yaw angle of zero degree. By choosing a higher yaw angle penalty and lower velocity penalty (parameter setup 2), the vehicle is reorientated at the end of the maneuver but achieves slower reduction of the velocity during the evasion.

Higher penalty values on the applied command values (parameter setup 3) lead to an avoidance of the collision with limited braking intervention and without full reorientation.

For the purpose of this thesis, parameter setup 1 is further used due to higher reduction of velocity during the evasive maneuver. After demonstrating the method in Scenario 1 with a single obstacle, Scenario 2 with two obstacles shall be considered to further investigate the performance. In Figure 4.13 the results of the method with parameter setup 1 on Scenario 2 is shown.

Compared to the performance in Scenario 1 in Figure 4.10, the performance in the second scenario is characterized by a longer counter steering phase to avoid collision with the second obstacle. The braking characteristic is comparable to Scenario 1. The figure shows a peak reduction in deceleration command in the middle of the maneuver which helps the vehicle to achieve faster reorientation in a short time.

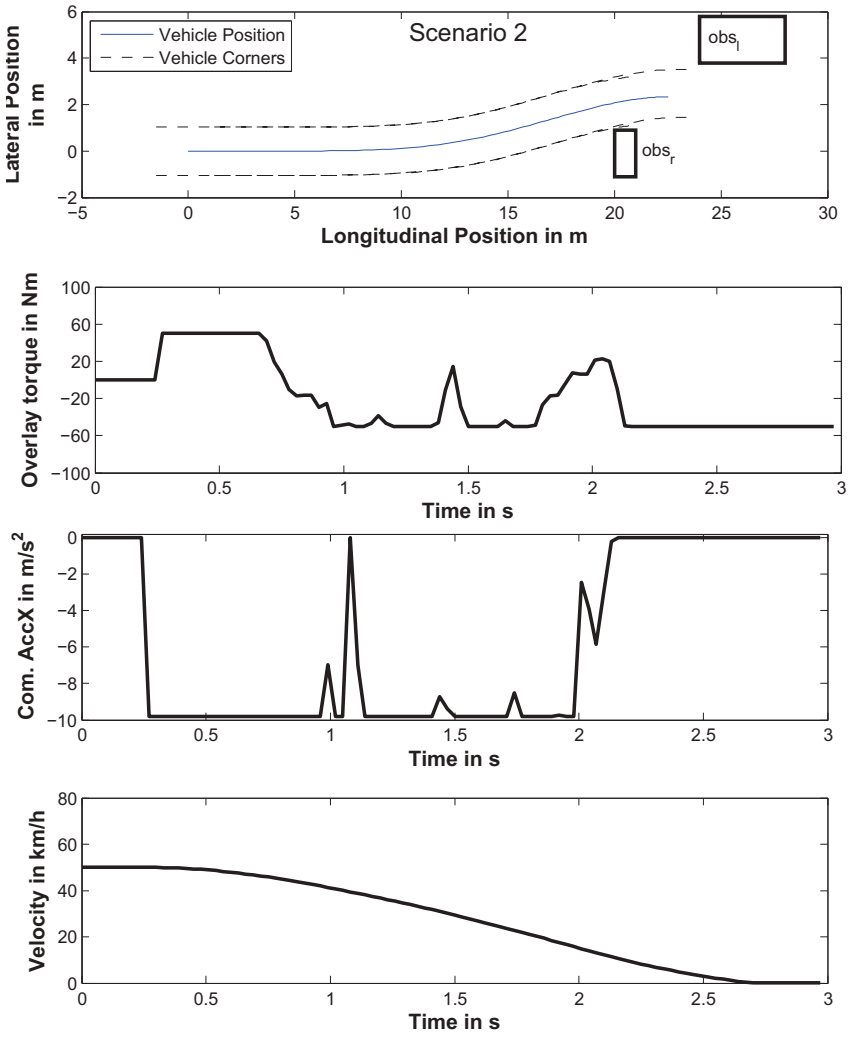

Figure 4.13: Simulation results of the nonlinear integrated trajectory planning and vehicle dynamics control method with parameter setup 1 in Scenario 2

4.7.4 Terminal Collision Avoidance

The terminal collision avoidance constraint introduced in Section 4.4 shall lead to trajectories avoiding a collision with obstacles outside of the prediction horizon.

In the first step of this section, the integrated method is applied without the terminal collision avoidance constraint in Scenario 2 with two obstacles while reusing parameter setup 3 (Table 4.3). The result is shown in Figure 4.14, where the ego vehicle drives around the first obstacle, but cannot avoid collision with the second obstacle, because the second obstacle is being considered in the planning horizon too late.

In a second step, the terminal collision avoidance constraint for a subsequent evasive maneuver shall be implemented and the method applied to Scenario 2 with the same parameter setup. The result in Figure 4.15 shows that collision with the obstacles has been successfully avoided by strong braking and steering at maneuver start followed by strong counter steering. It should be emphasized that this result could be achieved without extra tuning of the parameters.

In the third and final step, the terminal collision avoidance constraint for a braking maneuver in (4.16) can even be deployed to ensure collision avoidance in Scenario 3, which requires braking in front of a traffic jam as shown in Figure 4.16. This is achieved by considering the traffic jam from the beginning of the maneuver through the terminal collision avoidance constraint.

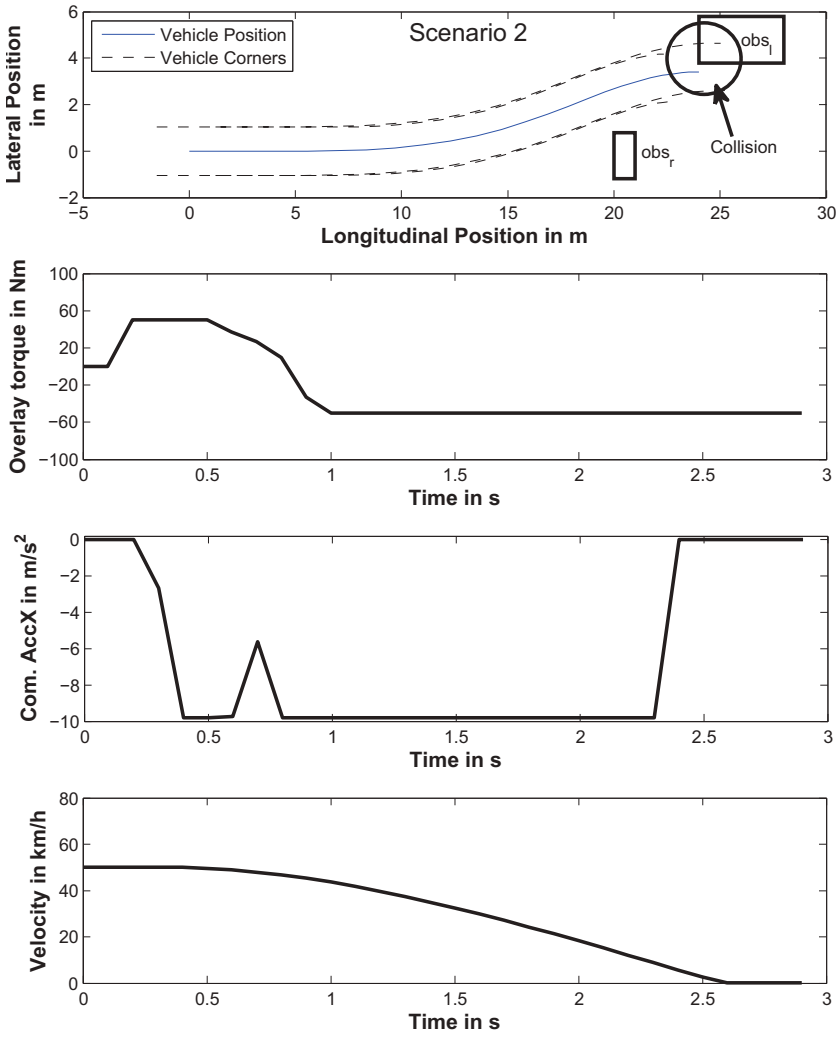

Figure 4.14: Simulation results of the nonlinear integrated trajectory planning and vehicle dynamics control method with parameter setup 3 in Scenario 2 without terminal collision avoidance constraint

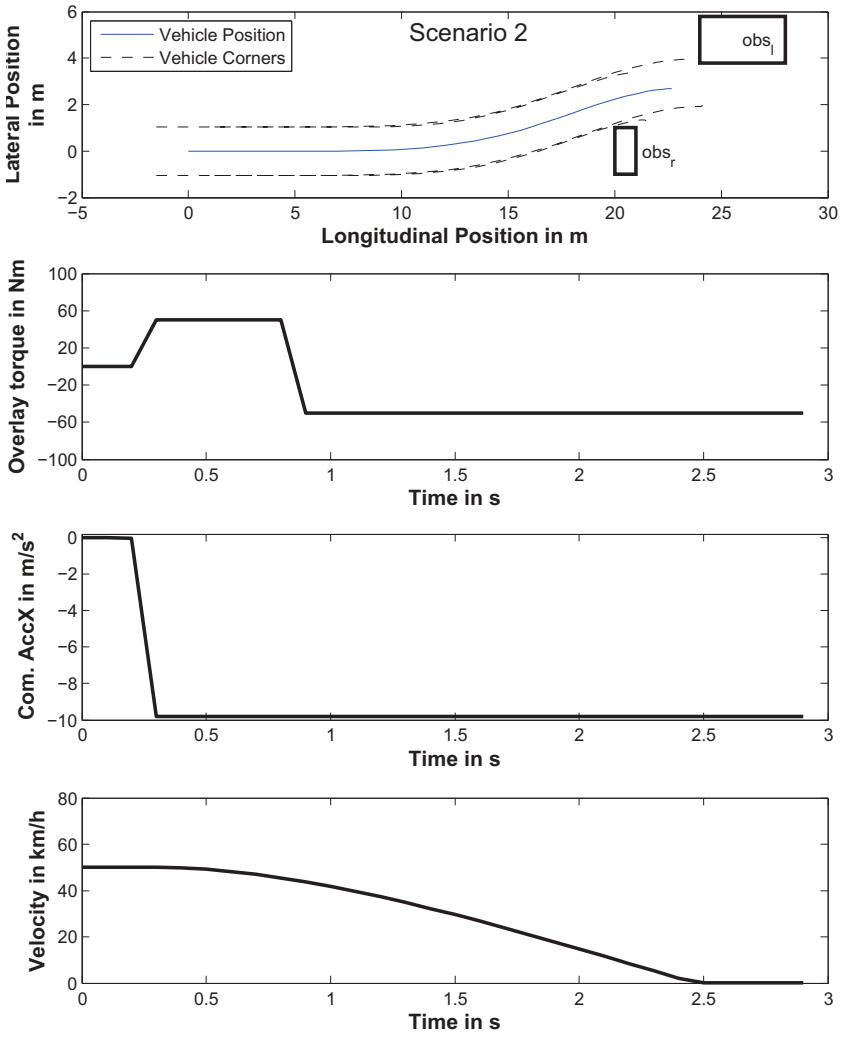

Figure 4.15: Simulation results of the nonlinear integrated trajectory planning and vehicle dynamics control method with parameter setup 3 in Scenario 2 with terminal collision avoidance constraint

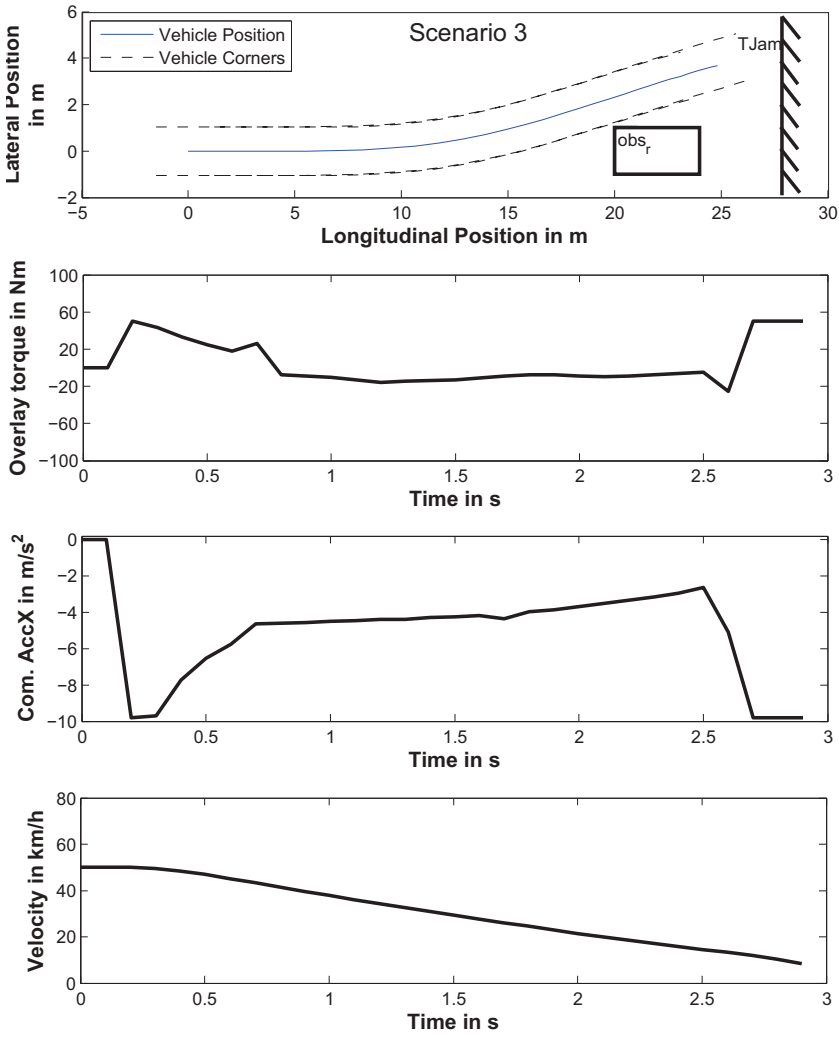

Figure 4.16: Simulation results of the nonlinear integrated trajectory planning and vehicle dynamics control method with parameter setup 3 in Scenario 3 with terminal collision avoidance constraint

4.8 Discussion

The integrated planning and control method considers a combined vehicle dynamics model and avoids collision by considering any obstacles as well as road information. The terminal collision avoidance constraint enables consideration of obstacles outside of the prediction horizon. The performance of the method on all scenarios has been discussed in Section 4.7. Table 4.4 shows the metric values introduced in Section 4.7.1, the relative velocity reduction at potential crash on the first obstacle obs_r and the final yaw angle, for the proposed method applied to Scenario 1 and 2 with parameter setup 1. The method successfully avoided the collision with the obstacles while reducing both the velocity and the yaw angle during the maneuver.

Table 4.4: Metric values of Nonlinear Integrated Planning and Control Method for typical scenarios in simulation

Scenarios	Velocity Reduction Δv_red	Final Yaw Angle φ_fnl	Computation Time t_cmp
Scenario 1	44.2 %	33 °	10 s - 15 s
Scenario 2	44.4 %	6 °	10 s - 15 s

The metric values of the proposed method and of the classical trajectory tracking method from Section 3.3 for Scenario 1 are shown in Table 4.5. The table demonstrates that the nonlinear integrated planning and control method achieves a higher performance level in terms of velocity reduction, but lower performance level for the final yaw angle in Scenario 1 compared to the classical concept. The performance of the integrated method is strongly influenced by the selection of the parameter setup as shown in section 4.7.3 and has been selected to deliever a maneuver performance with high velocity reduction in this thesis.

Table 4.5: Metric values of planning and control concepts for Scenario 1 in simulation

Metrics/ Requirements	Classical Tracking	Nonlinear Integrated
Velocity Reduction Δv_{red}	35 %	44.2 %
Final Yaw Angle φ_{fnl}	0 °	33 °
Computation Time t_{cmp}	0.006 s - 0.01 s	10 s - 15 s
Environmental Information	-	+
Tuning Effort	-	+

Furthermore, there are several key advantages of the proposed integrated planning and control concept compared to the classical control concept. First, the planning module is flexible and can adapt to scenarios with multiple obstacle and even newly detected obstacles to find a collision-free trajectory. Next, the terminal collision avoidance constraints enable planning of collision-free trajectories even with parameters not being tuned to the specific scenario and with obstacles outside the prediction horizon. Finally, the integrated concept reduces tuning and adaptation efforts of the trajectory planning module to the performance of the control module.

Challenges of the nonlinear integrated planning and control method are numerical weaknesses, such as convexity problems and problems at local minima, as well as the computation time. Due to the high computational burden required to solve the optimization problem, the method cannot be applied in real time on a test vehicle. In Chapter 5, these challenge will be addressed by suitable modifications of the proposed method.

5 Fast Integrated Planning and Control

The nonlinear integrated trajectory planning and vehicle dynamics control method presented in Chapter 4 achieves the desired goal of collision avoidance using nonlinear constraints to consider obstacles and a vehicle dynamics model for combined longitudinal and lateral dynamics in the simulative environment. As already mentioned before, a big weakness of the method is the high computational complexity which prevents its application in a real vehicle. This chapter addresses this weakness by exploiting linearization techniques and reformulating the nonlinear optimization problem into efficient linear optimization problems.

The structure of this enhanced method, to be called fast integrated planning and control method, is illustrated in Figure 5.1. The main difference to the structure in Chapter 4 is the linearization of all nonlinear constraints using the successive linearization technique. This technique and its application in this thesis will be explained in detail in Section 5.1. To compensate for linearization errors and uncertainties, a robust tube based approach is exploited to guarantee stability and constraint satisfaction in Section 5.2. The resulting MPC formulation is presented in Section 5.3. Finally, Section 5.4 shall demonstrate the performance of the fast integrated method for predefined scenarios in a simulation environment and in test drives with a real vehicle.

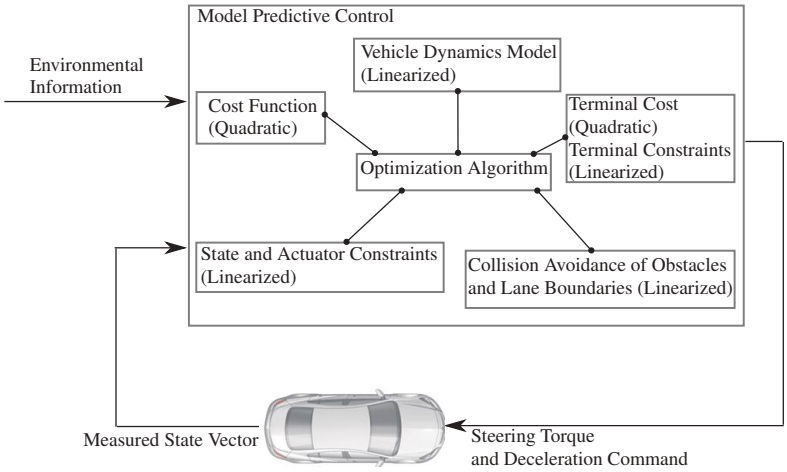

Figure 5.1: MPC structure of Fast Integrated Planning and Control Method

5.1 Successive linearization of nonlinear constraints

The successive linearization technique transforms nonlinear constraints into linear time varying constraints by linearizing nonlinearities around predicted operation points from the previous control step. It is a promising method for this task, allowing the use of efficient solvers [13][14][69][74].

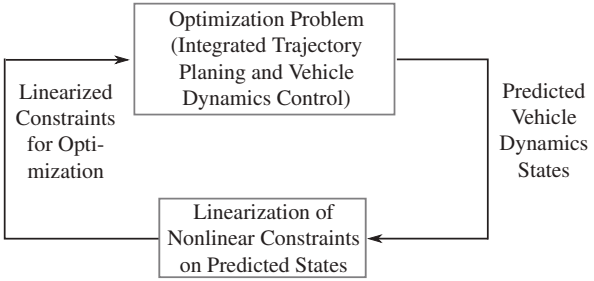

Figure 5.2: Principle of Successive Linerization

The principle of successive linearization in optimization problems is illustrated in Figure 5.2. The first module solves the optimization problem which may consist of the problem resulting from the integrated planning and control method. The outcomes are predicted vehicle dynamics states which can be used in a second step to linearize nonlinear constraints. With the linearized constraints, the optimization problem can be reformulated into an efficient convex optimization problem structure. Suitable solvers can then be applied to calculate the result. Successive linearization is based on valid prediction results in each consecutive control step and small control sampling time t_{ctrl}, so that consecutive predictions have little deviations. For the first control step, an appropriate trajectory must be chosen as base for the linearization of the nonlinear equations.
Several nonlinear constraints have been introduced for the nonlinear integrated planning and control method. The nonlinear vehicle dynamics model for combined lateral and longitudinal dynamics, with a single track model for the lateral dynamics and a PT1 characteristic for the longitudinal dynamics has been presented in Section 3.1.3. The nonlinear equation for the acceleration circle represents the maximum transferable forces of the tire according to the friction circle. Further, nonlinear collision avoidance constraints have been presented considering lateral position and yaw angle in dependence with the longitudinal position of the vehicle and of the obstacle.

5.1.1 Vehicle Dynamics Model

The vehicle dynamics model introduced in Section 3.1 is nonlinear due to the dependance of the lateral dynamics states with the longitudinal state, the velocity, (3.6). Assume the predicted state and input vector of the last control step $k-1$ for the prediction step i be given by $\mathbf{x}_{\text{i,k-1}}$ and $\mathbf{u}_{\text{i,k-1}}$, then the state space matrices of the linearized system for the prediction steps i (similarly to Section 3.3.2) are given by

$$\mathbf{A}_{\mathrm{c,i}} = \frac{\partial \mathbf{f}(\mathbf{x}_{\mathrm{i,k-1}}, \mathbf{u}_{\mathrm{i,k-1}})}{\partial \mathbf{x}} \tag{5.1}$$

$$\mathbf{B}_{\mathrm{c,i}} = \frac{\partial \mathbf{f}(\mathbf{x}_{\mathrm{i,k-1}}, \mathbf{u}_{\mathrm{i,k-1}})}{\partial \mathbf{u}} \tag{5.2}$$

$$\mathbf{E}_{\mathrm{c,i}} = \mathbf{f}(\mathbf{x}_{\mathrm{i,k-1}}, \mathbf{u}_{\mathrm{i,k-1}}) - \mathbf{A}_{\mathrm{c,i}}, \mathbf{x}_{\mathrm{i,k-1}} - \mathbf{B}_{\mathrm{c,i}} \mathbf{u}_{\mathrm{i,k-1}} \tag{5.3}$$

and the state space equation is

$$\dot{\mathbf{x}} = \mathbf{A}_{\mathrm{c,i}} \mathbf{x} + \mathbf{B}_{\mathrm{c,i}} \mathbf{u} + \mathbf{E}_{\mathrm{c,i}} \tag{5.4}$$

with $\mathbf{A}_{\mathrm{c,i}} =$

$$\begin{bmatrix}
A_{11} & A_{12} & 0 & 0 & 0 & \frac{c_{\alpha_{\mathrm{f}},\mathrm{i,k-1}}}{m v_{\mathrm{i,k-1}} i_{\mathrm{L}}} & 0 & A_{18} & 0 \\
A_{21} & A_{22} & 0 & 0 & 0 & A_{26} & 0 & A_{28} & 0 \\
0 & 1 & 0 & 0 & 0 & 0 & 0 & 0 & 0 \\
v & 0 & v & 0 & 0 & 0 & 0 & 0 & 0 \\
\frac{2D_{\mathrm{f}}}{J_{\mathrm{st}}} & \frac{2l_{\mathrm{f}}D_{\mathrm{f}}}{v_{\mathrm{i,k-1}}J_{\mathrm{st}}} & 0 & 0 & -\frac{d_{\mathrm{st}}}{J_{\mathrm{st}}} & \frac{-2D_{\mathrm{f}}}{i_{\mathrm{L}}J_{\mathrm{st}}} & 0 & A_{58} & 0 \\
0 & 0 & 0 & 0 & 1 & 0 & 0 & 0 & 0 \\
0 & 0 & 0 & 0 & 0 & 0 & 0 & 1 & 0 \\
0 & 0 & 0 & 0 & 0 & 0 & 0 & 0 & -\frac{1}{t_{\mathrm{del}}}
\end{bmatrix}$$

$$A_{11} = -\frac{c_{\alpha_{\mathrm{f}},i,k-1} + c_{\alpha_{\mathrm{r}},\mathrm{i,k-1}}}{m v_{\mathrm{i,k-1}}}; A_{12} = \frac{c_{\alpha_{\mathrm{r}},\mathrm{i,k-1}} l_{\mathrm{r}} - c_{\alpha_{\mathrm{f}},\mathrm{i,k-1}} l_{\mathrm{f}}}{m v_{\mathrm{i,k-1}}^2} - 1;$$

$$A_{18} = \frac{c_{\alpha_{\mathrm{f}},\mathrm{i,k-1}} + c_{\alpha_{\mathrm{r}},\mathrm{i,k-1}}}{m v_0^2} \beta_{\mathrm{i,k-1}} - 2\frac{c_{\alpha_{\mathrm{r}},\mathrm{i,k-1}} l_{\mathrm{r}} - c_{\alpha_{\mathrm{f}},\mathrm{i,k-1}} l_{\mathrm{f}}}{m v_{\mathrm{i,k-1}}^3} \dot{\varphi}_{\mathrm{i,k-1}} - \frac{c_{\alpha_{\mathrm{f}},\mathrm{i,k-1}}}{i_{\mathrm{L}} m v_{\mathrm{i,k-1}}^2} \delta_{\mathrm{i,k-1}}$$

$$A_{21} = \frac{c_{\alpha_{\mathrm{r}},\mathrm{i,k-1}} l_{\mathrm{r}} - c_{\alpha_{\mathrm{f}},\mathrm{i,k-1}} l_{\mathrm{f}}}{J_{\mathrm{z}}}; A_{22} = \frac{c_{\alpha_{\mathrm{r}},\mathrm{i,k-1}} l_{\mathrm{r}}^2 - c_{\alpha_{\mathrm{f}},\mathrm{i,k-1}} l_{\mathrm{f}}^2}{J_{\mathrm{z}} v_{\mathrm{i,k-1}}};$$

$$A_{26} = -\frac{c_{\alpha_{\mathrm{r}},\mathrm{i,k\text{-}1}} l_{\mathrm{r}}^2 + c_{\alpha_{\mathrm{f}},\mathrm{i,k\text{-}1}} l_{\mathrm{f}}^2}{J_z v_{\mathrm{i,k\text{-}1}}}$$

$$A_{28} = \frac{c_{\alpha_{f,i,k-1}} l_{\mathrm{f}}^2 + c_{\alpha_{r,i,k-1}} l_{\mathrm{r}}^2}{J_{\mathrm{z}} v_{\mathrm{i,k\text{-}1}}^2} \dot{\varphi}_{\mathrm{i,k\text{-}1}}; A_{58} = \frac{-2 l_{\mathrm{f}} D_{\mathrm{f}}}{J_{\mathrm{st}} v_{\mathrm{i,k\text{-}1}}^2} \dot{\varphi}_{\mathrm{i,k\text{-}1}};$$

$$\mathbf{B}_{\mathrm{c,i}} = \begin{bmatrix} 0 & 0 \\ 0 & 0 \\ 0 & 0 \\ 0 & 0 \\ \frac{1}{J_{\mathrm{st}}} & 0 \\ 0 & 0 \\ 0 & 0 \\ 0 & 0 \\ 0 & \frac{1}{t_{del}} \end{bmatrix} \quad \mathbf{E}_{\mathrm{c,i}} = \begin{bmatrix} \frac{F_{\mathrm{yf,0,i,k\text{-}1}} + F_{\mathrm{yr,0,i,k\text{-}1}}}{m v_{\mathrm{i,k\text{-}1}}} - A_{18} v_{\mathrm{i,k\text{-}1}} \\ \frac{F_{\mathrm{yf,0,i,k\text{-}1}} l_f + F_{\mathrm{yr,0,i,k\text{-}1}} l_r}{J_{\mathrm{z}}} - A_{28} v_{\mathrm{i,k\text{-}1}} \\ 0 \\ 0 \\ -A_{58} v_{\mathrm{i,k\text{-}1}} \\ 0 \\ 0 \\ 0 \\ 0 \end{bmatrix}$$

Note that $v_{\mathrm{i,k\text{-}1}}$, $\varphi_{i,k-1}$, $\dot{\varphi}_{\mathrm{i,k\text{-}1}}$ and $\beta_{\mathrm{i,k\text{-}1}}$ are the velocity, yaw angle, yaw rate and side slip angle predicted for the prediction step i at control time step $k-1$ and $c_{\alpha_{\mathrm{f}},\mathrm{i,k\text{-}1}}, c_{\alpha_{\mathrm{r}},\mathrm{i,k\text{-}1}}, F_{\mathrm{yf,0,i,k\text{-}1}}$ as well as $F_{\mathrm{yr,0,i,k\text{-}1}}$ correspond to predicted cornering stiffnesses and tire force biases for the predicted slip angles $\alpha_{\mathrm{r,i,k\text{-}1}}$ and $\alpha_{\mathrm{f,i,k\text{-}1}}$, the predicted wheel loads $F_{\mathrm{zf,i,k\text{-}1}}$ and $F_{\mathrm{zr,i,k\text{-}1}}$ as well as the predicted friction coefficient $\mu_{\mathrm{yf,i,k\text{-}1}}$ and $\mu_{\mathrm{yr,i,k\text{-}1}}$ with

$$c_{\alpha_{\mathrm{f}},\mathrm{i},\mathrm{k}-1} = F_{\mathrm{zf},\mathrm{i},\mathrm{k}-1} \frac{\partial \mu_{\mathrm{y}}}{\partial \alpha_{\mathrm{f}}} |_{\alpha_{\mathrm{f},\mathrm{i},\mathrm{k}-1}} \tag{5.5}$$

$$c_{\alpha_{\mathrm{r}},\mathrm{i},\mathrm{k}-1} = F_{\mathrm{zr},\mathrm{i},\mathrm{k}-1} \frac{\partial \mu_{\mathrm{y}}}{\partial \alpha_{\mathrm{r}}} |_{\alpha_{\mathrm{r},\mathrm{i},\mathrm{k}-1}}$$

$$F_{\mathrm{f},0,\mathrm{i},\mathrm{k}-1} = F_{\mathrm{zf},\mathrm{i},\mathrm{k}-1} \mu_{\mathrm{y},\mathrm{i},\mathrm{k}-1} - c_{\alpha_{\mathrm{f}},\mathrm{i},\mathrm{k}-1} \alpha_{\mathrm{f},\mathrm{i},\mathrm{k}-1} \tag{5.6}$$

$$F_{\mathrm{r},0,\mathrm{i},\mathrm{k}-1} = F_{\mathrm{zr},\mathrm{i},\mathrm{k}-1} \mu_{\mathrm{y},\mathrm{i},\mathrm{k}-1} - c_{\alpha_{\mathrm{r}},\mathrm{i},\mathrm{k}-1} \alpha_{\mathrm{r},\mathrm{i},\mathrm{k}-1}$$

To illustrate the effect of successive linearization for the vehicle dynamics model, Figure 5.3 shows the linearization of the tire equation for consecutive control steps. Assume the nonlinear tire model be given in Figure 5.3.a.
At maneuver start $k = 0$ in Figure 5.3.b, the tire equation for all predicted operation points are linearized at the same constant angle, the slip angle at the current time step α_0. The linearized tire equations for the predicted time steps are represented by g_1, g_2 and g_3. At the following step $k = 1$ in Figure 5.3.c, the predicted slip angle positions taken from the result of the optimization problem are considered for the linearization of the tire equation. Following this principle the predicted operation point will be adapted at each consecutive control step as shown exemplarily for $k = 2$ in Figure 5.3.d. The linearized tire parameters can then be used for the linearized vehicle dynamics model.
For the MPC method, the linearized continuous vehicle dynamics model equation 5.4 will be discretized, such that the discrete state space equation is

$$\mathbf{x}_{i+1} = \mathbf{A}_{\mathrm{i}+1} \mathbf{x}_i + \mathbf{B}_{\mathrm{i}} \mathbf{u}_i + \mathbf{E} \quad \forall \mathrm{i} = 0, \cdots, \mathrm{N} \tag{5.7}$$

The affine time varying state space equation is continuous on the state $\mathbf{x}$ and input $\mathbf{u}$ at each prediction step, such that Assumption 1 is satisfied. This affine model will be transformed into a linear model in Section 5.2 to calculate the penalty matrix and to apply the robust control design in Section 3.2.2.

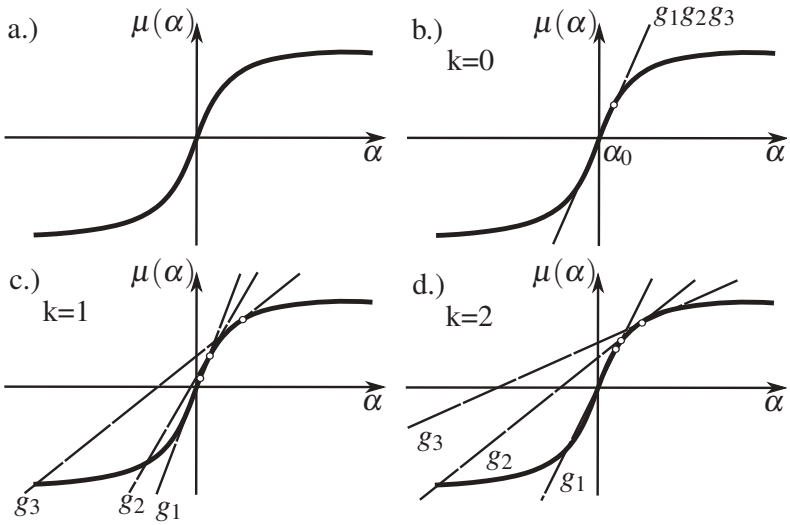

Figure 5.3: Successive linearization of tire equation - a.) Nonlinear Tire model b.) Linearization on current slip angle α_0 c.) Linearization on predicted operation points d.) Linearization on consecutive prediction points

5.1.2 Collision Avoidance Constraints

Collision avoidance has been achieved using nonlinear inequality constraints in Chapter 4. The nonlinear collision avoidance constraints depends on the longitudinal position, the lateral position and the yaw angle. In this section, the nonlinear constraints will be transformed to linear constraints for the lateral position and the yaw angle. According to the principles of successive linearization, the longitudinal position at each control step can be estimated using the longitudinal position prediction of the last control step. With the predicted positions, suitable constraints for the lateral position and the yaw angle can be determined.

In Chapter 4 the nonlinear inequality constraints in (4.5) required the calculation of y_{Br} and y_{Bl} given by

$$\begin{aligned} y_{\mathrm{Br}} &= y - \frac{w}{2\cos\varphi(k)} + \Delta x \tan\varphi \\ y_{\mathrm{Bl}} &= y + \frac{w}{2\cos\varphi(k)} + \Delta x \tan\varphi \end{aligned} \tag{5.8}$$

and the constraints

$$\begin{aligned} y_{\mathrm{Br}} &> y_{\mathrm{obsr}} + w_{\mathrm{obsr}}/2 \\ y_{\mathrm{Bl}} &< y_{\mathrm{obsr}} - w_{\mathrm{obsr}}/2\ . \end{aligned} \tag{5.9}$$

In this section, the inequalities are first simplified using small angles approximation to

$$\begin{aligned} y_{\mathrm{Br}} &= y - \frac{w}{2} + \Delta x\varphi \\ y_{\mathrm{Bl}} &= y + \frac{w}{2} + \Delta x\varphi. \end{aligned} \tag{5.10}$$

Note that (4.5) and (4.7) involve nonlinearities such as if-else structures and min-max operations. The effects of these nonlinear operations need to be approximated by linear equations. First, the if-else structure, which depends on the vehicle states of the predicted step i, is replaced by an approximation using predicted vehicle states of time step $k-1$ and the corresponding prediction step i. The equations are given as

$$y_{\mathrm{Br}} \geq y_{\mathrm{obsr}} + w_{\mathrm{obsr}}/2 \tag{5.11}$$
$$\forall(x_{\mathrm{fr,i,k\text{-}1}} > x_{\mathrm{obsr}}) \cap (x_{\mathrm{rr,i,k\text{-}1}} < x_{\mathrm{obsr}} + l_{\mathrm{obsr}})$$
$$y_{\mathrm{Bl}} \leq y_{\mathrm{obsl}} - w_{\mathrm{obsl}}/2 \tag{5.12}$$
$$\forall(x_{\mathrm{fl,i,k\text{-}1}} > x_{obsl}) \cap (x_{\mathrm{rl,i,k\text{-}1}} < x_{\mathrm{obsl}} + l_{\mathrm{obsl}})\ .$$

The parameters $x_{\text{fr,i,k-1}}$, $x_{\text{fl,i,k-1}}$, $x_{\text{rr,i,k-1}}$ and $x_{\text{rl,i,k-1}}$ are obtained from the preceding optimization step, such that the dependancy on the longitudinal position of the current control step k is eliminated and inequality constraints become linear. The collision avoidance set is transformed to

$$\begin{aligned}\mathbb{C} := \{\mathbf{x} \in \mathbb{R}^9 |\ & (y_{\text{Br}} \geq y_{\text{obsr}} + w_{\text{obsr}}/2, \forall x \in \mathbb{X}_{\text{or}}) \cap \\ & (y_{\text{Bl}} \leq y_{\text{obsl}} - w_{\text{obsl}}/2, \forall x \in \mathbb{X}_{\text{ol}})\}\end{aligned}$$

with

$$\mathbb{X}_{\text{or}} := \{x \in \mathbb{R} | (x_{\text{fr,i,k-1}} > x_{\text{obsr}}) \cap (x_{\text{rr,i,k-1}} < x_{\text{obsr}} + l_{\text{obsr}})\}$$

$$\mathbb{X}_{\text{ol}} := \{x \in \mathbb{R} | (x_{\text{fl,i,k-1}} > x_{\text{obsl}}) \cap (x_{\text{rl,i,k-1}} < x_{\text{obsl}} + l_{\text{obsl}})\}\ .$$

The approach is illustrated in Figure 5.4. At maneuver start $k = 0$, when no longitudinal position predictions are available, the considered longitudinal position for the prediction steps are approximated by the constant velocity assumption (constant measured velocity $v_{0,\text{k}}$ for all prediction steps) illustrated with the equidistant position marks (vertical dashed lines) for the corresponding prediction time steps $i = 0, \cdots, N$ in Figure 5.4.a. After solving the optimization problem, a trajectory will result in Figure 5.4.b which satisfies the linearized constraints on the lateral position from the considered longitudinal positions in Figure 5.4.a. The predicted longitudinal positions extracted from the result of the optimization problem in Figure 5.4.b can then be used to update the linearized lateral position constraints. Note that the predicted longitudinal position between consecutive control steps change, in general, due to change in the predicted velocities between each control step. This procedure continues with each consecutive control step, shown exemplarily for $k = 0$ and $k = 1$ in Figure 5.4.b and 5.4.c.

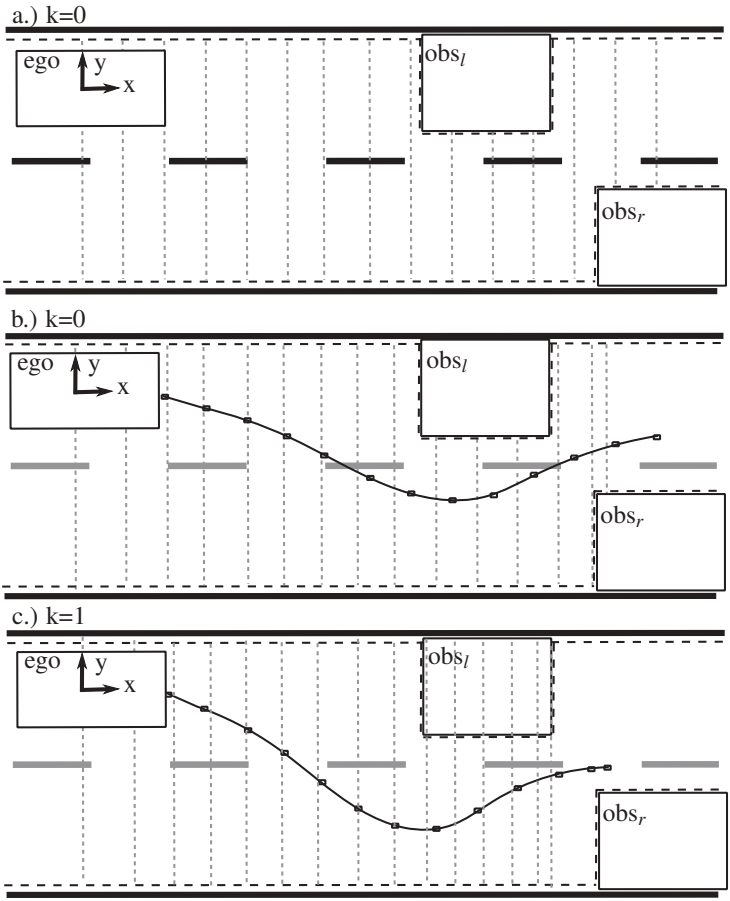

Figure 5.4: Successive linearization of collision avoidance constraints; a.) Constant velocity prediction at maneuver start leads to equidistant longitudinal position distances (vertical dashed lines) for predictive time steps; (b) Calculated trajectory satisfying constraints at lateral position; (c) Predicted longitudinal positions are used for further linearization of constraints in the next time step

Following this principle the constraints to keep the vehicle in the lane

$$\begin{aligned} \min(y_{\mathrm{fr}}, y_{\mathrm{rr}}) &> y_{\mathrm{R}}(x) \\ \max(y_{\mathrm{fl}}, y_{\mathrm{rl}}) &< y_{\mathrm{L}}(x) \\ \text{with } y_{\mathrm{fr}} &= y + l_{\mathrm{f}} \sin(\varphi) - \frac{w}{2}\cos(\varphi) \\ y_{\mathrm{rr}} &= y - l_{\mathrm{r}} \sin(\varphi) - \frac{w}{2}\cos(\varphi) \\ y_{\mathrm{fl}} &= y + l_{\mathrm{f}} \sin(\varphi) + \frac{w}{2}\cos(\varphi) \\ y_{\mathrm{rl}} &= y - l_{\mathrm{r}} \sin(\varphi) + \frac{w}{2}\cos(\varphi) \end{aligned} \tag{5.13}$$

can be transformed accordingly to

$$\begin{aligned} y + c_{\mathrm{r}}\varphi &> y_{\mathrm{R}}(x_{\mathrm{i,k\text{-}1}}) + \frac{w}{2} \\ y + c_{\mathrm{l}}\varphi &< y_{\mathrm{L}}(x_{\mathrm{i,k\text{-}1}}) - \frac{w}{2} \\ \text{with } c_{\mathrm{r}} &= \begin{cases} l_{\mathrm{f}} & y_{\mathrm{fr,i,k\text{-}1}} < y_{\mathrm{rr,i,k\text{-}1}} \\ -l_{\mathrm{r}} & y_{\mathrm{fr,i,k\text{-}1}} > y_{\mathrm{rr,i,k\text{-}1}} \end{cases} \\ c_l &= \begin{cases} -l_{\mathrm{r}} & y_{\mathrm{fl,i,k\text{-}1}} < y_{\mathrm{rl,i,k\text{-}1}} \\ l_{\mathrm{f}} & y_{\mathrm{fl,i,k\text{-}1}} > y_{\mathrm{rl,i,k\text{-}1}} \end{cases} . \end{aligned} \tag{5.14}$$

Here $y_{\mathrm{fr,i,k\text{-}1}}$, $y_{\mathrm{fl,i,k\text{-}1}}$, $y_{\mathrm{rr,i,k\text{-}1}}$ and $y_{\mathrm{rl,i,k\text{-}1}}$ are predicted positions for the vehicle corners of the last control step $k-1$ for the prediction step i. The corresponding set is transformed to

$$\begin{aligned} \mathbb{L}_q = \{\mathbf{x} \in \mathbb{R}^9 \mid\ & y + c_{\mathrm{r}}\varphi \geq y_{\mathrm{R}}(x_{\mathrm{i,k\text{-}1}}) + \frac{w}{2}\ , \\ & y + c_{\mathrm{l}}\varphi \leq y_{\mathrm{L}}(x_{\mathrm{i,k\text{-}1}}) - \frac{w}{2}\} \\ \text{with } c_r &= \begin{cases} l_{\mathrm{f}} & y_{\mathrm{fr,i,k\text{-}1}} < y_{\mathrm{rr,i,k\text{-}1}} \\ -l_{\mathrm{r}} & y_{\mathrm{fr,i,k\text{-}1}} > y_{\mathrm{rr,i,k\text{-}1}} \end{cases} \end{aligned} \tag{5.15}$$

$$c_l = \begin{cases} -l_\mathrm{r} & y_\mathrm{fl,i,k\text{-}1} < y_\mathrm{rl,i,k\text{-}1} \\ l_\mathrm{f} & y_\mathrm{fl,i,k\text{-}1} > y_\mathrm{rl,i,k\text{-}1} \end{cases} .$$

The sets $\mathbb{C}_\mathrm{q}$ and $\mathbb{L}_\mathrm{q}$ are closed sets for the state vector, fulfilling Assumption 2. A fundamental difference between the nonlinear collision avoidance constraints in Section 4.3 and the collision avoidance constraints in this section is that the nonlinearity is linearized prior to the optimization in this section so that the quadratic solver calculates the solution based on linearized position constraints for each prediction step.

5.1.3 Terminal Collision Avoidance

Section 4.4 introduced nonlinear terminal collision avoidance constraints to consider relevant obstacles outside of the prediction horizon. Successive linearization will be exploited in this section to acquire linear terminal collision avoidance constraints.
The nonlinear constraint for Scenario 3 in Section 4.4 is

$$\begin{aligned} &\Delta x \geq x_\mathrm{B} \\ \equiv\ &(x_\mathrm{Tjam} - x(N)) \geq \frac{v(N)^2 \cos(\varphi(N))}{2a_\mathrm{x}(N)} . \end{aligned} \tag{5.16}$$

This inequality can be linearized to

$$\begin{aligned} \equiv\ &(x_\mathrm{Tjam} - x(N)) \geq \frac{v_0^2 \cos(\varphi_0(N))}{2a_\mathrm{x0}} + \frac{v_0 \cos(\varphi_0(N))}{a_\mathrm{x0}} (v(N) - v_0(N)) \\ &- \frac{v_0^2 \cos(\varphi_0(N))}{2a_\mathrm{x,0}^2} (a_x(N) - a_\mathrm{x,0}) - \frac{v_0^2 \sin(\varphi_0(N))}{2a_\mathrm{x,0}} (\varphi(N) - \varphi_0(N)) \\ \equiv\ &\mathbf{L}_\mathrm{B}\mathbf{x}(N) \leq c_\mathrm{B} \end{aligned}$$

where $v_0(N), \varphi_0(N)$ and $a_\mathrm{x,0}(N)$ correspond to predicted state values of the last control time for the N-th prediction step.

Similarly the nonlinear inequality for Scenario 2 is

$$\begin{aligned} &\Delta x(N) \geq x_{\mathrm{E}}(N) \\ &\equiv (x_{\mathrm{obsl}} - x(N)) \geq v(N)\sqrt{\frac{2y_{\mathrm{E}}(N)}{a_{\mathrm{y}}(N)}} \end{aligned} \tag{5.17}$$

and the linear constraints are calculated using the Taylor linearization below. For convenience of calculation y_{E} has been set to the constant predicted value of previous control step $y_{\mathrm{E},0}$ and is not linearized as a variable.

$$\begin{aligned} &\equiv (x_{\mathrm{obsl}} - x_0(N))^2(\dot{\varphi}(N) + \dot{\beta}(N)) + v_0(N)y_{\mathrm{E},0}\varphi(N) \\ &\quad - 2(\dot{\varphi}_0(N) + \dot{\beta}_0(N))(x_{\mathrm{obsl}} - x_0(N))x(N) \\ &\quad + \tan\varphi_0(N)y_{\mathrm{E},0}(N)v(N) \leq -v_0(N)y_{\mathrm{E},0}(N)\tan\varphi_0(N) \\ &\quad - 2(\dot{\varphi}_0(N) + \dot{\beta}_0(N))(x_{\mathrm{obsl}} - x_0(N))x_0(N) + 2\varphi_0(N)y_{\mathrm{E},0}(N)v(N) \\ &\equiv \mathbf{L}_{\mathrm{N}}\mathbf{x}_{\mathrm{N}} + \mathbf{L}_{\mathrm{N\text{-}1}}\mathbf{x}_{\mathrm{N\text{-}1}} \leq c_{\mathrm{E}} \end{aligned}$$

The sets to consider for collision avoidance in the scenarios are

$$\mathbb{G}_{\mathrm{B}} := \{\mathbf{x} \in \mathbb{R}^9 | \mathbf{L}_{\mathrm{B}}\mathbf{x}(N) \leq c_{\mathrm{B}}\} \quad \text{and} \tag{5.18}$$

$$\mathbb{G}_{\mathrm{E}} := \{\mathbf{x} \in \mathbb{R}^9 | \mathbf{L}_{\mathrm{N}}\mathbf{x}(N) + \mathbf{L}_{\mathrm{N\text{-}1}}\mathbf{x}(N-1) \leq c_{\mathrm{E}}\}\ . \tag{5.19}$$

5.1.4 Acceleration Circle

The nonlinear acceleration circle, representing the effect of the friction circle on each wheel, introduced in Section 3.1.4 will be modified in this section. A similar approximation approach was first introduced in [19], where the nonlinear friction circle is replaced by several linear inequalities. In this thesis, the circle will be approximated by the linear inequalities illustrated in Figure 5.5.

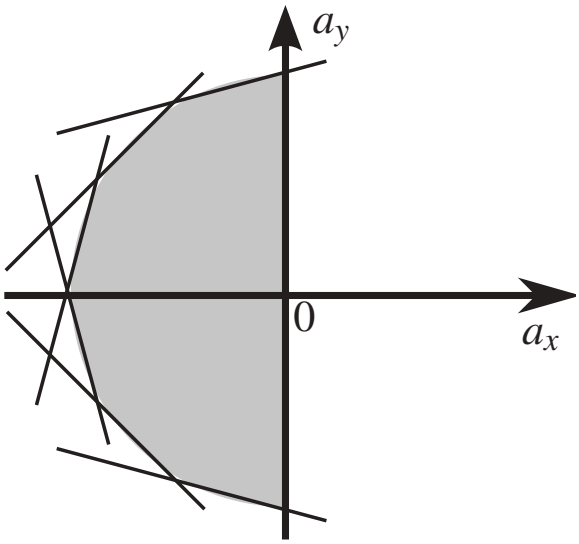

Figure 5.5: Approximation of the friction circle by linear inequalities

The considered model with the vehicle dynamics states does not directly represent the lateral acceleration but can be calculated by

$$a_{\mathrm{y}}(i,k) = \left(\frac{\beta(i+1,k) - \beta(i,k)}{t_{\mathrm{pred}}} + \dot{\varphi}(i,k) \right) \cdot v(i,k) \ . \tag{5.20}$$

This equation is not linear on the vehicle dynamic states in (3.21) and will again be modified by successive linearization. In this section, successive linearization is proposed to approximate the result. In the equation above $v(i,k)$ will be substituted by $v_{\mathrm{i,k\text{-}1}}$, which is the predicted speed value of the preceding control time $k-1$ for the prediction step i.

$$a_{\mathrm{y}}(i,k) = \left(\frac{\beta(i+1,k) - \beta(i,k)}{t_{\mathrm{pred}}} + \dot{\varphi}(i,k) \right) \cdot v_{\mathrm{i,k\text{-}1}} \tag{5.21}$$

The approximation of the acceleration circle with 6 linear inequalities is expressed by

$$\mathbf{L}_{\mathrm{y}}\left(\frac{\beta(i+1,k)-\beta(i,k)}{t_{\mathrm{pred}}}+\dot{\varphi}(i,k)\right)\cdot v_{\mathrm{i,k\text{-}1}}+\mathbf{L}_{\mathrm{x}}a_{\mathrm{x}}(i,k)<\mathbf{M} \tag{5.22}$$

$$\mathbf{L}_{\mathrm{y}}=\begin{bmatrix}\sin((4)\frac{2\pi}{8}-\frac{\pi}{8})\\ \sin((5)\frac{2\pi}{8}-\frac{\pi}{8})\\ \vdots\\ \sin((9)\frac{2\pi}{8}-\frac{\pi}{8})\end{bmatrix},\mathbf{L_x}=\begin{bmatrix}\cos((4)\frac{2\pi}{n}-\frac{\pi}{8})\\ \cos((5)\frac{2\pi}{n}-\frac{\pi}{8})\\ \vdots\\ \cos((9)\frac{2\pi}{n}-\frac{\pi}{8})\end{bmatrix},\mathbf{M}=\begin{bmatrix}\lambda\mu a_{\max}\\ \lambda\mu a_{\max}\\ \vdots\\ \lambda\mu a_{\max}\end{bmatrix}$$

with the parameter $\lambda=\frac{5\pi}{12}$ as proposed by [19]. The set of possible vehicle dynamics states is transformed to

$$\mathbb{V}_{\mathrm{q}}=\{\mathbf{x}\in\mathbb{R}^9\mid v\geq 0,\ a_{\mathrm{x}}(k)\leq 0 \qquad \text{and} \tag{5.23}$$

$$\mathbf{L}_{\mathrm{y}}\left(\frac{\beta(i+1,k)-\beta(i,k)}{t_{\mathrm{pred}}}+\dot{\varphi}(i,k)\right)\cdot v_{\mathrm{i,k\text{-}1}}+\mathbf{L}_{\mathrm{x}}a_{\mathrm{x}}(i,k)<\mathbf{M}. \tag{5.24}$$

The inequality constraints in the set are closed fulfilling Assumption 2.

5.2 Compensation of Linearization Errors

In the last section approximation techniques have been presented to linearize nonlinear constraints of the nonlinear integrated planning and control method. By exploiting these techniques the nonlinear optimization problem can be reformulated into the anticipated quadratic program to achieve an efficient, fast optimization problem. However, linearization of the nonlinear constraints leads to the side effects of linearization errors which can threaten the stability and the satisfaction of constraints. This section shall show how these errors can be

considered to ensure stability and constraint satisfaction by exploiting the principles of robust tube based MPC presented in Section 3.2.2.
Following this method, a linear feedback vector needs to be calculated and constraint tightening shall be applied. The linear feedback vector **k**, similarly to Section 3.3.5, is calculated by solving the Ricatti equation for the matrix **P** with the linear state space model

$$\begin{bmatrix} \mathbf{x}_{k+1} \\ 1 \end{bmatrix} = \begin{bmatrix} \mathbf{A}(\theta) & \mathbf{E}(\theta) \\ 0 & 1 \end{bmatrix} \begin{bmatrix} \mathbf{x}_k \\ 1 \end{bmatrix} + \begin{bmatrix} \mathbf{B}(\theta) \\ 0 \end{bmatrix} \mathbf{u}_k \tag{5.25}$$

which have been transformed from (5.7). The Ricatti equation is then given by

$$\begin{bmatrix} \mathbf{A}(\theta) & \mathbf{E}(\theta) \\ 0 & 1 \end{bmatrix}^T \mathbf{P} + \mathbf{P} \begin{bmatrix} \mathbf{A}(\theta) & \mathbf{E}(\theta) \\ 0 & 1 \end{bmatrix} \leq \begin{bmatrix} -\mathbf{Q} & 0 \\ 0 & 0 \end{bmatrix} \tag{5.26}$$

for $\theta \in \Theta$ and $\mathbf{Q}$ as defined in (4.1). Here Θ is the set of 2^3 possible parameter combinations describing the extreme points of the uncertain parameter vector similar to the robust control design in [84].

$$\theta = [v, \alpha_\mathrm{r}, \alpha_\mathrm{f}] \tag{5.27}$$

with the set given by their limits

$$\Theta := \{\theta \in \mathbb{R}^3 | v \in [v_\mathrm{min}, v_\mathrm{max}], \alpha_\mathrm{r} \in [0, \alpha_\mathrm{r,max}], \alpha_\mathrm{f} \in [0, \alpha_\mathrm{f,max}]\} \tag{5.28}$$

This problem has been solved by linear matrix inequalities [44] in Section 3.3.5, so that the feedback vector can stabilize the system in any dynamics range of the maneuver defined by the limits $v_\mathrm{min}, v_\mathrm{max}, \alpha_\mathrm{r,max}$ and $\alpha_\mathrm{f,max}$. Here $\mathbf{Q}$ is positive semi-definite and $\mathbf{P}$ is symmetric positive semi-definite. The linear feedback vector can then be calculated by

$$\mathbf{k} = -\mathbf{R}^{-1} \begin{bmatrix} \mathbf{B}(\theta) \\ 0 \end{bmatrix}^T \mathbf{P} \,. \tag{5.29}$$

The terminal weight matrix $\mathbf{P}_\mathrm{f}$is calculated by

$$\mathbf{A}_\mathrm{k}(\theta)'\mathbf{P}_\mathrm{f}\mathbf{A}_\mathrm{k}(\theta) - \mathbf{P}_\mathrm{f} \leq -\mathbf{Q}, \tag{5.30}$$

$$\mathbf{A}_\mathrm{k}(\theta) = \begin{bmatrix} \mathbf{A}(\theta) & \mathbf{E}(\theta) \\ 0 & 1 \end{bmatrix}^T + \begin{bmatrix} \mathbf{B}(\theta) \\ 0 \end{bmatrix} \mathbf{k}$$

with $\mathbf{A}(\theta)$ and $\mathbf{B}(\theta)$ being the state space matrices with the parameter vector $\theta \in \Theta$. Equation (5.30) is derived from Assumption 6 with

$$V_\mathrm{f} = [\mathbf{x}; 1]^T \mathbf{P}_\mathrm{f} [\mathbf{x}; 1] \tag{5.31}$$

$$\begin{aligned} \mathbb{X}_\mathrm{f} := \{\mathbf{x} \in \mathbb{R}^9 | & v_{\min} \leq v \leq v_{\max}, \\ & -\alpha_{\mathrm{f,max}} \leq \alpha_\mathrm{f} \leq \alpha_{\mathrm{f,max}}, \\ & -\alpha_{\mathrm{r,max}} \leq \alpha_r \leq \alpha_{\mathrm{r,max}} \quad . \end{aligned} \tag{5.32}$$

Let $\mathbb{X}$ and $\mathbb{U}$ be defined by

$$\begin{aligned} \mathbb{X} &= \mathbb{S} \cap \mathbb{L} \cap \mathbb{C}_\mathrm{q} \cap \mathbb{V}_\mathrm{q} \\ \mathbb{X} &:= \{\mathbf{c}_\mathrm{i}\mathbf{x} \leq d_\mathrm{i}\} \\ \mathbb{U} &:= \{\mathbf{a}_\mathrm{i}\mathbf{u} \leq b_\mathrm{i}\} \end{aligned}$$

with i being the index over all considered constraints, then the sets $\mathbb{Z}$ and $\mathbb{V}$ for the nominal system can be given by

$$\mathbb{Z} := \{\mathbf{c}_\mathrm{i}\mathbf{z} \leq d_\mathrm{i} - \max_\mathrm{j}\{\mathbf{c}_\mathrm{i}\mathbf{e}_\mathrm{ij} | \mathbf{w}_\mathrm{j} \in \mathbb{W}\}\} \tag{5.33}$$

$$\mathbb{V} := \{\mathbf{a}_\mathrm{i}\mathbf{v} \leq b_\mathrm{i} - \max_\mathrm{j}\{\mathbf{a}_\mathrm{i}\mathbf{k}\mathbf{e}_\mathrm{ij} | \mathbf{w}_\mathrm{i,j} \in \mathbb{W}\}\} \tag{5.34}$$

with the set $\mathbb{W}$ and the additive uncertainty vector $\mathbf{w}_\mathrm{j}$ calculated according to (3.2.2) with the parameter vector $\theta_\mathrm{j} \in \Theta$. In the equation above the additive uncertainty vector is chosen which has the maximum effect on the considered constraint with the linearization error $\mathbf{e}_\mathrm{ij}$. The dynamic of the linearization error is given by

$$\mathbf{e}_\mathrm{i,j} = \mathbf{A}_\mathrm{k}^{i}\mathbf{e}_0 + \sum_{l=0}^{i-1} \mathbf{A}_\mathrm{k}^{l}\mathbf{w}_\mathrm{j} \tag{5.35}$$

with

$$\begin{gathered}\mathbf{w}_\mathrm{j} = (\mathbf{A}(\theta_\mathrm{j}) - \mathbf{A})\mathbf{x} + (\mathbf{B}(\theta_\mathrm{j}) - \mathbf{B})\mathbf{u} + \mathbf{E}(\theta_j) \\ \theta_j = \theta_0 + \Delta\theta_j \in \Theta \\ (\mathbf{x}, \mathbf{u}) \in \mathbb{X} \times \mathbb{U}\end{gathered}$$

Here θ_0 is the nominal parameter vector and $\Delta\theta_\mathrm{j}$ is the set of parameter deviations with

$$\begin{aligned}\Delta\theta_\mathrm{j} \in \{&[\Delta v, \Delta\alpha_\mathrm{f}, \Delta\alpha_\mathrm{r}];\ [\Delta v, \Delta\alpha_\mathrm{f}, -\Delta\alpha_\mathrm{r}] \\ &[\Delta v, -\Delta\alpha_\mathrm{f}, \Delta\alpha_\mathrm{r}];\ [-\Delta v, \Delta\alpha_\mathrm{f}, \Delta\alpha_\mathrm{r}] \\ &[-\Delta v, -\Delta\alpha_\mathrm{f}, \Delta\alpha_\mathrm{r}];\ [\Delta v, -\Delta\alpha_\mathrm{f}, -\Delta\alpha_\mathrm{r}] \\ &[-\Delta v, \Delta\alpha_\mathrm{f}, -\Delta\alpha_\mathrm{r}];\ [-\Delta v, -\Delta\alpha_\mathrm{f}, -\Delta\alpha_\mathrm{r}]\}\end{aligned}$$

where Δv, $\Delta\alpha_\mathrm{f}$ and $\Delta\alpha_\mathrm{r}$ determine the range of parameter deviations (linearization errors). In this thesis the range is set to the maximum deviation between the predicted state at the current and the last control step.

$$\begin{aligned}\Delta\alpha_\mathrm{f} &= \max_i(\alpha_\mathrm{f,i,k} - \alpha_\mathrm{f,i,k\text{-}1}) \\ \Delta\alpha_\mathrm{r} &= \max_i(\alpha_\mathrm{r,i,k} - \alpha_\mathrm{r,i,k\text{-}1}) \\ \Delta v &= \max_i(v_\mathrm{i,k} - v_\mathrm{i,k\text{-}1})\end{aligned}$$

5.3 MPC Formulation

The fast integrated planning and control problem is finally formulated in this section. The MPC has a similar structure as the formulation in (4.6). Instead of nonlinear constraints, linearized constraint equations are used, which have been derived by successive linearization in this chapter. The constraints are modified to consider the maximum effect of linearization errors in $\mathbb{V}$ and $\mathbb{Z}$.

$$\begin{aligned}
\min_{\mathbf{u}} \; & J = \sum_{i=1}^{N} \mathbf{z}(i,k)^T \mathbf{Q}\mathbf{z}(i,k) + \mathbf{v}(i,k)^T \mathbf{R}\mathbf{v}(i,k) \\
& \quad + [\mathbf{z}(N,k)^T \; 1]\mathbf{P}_{\mathrm{f}}[z(N,k)^T \; 1]^T + \mathbf{Q}_s s_{\mathrm{obs}}(i,k)^2 \\
\text{s.t.} \; & \mathbf{z}(i+1,k) = \mathbf{A}_{\mathrm{i}}\mathbf{z}(i,k) + \mathbf{B}_{\mathrm{i}}\mathbf{v}(i,k) + \mathbf{E}_{\mathrm{i}} \\
& \mathbf{v}(i,k) \in \mathbb{V} \\
& \mathbf{z}(i,k) \in \mathbb{Z} \\
& \mathbf{z}(0,k) = \mathbf{z}_0 \\
& i = 1, \cdots, N \\
& \mathbf{z}(N,k) \in \mathbb{G}_{\mathrm{B/E}} \text{ if terminal collision avoidance is applied}
\end{aligned} \tag{5.36}$$

The MPC is calculated by the steps given as follows:

Robust Control Algorithm:
Initilization: At time $k = 0$ set $\mathbf{z}_0$=$\mathbf{x}_0$, where $\mathbf{x}(0)$ is the measured state.
Step 1 - Linearization: Linearize nonlinear constraints according to the sections 5.1.1, 5.1.2, 5.1.3 and 5.1.4.
Step 2 - Compute control: Compute control at time k and current states $(\mathbf{z}, \mathbf{v})$ according to the optimization problem in (5.36), solve the nominal optimal control problem to obtain nominal control vector $\mathbf{v}$ and apply control action $\mathbf{u} = \mathbf{v}(0,k) + \mathbf{k}([\mathbf{x}^T(0,k) \; 1]^T - [\mathbf{z}^T(0,k) \; 1])^T$. Save predicted state vectors $\mathbf{z}(i,k), i = 1, \cdots, N$
Step 3 - Apply control: Apply control $\mathbf{u}$ to the system.

Step 4 - Update: Measure the successor state $\mathbf{x}^+$ of the system according to (3.35) and compute the successor state $\mathbf{z}^+ = f(\mathbf{z}(0,k),\mathbf{v}(0,k))$ of the nominal system.
Step 5: Set $(\mathbf{x}(0,k),\mathbf{z}(0,k)) = (\mathbf{x}^+,\mathbf{z}^+)$, set k=k+1, and go to Step 1.

5.4 Results

In previous sections, the fast model predictive approach for integrated trajectory planning and vehicle dynamics control has been presented. Furthermore, the robust tube MPC approach has been discussed to compensate linearization errors. In this section, the method will be demonstrated on Scenario 1 and 2 defined in Section 4.7.2 and compared with the nonlinear MPC approach from Chapter 4. Finally, experimental results will show the performance of the proposed method in the real vehicle.
In the simulation environment, the optimization is solved with an interior point algorithm implemented in MATLAB Simulink. The applied vehicle dynamics model is the nonlinear vehicle dynamcis model in Section 3.1.3 The computer is equipped with an Intel(R) Core(TM) i5-3380M with 2.9h GHz, 8 GB RAM and Windows 7 SP1 as the given operating system.
In the real vehicle, the algorithm runs on a dSpace MicroAutobox II from dSpace. It has a IBM PPC 750 GL 900Mhz processor and 16 MB main memory. The optimization is solved with the CVXGEN solver [46].

5.4.1 Simulation of Typical Scenarios

The performance of the fast integrated planning and control method with parameter setup 4 in Table 5.1 is demonstrated for Scenario 1 in Figure 5.6.
The parameter setup is the same as parameter setup 1 in Chapter 4 except for the slack variable. The difference in the slack variable penalty can be explained by the different characteristic of tube planning compared to the planning of the nominal trajectory in Chapter 4.
Figure 5.6 illustrates the position, the steering torque command, the deceleration command and the velocity of the simulated vehicle during the maneuver. Similarly to Chapter 4, the maneuver is marked at characteristic time marks. In the steering phase, starting at ①, the maximum torque limit and the maximum deceleration command is applied. The steering phase is interrupted shortly by an alternating switching behaviour of steering torque and deceleration command at ②. This effect can be explained by transient dynamics of successive linearization before the predicted dynamics converge. The counter steering phase starting at ③ is characterized by a negative steering torque and a maximum deceleration command. After passing the obstacle the velocity is reduced to a standstill at ④.
The performance in Scenario 2 with two obstacles is illustrated in Figure 5.7. The figure shows that the control method can successfully avoid collision with two obstacles. A difference lies in the longer counter steering phase in Figure 5.7 to avoid collision with the second obstacle obs_l.

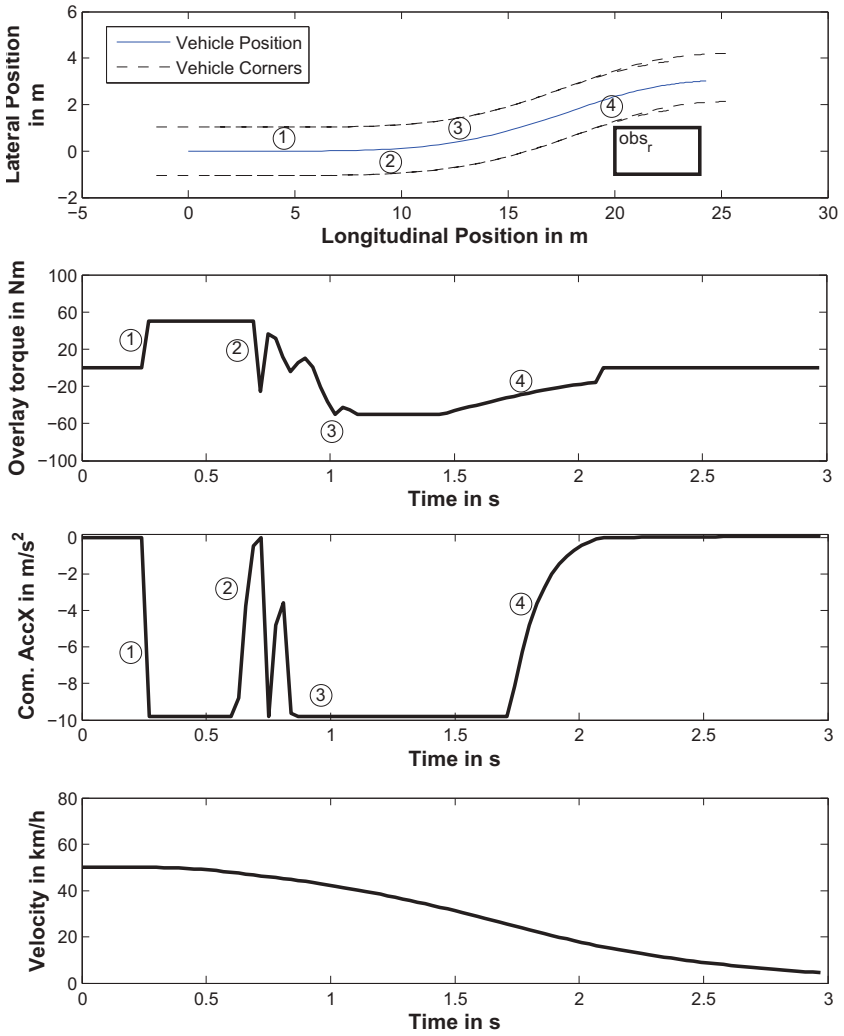

Figure 5.6: Simulation results of the fast integrated trajectory planning and vehicle dynamics control method with parameter setup 4 in Scenario 1

Table 5.1: Parameter setup 4 for the Fast Integrated Planning and Control Method

Parameter	Symbol	Value	Unit
Prediction horizon length	N	15	(none)
Prediction horizon step size	dt_{pred}	0.14	s
Controller time step size	dt_{ctrl}	0.1	s
Penalty of slack variable	q_{s}	10^6	$1/\text{m}^2$
Penalty of yaw angle	q_{φ}	$3{\cdot}10^3$	$1/\text{rad}^2$
Penalty of velocity	q_{v}	10	s^2/m^2
Penalty of steering torque command	r_{T}	0.1	$1/\text{Nm}^2$
Penalty of deceleration command	r_{a_x}	0.1	s^4/m^2
Limit of steering system	T_{max}	50	Nm
Limit of braking system	$a_{\text{x,cmd,max}}$	-9.81	m/s^2

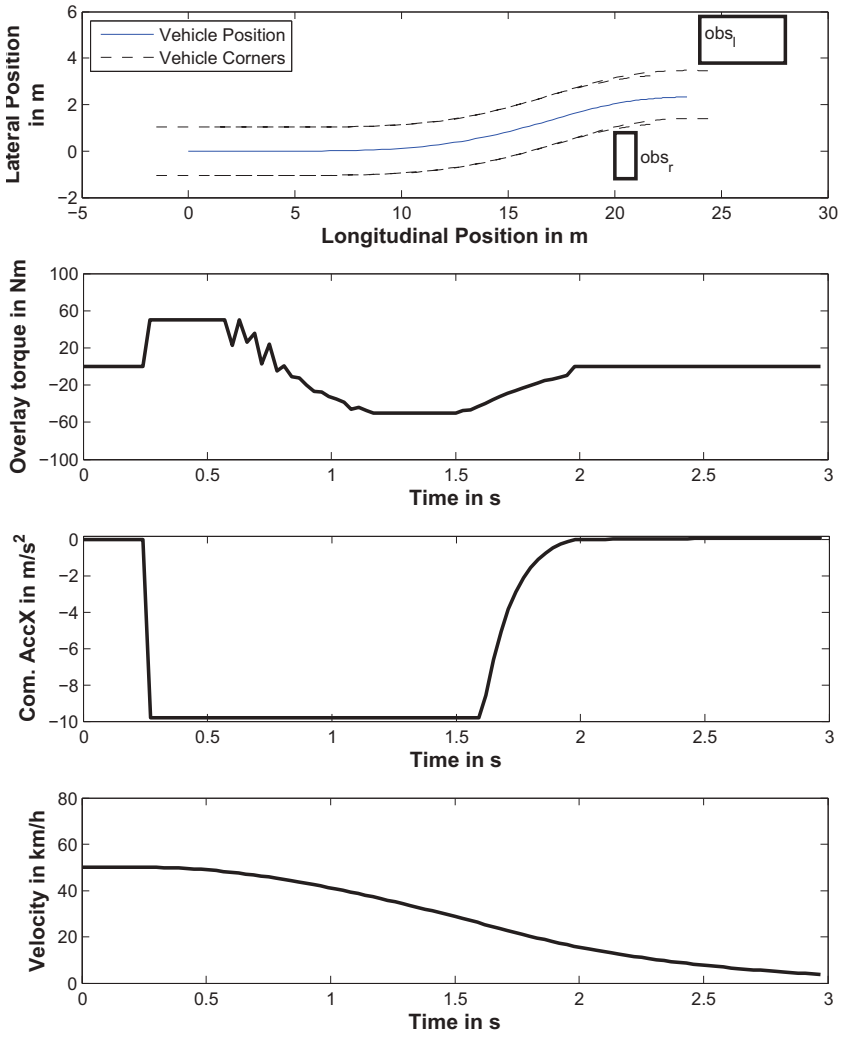

Figure 5.7: Simulation results of the fast integrated trajectory planning and vehicle dynamics control method with parameter setup 4 in Scenario 2

5.4.2 Simulation with Terminal Collision Avoidance

Similarly to Section 4.4, this section shall demonstrate the effect of the terminal collision avoidance constraint in the fast integrated planning and control method. In this section, parameter setup 5 in Table 5.2 is chosen which has the same parameter values as parameter setup 3 in Table 4.3. It has a shorter prediction horizon compared to the setup in Table 5.1 and higher penalty on the command signals. As has been demonstrated in Section 4.7.4, the method with this parameter setup was able avoid collision with the obstacle in Scenario 1 and does not reduce the velocity to standstill at the end of maneuver. Furthermore, the method with this parameter setup cannot avoid collision with the obstacle, as the obstacle has been detected too late.

Table 5.2: Parameter setup 5 for the Fast Integrated Planning and Control Method

Parameter	Symbol	Value	Unit
Prediction horizon length	N	15	(none)
Prediction horizon step size	dt_{pred}	0.07	s
Controller time step size	dt_{ctrl}	0.1	s
Penalty of slack variable	q_{s}	$3{\cdot}10^6$	$1/\text{m}^2$
Penalty of yaw angle	q_{φ}	10^4	$1/\text{rad}^2$
Penalty of velocity	q_{v}	0	s^2/m^2
Penalty of steering torque command	r_{T}	1	$1/\text{Nm}^2$
Penalty of deceleration command	r_{a_x}	10	s^4/m^2
Limit of steering system	$T_{\max}$	50	Nm
Limit of braking system	$a_{\text{x,cmd,max}}$	-9.81	m/s^2

The performance of the terminal collision avoidance constraint for an evasive maneuver in (5.19) is shown in Figure 5.8. By considering the proposed linearized terminal collision avoidance constraint, the collision is avoided.

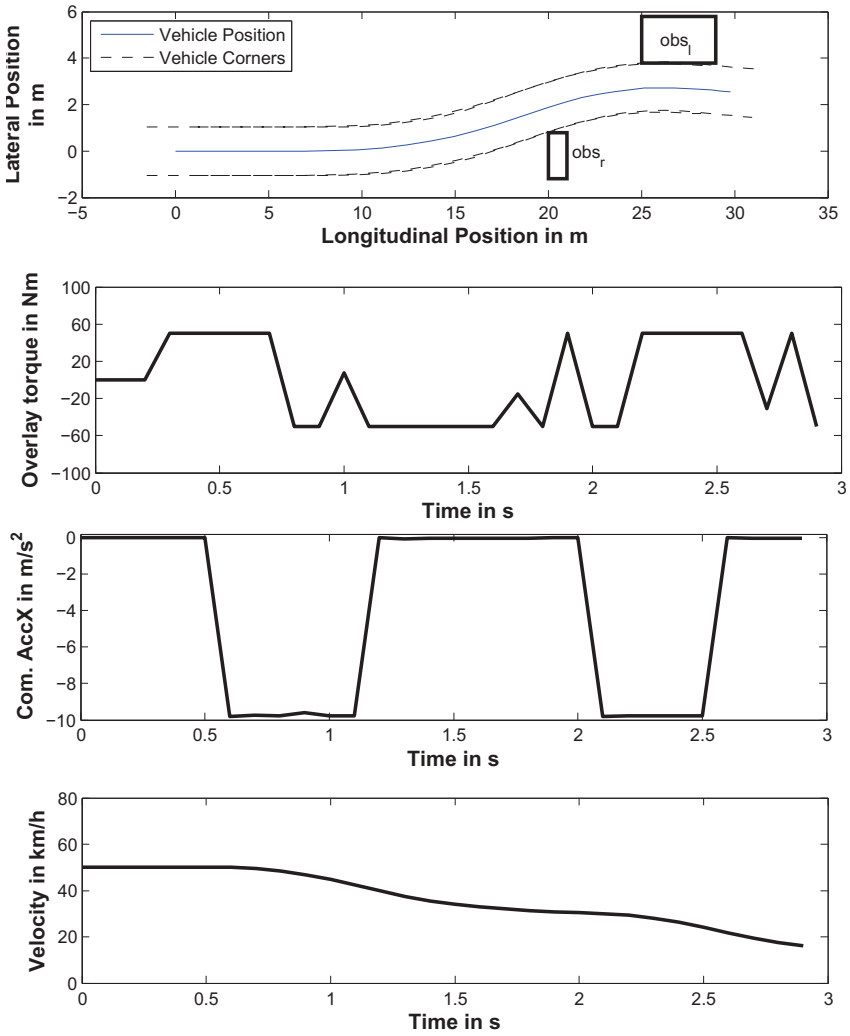

Figure 5.8: Simulation results of the fast integrated trajectory planning and vehicle dynamics control method with parameter setup 5 in Scenario 2 with terminal collision avoidance constraint

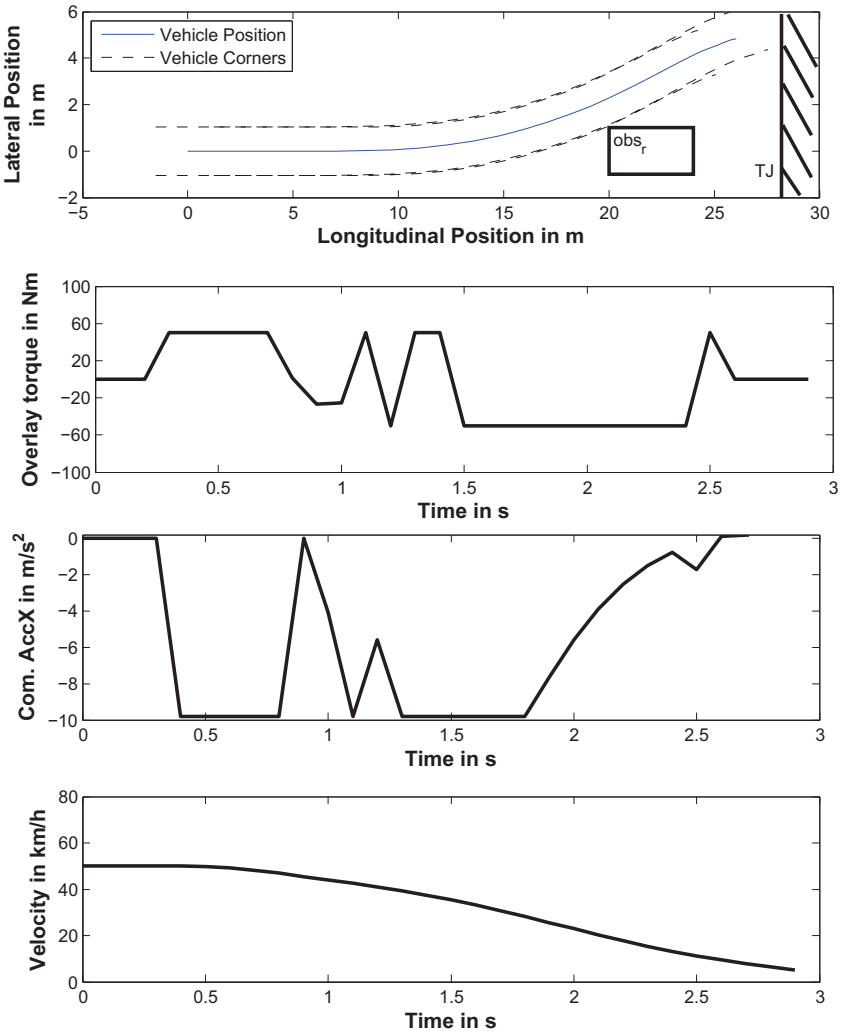

Figure 5.9: Simulation results of the fast integrated trajectory planning and vehicle dynamics control method with parameter setup 5 in Scenario 3 with terminal collision avoidance constraint

Finally, the terminal collision avoidance constraint for a braking maneuver in (5.18) will be used to ensure collision avoidance in Scenario 3, which requires braking in front of a traffic jam as shown in Figure 4.16. The figures illustrates that the implemented terminal collision avoidance constraint is able to reduce velocity to standstill before colliding with obstacles in the traffic jam and can thus be used to guarantee collision avoidance with the obstacle in the scenarios.

5.4.3 Real Vehicle Application

The proposed fast integrated planning and control method can be solved with fast and efficient solvers like [46] on a real time computer platform. It has been implemented in a dSpace MicroAutobox on a test vehicle and tested in the predefined scenarios. The obstacles have been simulated in a vehicle-in-the-loop (VIL) environment.

Figure 5.10 shows the result of the fast integrated planning and control method with parameter setup 6 in Table 5.3 for Scenario 1 in the test vehicle. The maneuver starts with the steering phase at ① where the maximum steering torque and deceleration command are commanded. At ② the counter-steering phase starts where the deceleration command is reduced for a short period. In the stabilization phase from ③ to ④ the method reorientates the vehicle to zero yaw angle and brakes the vehicle to a standstill. Comparing Figure 5.6 with Figure 5.10 indicates that the velocity reduction is stronger in the simulation results though the deceleration command characteristic is similar. The deviation can be explained by ESC and ABS interventions. As illustrated the ABS and the ESC are activated during a large time period of the maneuver, which weakens the velocity reduction by the intervention during the evasive maneuver.

Furthermore, the proposed method has been demonstrated in Scenario 2 shown in Figure 5.11. The vehicle successfully avoids the collision with the obstacles and brakes the velocity to zero at the end of the maneuver.

Table 5.3: Parameter setup 6 for the Fast Integrated Planning and Control Method in real vehicle application

Parameter	Symbol	Value	Unit
Prediction horizon length	N	10	(none)
Prediction horizon step size	dt_{pred}	0.2	s
Controller time step size	dt_{ctrl}	0.13	s
Penalty of slack variable	q_{s}	$3{\cdot}10^2$	$1/\text{m}^2$
Penalty of yaw angle	q_{φ}	$3{\cdot}10^3$	$1/\text{rad}^2$
Penalty of velocity	q_{v}	10	s^2/m^2
Penalty of steering torque command	r_{T}	0.1	$1/\text{Nm}^2$
Penalty of deceleration command	r_{a_x}	0.1	s^4/m^2
Limit of steering system	T_{max}	50	Nm
Limit of braking system	$a_{\text{x,cmd,max}}$	-9.81	m/s^2

5.5 Discussion

This chapter presented successive linearization as an efficient technique to approximate nonlinearities in MPC by linear equation and reformulate nonlinear optimization problems into quadratic programs. Linearization errors may threaten the stability of the system and must be considered in constraint formulations. The robust tube based MPC approach has been deployed to consider linearization errors as additive uncertainties and derive modified constraints to guarantee stability for the uncertain system. The performance of the planning and control method has been demonstrated in simulation and in experiments, showing the applicability of the algorithm in real time.

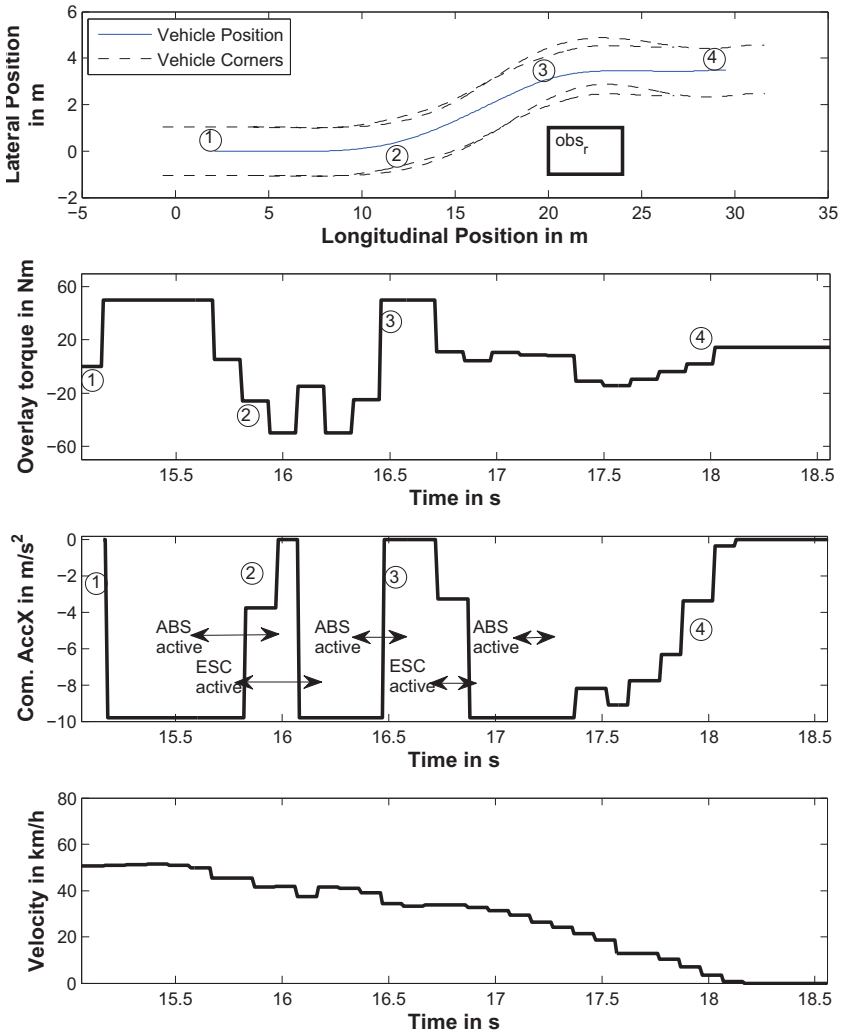

Figure 5.10: Results in real vehicle of the fast integrated trajectory planning and vehicle dynamics control method with parameter setup 4 in Scenario 1

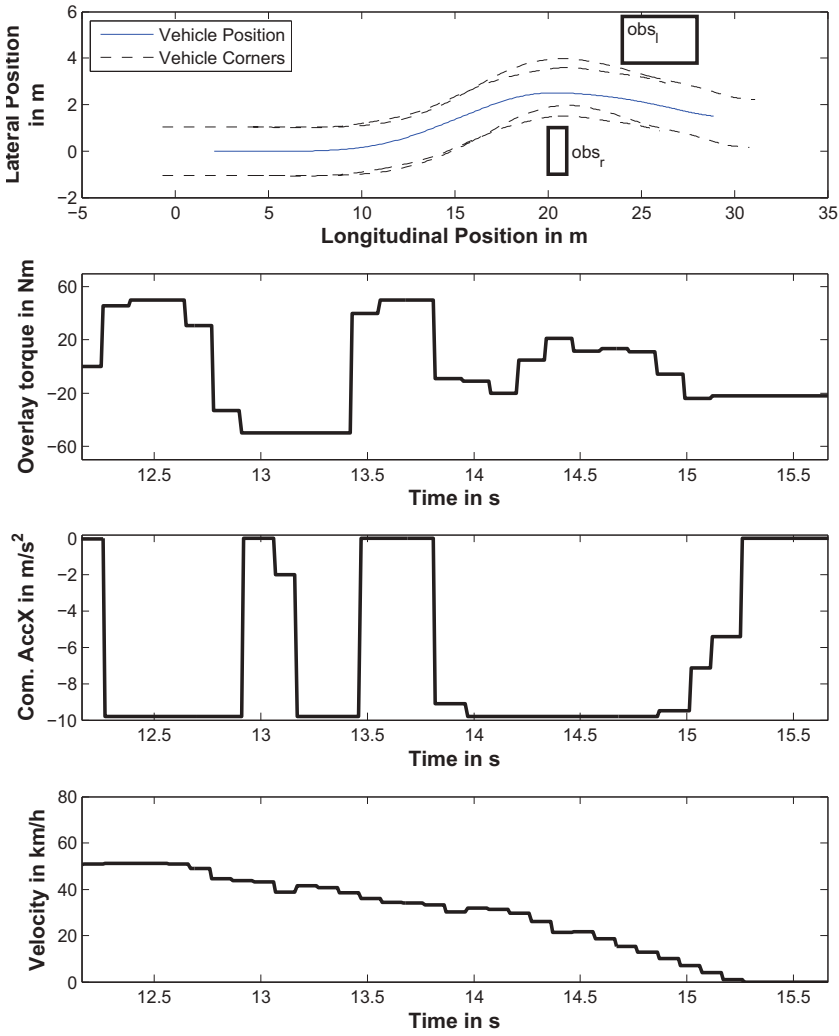

Figure 5.11: Results in real vehicle of the fast integrated trajectory planning and vehicle dynamics control method with parameter setup 4 in Scenario 2

Table 5.4: Metric values of planning and control concepts in simulation

Scenarios	Velocity Reduction Δv_{red}	Final Yaw Angle φ_{fnl}	Computation Time t_{cmp}
Scenario 1			
Nonlinear Integrated	44%	33°	$10s - 15s$
Fast Integrated	36%	14°	$0.15s$
Scenario 2			
Nonlinear Integrated	44.2%	6°	$10s - 15s$
Fast Integrated	45%	1°	$0.15s$

Table 5.4 shows the performance of the nonlinear and the fast integrated method in Scenario 1 and 2 in simulation. The nonlinear integrated planning and control method provides the flexibility needed to adapt to multiple obstacle scenarios and lead to reduced tuning effort of both planning and control module. The fast method inherits the flexibility required to plan in complex scenarios and can be calculated in approximately hundred of milliseconds. In Scenario 1, the fast method was able to drastically reduce the final yaw angle compared to the nonlinear method even though the same parameter setup have been chosen for both simulations. This has been explained by transient dynamics caused by successive linearization of the fast method, which disturb the deceleration command, extend the maneuver distance and thus enables the algorithm to re-orientate the vehicle. It is expected that the effect of the transient dynamics can be reduced with lower sampling time, which is possible when applied on computer platforms with higher processing power. In Scenario 2, the performance of both methods are very similar and the fast method shows has a significant of computation time.

Finally, Table 5.5 summarizes the performance metric values of the fast integrated planning and control method for the presented scenarios. The applied simulation environment showed to be sufficiently correlated with the test vehicle characteristic to develope and optimize the method in this thesis.

Table 5.5: Metric values of the Fast Integrated Planning and Control method for typical scenarios in simulation and in real vehicle

Scenarios	Velocity Reduction Δv_{red}	Final Yaw Angle φ_{fnl}	Computation Time t_{cmp}
Scenario 1			
Simulation	36.1%	14 °	0.15s
Real Vehicle	31.2%	1 °	0.13s
Scenario 2			
Simulation	42.5%	1 °	0.15s
Real Vehicle	28.2%	−9 °	0.13s

The Table shows little deviation in the final yaw angle and higher deviation in the velocity reduction metric between both environment. First, this can be explained with model deviations and sensor errors especially during phases with suspended braking intervention. Furthermore, the deviation may result from the intervention of the ABS and the ESC system which reduce the pressure in the brake line to improve the overall vehicle dynamics stability. Though the computation time in simulation and in the real vehicle are similar, it must be noted that the prediction horizon in simulation has 15 prediction steps and the horizon in the real vehicle has 10 prediction steps. All in all the proposed method is able to avoid collision in both environments with similar parameter setups.

6 Conclusion and Outlook

Recent developments in advanced driver assistance systems have increased the qualitative degree as well as the quantitative extent of system features in vehicles. Among these system features collision avoidance systems play a crucial role in protecting the vehicle and improve the overall safety of traffic participants. Automated emergency braking systems as an important representative have significantly reduced the rate of accidents by initiating a braking maneuver in critical situations.

To enhance the effectiveness of collision avoidance systems, the exploitation of the lateral maneuver space by evasive maneuvers shall be investigated.

Effective avoidance systems drive the need for holistic integrated approaches to cover planning and control in one method. The key research question as established in this thesis leads to an integrated method considering all known constraints. A key advantage comes along with the optimization based upon one physical model for both planning and control tasks. Another characteristic of this concept allows for reduction of the necessary tuning effort by reducing the number of design parameters in the overall system.

A nonlinear integrated planning and control method has been presented to design and realize optimal evasion maneuvers. Combined planning of longitudinal and lateral dynamics together with non-linear optimization supports the full exploitation of the available maneuver space at the limit of the given vehicle dynamics. The underlying model predictive control method provides the prerequisites to consider actuator limitations and stability limits through input and state constraints. Environmental information is explicitly considered by obstacle and maneuver space constraints. An extension of the method provides

a solution for the well-known issue associated limited planning horizons. The concept of terminal collision avoidance has been introduced in this work to take into account objects outside of the prediction horizon.
The interaction between the longitudinal and the lateral vehicle dynamics leads to nonlinear constraints and thus to a nonlinear optimization problem. The application of concepts for maneuver planning requires computationally efficient algorithms to cope with limited calculation power. The successive linearization technique transforms the nonlinear constraints into linear ones and enables the application of design principles in real vehicles. The robust tube based model predictive approach is exploited to explicitly consider linearization errors for the satisfaction of constraints and the guarantee of control stability.
The resulting fast integrated planning and control method shows a control performance comparable to the nonlinear method in a simulation environment for all characteristic scenarios. Furthermore, the applicability of the algorithm in real time has been verified in a test vehicle. The results underline a high degree of conformance in control characteristics for simulation and for real vehicle application.
The proposed integrated planning and control method may serve as the foundation for a number of potential future investigations.
The design of the collision avoidance constraints presented in this work represent a base for planning of trajectories in complex scenarios with arbitrary information about the road participants. In this thesis, simple scenarios have been chosen with static obstacles represented by rectangular shapes to demonstrate the applicability of the proposed planning and control method. In a next step, the proposed method can easily be modified to take into account moving obstacles as well as predicted obstacle trajectories based on statistical representations or Markov based models for the planning task.
Driver related factors have a huge impact in collision avoidance scenarios and require specific design of actuator components. To fully compensate for possible driver disturbances during the execution of collision avoidance maneuvers, suitable actuator systems such as steer-by-wire or steer-angle-overlay may be

investigated in future work to overcome weaknesses of existing actuator components. As characteristics and limitations of actuators have been reflected in this thesis, the proposed method can be easily modified to handle different and more actuators.

The design of the proposed methods in this thesis focused on the requirements and scenarios for evasive collision avoidance maneuvers in an advanced driver assistance system. In the future, the proposed framework has big potentials for general automated driving tasks where the driver is out of the control loop. Further, the design goals may be modified to integrate traffic rule information into the method such as the maximum allowed speed and the traffic light status.

High standards are set for trajectory planning and vehicle dynamics control modules in order to enable automated driving functionality. The proposed fast integrated planning and control method lays the foundation for the full exploitation of the available vehicle dynamics and the available space during the maneuver execution. The design concepts investigated in this thesis are promising to accelerate the realization of future design principles and thereby contribute to the overall development of automated driving technologies.

References

[1] J. Ackermann, J. Guldner, W. Sienel, R. Steinhauser, and V. I. Utkin. Linear and Nonlinear Controller Design for Robust Automatic Steering. In: *Control System Technology* 3 (1995), pp. 132–143.

[2] K. J. Astroem and T. Haegglund. *Advanced PID Control*. The Instrumentation, Systems, and Automation Society, North Carolina, 2006.

[3] E. Bauer and U. Konigorski. Ein modellprädiktiver Querplanungsansatz zur Kollisionsvermeidung. In: *Steuerung und Regelung von Fahrzeugen und Motoren*. Baden-Baden, 2013.

[4] E. Bauer, F. Lotz, M. Pfromm, M. Schreier, B. Abendroth, S. Cieler, A. Eckert, A. Hohm, S. Lüke, P. Rieth, et al. PRORETA 3: An Integrated Approach to Collision Avoidance and Vehicle Automation. In: *at-Automatisierungstechnik Methoden und Anwendungen der Steuerungs-, Regelungs-und Informationstechnik* 60 (12) (2012), pp. 755–765.

[5] C. E. Beal. Applications of model predictive control to vehicle dynamics for active safety and stability. PhD thesis. Stanford University, 2011.

[6] C. E. Beal and C. Gerdes. Model Predictive Control for Vehicle Stabilization at the Limits of Handling. In: *IEEE Transactions on Control Systems Technology* 21 (4) (2013), pp. 1258–1269.

[7] A. G. Beccuti, S. Mariéthoz, S. Cliquennois, S. Wang, and M. Morari. Explicit model predictive control of DC–DC switched-mode power supplies with extended Kalman filtering. In: *IEEE Transactions on Industrial Electronics* 56 (6) (2009), pp. 1864–1874.

[8] P. Bender, Ö. S. Tas, J. Ziegler, and C. Stiller. The combinatorial aspect of motion planning: Maneuver variants in structured environments. In: *IEEE Intelligent Vehicles Symposium, Seoul*. 2015.

[9] F. Borrelli, A. Bemporad, M. Fodor, and D. Hrovat. A hybrid approach to traction control. In: *International Workshop on Hybrid Systems: Computation and Control, Rome*. 2001.

[10] F. Borrelli, A. Bemporad, and M. Morari. Predictive Control for Linear and Hybrid Systems, 2015. In: *http://www.mpc.berkeley.edu/mpc-course-material* (2015). Accessed 09 April 2017.

[11] S. Boyd, L. E. Ghaoui, E. Feron, and V. Balakrishnan. *Linear Matrix Inequalities in System and Control Theory*. Society for Industrial and Applied Mathematics, Philadelphia, 1994.

[12] D. Burton, A. Delaney, S. Newstead, D. Logan, and B. Fildes. Effectiveness of ABS and vehicle stability control systems. In: *Royal Automobile Club of Victoria, Adelaide* (2004).

[13] M. Cannon. Efficient nonlinear model predictive control algorithms. In: *Annual Reviews in Control* 28 (2) (2004), pp. 229–237.

[14] M. Cannon, J. Buerger, B. Kouvaritakis, and S. Rakovic. Robust tubes in nonlinear model predictive control. In: *IEEE Transactions on Automatic Control* 56 (8) (2011), pp. 1942–1947.

[15] M. Choi and S. B. Choi. Model Predictive Control for Vehicle Yaw Stability With Practical Concerns. In: *IEEE Transactions on Vehicular Technology* 63 (8) (2014), pp. 3539–3548.

[16] C. R. Cutler and B. L. Ramaker. Dynamic matrix control - a computer control algorithm. In: *Joint automatic control conference, San Francisco*. 1980.

[17] T. A. Dingus, F. Guo, S. Lee, J. F. Antin, M. Perez, M. Buchanan-King, and J. Hankey. Driver crash risk factors and prevalence evaluation using naturalistic driving data. In: *Proceedings of the National Academy of Sciences, Washington*. 2016.

[18] S. Engel. Regelungstechnische Konzepte zum Umgang mit dem Fahrer in Kollisionsvermeidungssystemen. MA thesis. Technische Universität Darmstadt, 2016.

[19] S. M. Erlien. Shared Vehicle Control Using Safe Driving Envelopes for Obstacle Avoidance and Stability. PhD thesis. Stanford University, 2015.

[20] P. Falcone, M. Tufo, F. Borrelli, J. Asgari, and H. E. Tseng. A linear time varying model predictive control approach to the integrated vehicle dynamics control problem in autonomous systems. In: *IEEE Conference on Decision and Control, New Orleans*. 2007.

[21] J. Farinella, C. Lay, and S. Bhandari. UAV Collision Avoidance using a Predictive Rapidly-Exploring Random Tree. In: *AIAA SciTech Forum, San Diego*. 2016.

[22] C. E. Garcia. Quadratic dynamic matrix control of nonlinear processes. An application to a batch reaction process. In: *AIChE annual meeting, San Francisco*. 1984.

[23] T. M. Gasser. *Vehicle Automation: Definitions, legal aspects, research needs*. Tech. rep. German Federal Highway Research Institute, Bergisch Gladbach, 2014.

[24] T. M. Gasser et al. Legal consequences of an increase in vehicle automation: English translation of BASt-Report F83 (Part 1). In: *Bundesanstalt für Straßenwesen* (Bergisch Gladbach, 2013).

[25] T. M. Gasser, C. Arzt, M. Ayoubi, A. Bartels, L. Bürkle, J. Eier, F. Flemisch, D. Häcker, T. Hesse, W. Huber, et al. Legal consequences of an increase in vehicle automation. In: *Die Bundesanstalt für Straßenwesen (BASt) Report F* 83 (Bergisch Gladbach, 2009).

[26] T. M. Gasser and R. Auerswald. Vervollständigung der Landkarte Fahrzeugautomatisierung - Ein Diskussionsentwurf. In: *URBAN Konferenz, Munich*. 2016.

[27] S. Gottschling. Integrierte Fahrdynamikregelung und Trajektorienplanung zur Kollisionsvermeidung. MA thesis. Technische Universität Darmstadt, 2016.

[28] Y. Hattori, E. Ono, and S. Hosoe. Optimum vehicle trajectory control for obstacle avoidance problem. In: *IEEE/ASME Transactions on Mechatronics* 11 (5) (2006), pp. 507–512.

[29] R. Hayashi, J. Isogai, P. Raksincharoensak, and M. Nagai. Autonomous collision avoidance system by combined control of steering and braking using geometrically optimised vehicular trajectory. In: *Vehicle System Dynamics* 50 (1) (2012), pp. 151–168.

[30] W. Hulshof, I. Knight, A. Edwards, M. Avery, and C. Grover. Autonomous emergency braking test results. In: *International Technical Conference on the Enhanced Safety of Vehicles*. 2013.

[31] Insurance Institute for Highway Safety. ESC reduces multiple-vehicle crashes as well as single-vehicle ones. http://www.iihs.org/iihs/sr/statusreport/article/41/5/2. Accessed: 2016-03-19. 2006.

[32] Insurance Institute for Highway Safety. *Volvo's City Safety prevents low-speed crashes and cuts insurance costs*. Status Report 46 (6). 2011.

[33] S. Kammel, J. Ziegler, B. Pitzer, M. Werling, T. Gindele, D. Jagzent, J. Schröder, M. Thuy, M. Goebl, F. v. Hundelshausen, O. Pink, C. Frese, and C. Stiller. Team AnnieWAY's Autonomous System for the 2007 DARPA Urban Challenge. In: *J. Field Robot.* 25 (9) (Sept. 2008), pp. 615–639.

[34] S. Karush. *They're working. Special issue: Crash Avoidance*. Tech. rep. 47(3). Insurance Institute for Highway Safety, 2012.

[35] A. Katriniok. Optimal vehicle dynamics control and state estimation for a low-cost GNSS-based collision avoidance system. PhD thesis. Rheinisch-Westfälische Technische Hochschule Aachen, 2013.

[36] J. Keisler. *Elementary calculus: An infinitesimal approach*. University of Wisconsin, Wisconsin, 2012.

[37] M. Keller, C. Haß, A. Seewald, et al. A vehicle lateral control approach for collision avoidance by emergency steering maneuvers. In: *International Munich Chassis Symposium, Munich*. 2015.

[38] M. Keller, C. Hass, A. Seewald, and T. Bertram. Ein modellprädiktives Planungs-und Fahrzeugquerregelungsverfahren zur Kollisionsvermeidung durch Notausweichmanöver. In: *Automotive meets Electronics, Dortmund*. 2015.

[39] O. Khatib. Real-time obstacle avoidance for manipulators and mobile robots. In: *The International Journal of Robotics Research* 5 (1) (1986), pp. 90–98.

[40] T. Kranz, S. Hahn, and K. Zindler. Nonlinear lateral vehicle control in combined emergency steering and braking maneuvers. In: *IEEE Intelligent Vehicles Symposium, Gothenburg*. 2016.

[41] K. Kritayakirana and J. C. Gerdes. Autonomous vehicle control at the limits of handling. In: *International Journal of Vehicle Autonomous Systems* 10 (4) (2012), pp. 271–296.

[42] B. Krogh and C. Thorpe. Integrated path planning and dynamic steering control for autonomous vehicles. In: *IEEE International Conference on Robotics and Automation, San Francisco*. 1986.

[43] Y. Kuwata, G. A. Fiore, J. Teo, E. Frazzoli, and J. P. How. Motion planning for urban driving using RRT. In: *IEEE/RSJ International Conference on Intelligent Robots and Systems, Nice*. 2008.

[44] J. Löfberg. YALMIP : a toolbox for modeling and optimization in MATLAB. In: *IEEE International Conference on Robotics and Automation, Barcelona*. 2004.

[45] T. N. Matsko. Internal model control for chemical recovery. In: *Chemical Engineering Progress* 81 (12) (1985), pp. 46–51.

[46] J. Mattingley and S. Boyd. CVXGEN: A code generator for embedded convex optimization. In: *Optimization and Engineering* 13 (1) (2012), pp. 1–27.

[47] R. K. Mehra, R. Rouhani, J. Eterno, J. Richalet, and A. Rault. Model algorithmic control: review and recent developments. In: *Engineering Foundation Conference on Chemical Process Control, New York*. 1982.

[48] H. S. Meinert. *Untersuchung von robusten modellprädiktiven Regelungen zur Anwendung in der Flugführung*. Verlag Dr. Hut, Munich, 2011.

[49] M. Mitschke and H. Wallentowitz. *Dynamik der Kraftfahrzeuge*. Springer Berlin, 2004.

[50] R. Möbus, M. Baotic, and M. Morari. Multi-object adaptive cruise control. In: *International Workshop on Hybrid Systems: Computation and Control, Prague*. 2003.

[51] M. Morari. Predicting the future of model predictive control. In: *AIChE Annual Meeting, Systems and Process Control Centennial Session, Philadelphia*. 2008.

[52] N. Moshchuk. Collision avoidance with steering: Towards autonomous driving: ADAS and role of steering systems. In: *Steering Systems, Detroit* (2014).

[53] N. Moshchuk, S. K. Chen, C. Zagorski, and A. Chatterjee. Optimal braking and steering control for active safety. In: *International IEEE Conference on Intelligent Transportation Systems, Crete*. 2012.

[54] O. Nelles. *Nonlinear System Identification: From Classical Approaches to Neural Networks and Fuzzy Models*. Springer, Berlin, 2001.

[55] G. C. Nunes. Design and analysis of multivariable predictive control applied to an oil-water-gas separator: A polynomial approach. PhD thesis. University of Florida, 2001.

[56] H. B. Pacejka. *Tyre and Vehicle Dynamics*. Automotive engineering. Butterworth-Heinemann, Waltham, 2006.

[57] F. G. Papi. Control Strategies for Collision Avoidance of Ground Vehicles. Bachelor's thesis. Universidade Federal de Santa Catarina, 2015.

[58] C. Pfeiffer. Fahrdynamikanalyse und Entwicklung eines Entscheideralgorithmus für ein Kollisionsvermeidungssystem. Bachelor's thesis. Hochschule Darmstadt, 2014.

[59] D. Pfeiffer and U. Franke. Efficient representation of traffic scenes by means of dynamic stixels. In: *IEEE Intelligent Vehicles Symposium, San Diego*. 2010.

[60] D. Pfeiffer and U. Franke. Towards a Global Optimal Multi-Layer Stixel Representation of Dense 3D Data. In: *British Machine Vision Conference, Dundee*. 2011.

[61] J. B. Rawlings and D. Q. Mayne. *Model predictive control: Theory and design*. Nob Hill Pub., Madison, 2009.

[62] J. Richalet, A. Rault, J. L. Testud, and J. Papon. Model Predictive heuristic control: application to an Industrial Process. In: *Automatica* 14 (5) (1978), pp. 413–428.

[63] P. Riekert and T. E. Schunck. *Zur Fahrmechanik des gummibereiften Kraftfahrzeugs*. Deutsche Kraftfahrtforschung. Technische Hochschule Stuttgart, 1940.

[64] On-Road Automated Vehicle Standards Committee. SAE J3016: Taxonomy and Definitions for Terms Related to On-Road Motor Vehicle Automated Driving Systems. In: *SAE International, Warrendale* (2014).

[65] N. R. Ruchika. Model predictive control: History and development. In: *International Journal of Engineering Trends and Technology (IJETT)* 4 (6) (2013), pp. 2600–2602.

[66] F. Schindler. Parameter Study and Robustness Analysis of Control Concepts for Collision Avoidance. Bachelor's thesis. Hochschule Rhein-Main, 2016.

[67] C. Schmidt. Fahrstrategien zur Unfallvermeidung im Straßenverkehr für Einzel- und Mehrobjektszenarien. PhD thesis. Karlsruhe Institute of Technology, 2013.

[68] M. Schorn. Quer- und Längsregelung eines Personenkraftwagens für ein Fahrerassistenzsystem zur Unfallvermeidung. PhD thesis. Technische Universität Darmstadt, 2007.

[69] H. Seki, S. Ooyama, and M. Ogawa. Nonlinear model predictive control using successive linearization-Application to chemical reactors. In: *Transactions-society of instrument and control engineers* 38 (1) (2002), pp. 61–66.

[70] S. Skogestad. Probably the best simple PID tuning rules in the world. In: *AIChE Annual Meeting, Reno*. 2001.

[71] U. Stählin. *Eingriffsentscheidung für ein Fahrerassistenzsystem zur Unfallvermeidung*. Berichte aus dem Institut für Automatisierungstechnik der TU Darmstadt. VDI-Verlag, Düsseldorf, 2008.

[72] H. Stübing. Entwicklung von Kriterien zur Bewertung von Kollisionsvermeidungssystemen. Bachelor's thesis. Hochschule Darmstadt, 2015.

[73] S. Thrun, M. Montemerlo, H. Dahlkamp, D. Stavens, A. Aron, J. Diebel, P. Fong, J. Gale, M. Halpenny, G. Hoffmann, et al. Stanley: The robot that won the DARPA Grand Challenge. In: *Journal of field Robotics* 23 (9) (2006), pp. 661–692.

[74] J. P. Timings and D. J. Cole. Minimum maneuver time calculation using convex optimization. In: *Journal of Dynamic Systems, Measurement, and Control* 135 (3) (2013).

[75] A. T. Van Zanten. *Bosch ESP systems: 5 years of experience*. Tech. rep. SAE Technical Paper, 2000.

[76] R. Vilanova and A. Visioli. *PID control in the third millennium*. Springer, London, 2012.

[77] M. Werling. Ein neues Konzept für die Trajektoriengenerierung und -stabilisierung in zeitkritischen Verkehrsszenarien. PhD thesis. Karlsruhe Institute of Technology, 2011.

[78] M. Werling, B. Gutjahr, S. Galler, and L. Gröll. Riccati-Trajektorienoptimierung für den aktiven Fußgängerschutz. In: *at-Automatisierungstechnik* 63 (3) (2015), pp. 202–210.

[79] M. Werling, J. Ziegler, S. Kammel, and S. Thrun. Optimal trajectory generation for dynamic street scenarios in a frenet frame. In: *IEEE International Conference on Robotics and Automation, Anchorage*. 2010.

[80] H. Wu. Fahrdynamikregelung von kombinierten Brems- und Ausweichmanövern. MA thesis. Technische Universität Darmstadt, 2014.

[81] B. Yi. Kombiniertes Ausweichen und Bremsen zum letztmöglichen Moment. In: *URBAN Konferenz*. Munich, 2016.

[82] B. Yi, P. Bender, F. Bonarens, and C. Stiller. Model Predictive Trajectory Planning for Automated Driving. In: *IEEE Transactions on Intelligent Vehicles* ((submitted on 27.06.2017)).

[83] B. Yi, J. Ferdinand, N. Simm, and F. Bonarens. Application of Local Linear Steering Models with Model Predictive Control for Collision Avoidance Maneuvers. In: *IFAC Symposium on Intelligent Autonomous Vehicles, Leipzig*. 2016.

[84] B. Yi, J. Ferdinand, and H. Wu. Robuste Fahrdynamikregelung zur Kollisionsvermeidung. In: *Automotive meets Electronics, Dortmund* (2015).

[85] B. Yi, S. Gottschling, J. Ferdinand, N. Simm, F. Bonarens, and C. Stiller. Real Time Integrated Vehicle Dynamics Control and Trajectory Planning with MPC for Critical Maneuvers. In: *IEEE Intelligent Vehicles Symposium*. Gothenburg, 2016.

[86] J. Ziegler, P. Bender, T. Dang, and C. Stiller. Trajectory planning for Bertha 2014; A local, continuous method. In: *IEEE Conference on Intelligent Vehicles Symposium, Ypsilanti*. 2014.

[87] J. Ziegler, P. Bender, M. Schreiber, H. Lategahn, T. Strauss, C. Stiller, T. Dang, U. Franke, N. Appenrodt, C. G. Keller, et al. Making bertha drive - an autonomous journey on a historic route. In: *IEEE Intelligent Transportation Systems Magazine* 6 (2) (2014), pp. 8–20.

Publications by the author

[81] B. Yi. Kombiniertes Ausweichen und Bremsen zum letztmöglichen Moment. In: *URBAN Konferenz*. Munich, 2016.

[82] B. Yi, P. Bender, F. Bonarens, and C. Stiller. Model Predictive Trajectory Planning for Automated Driving. In: *IEEE Transactions on Intelligent Vehicles* ((submitted on 27.06.2017)).

[83] B. Yi, J. Ferdinand, N. Simm, and F. Bonarens. Application of Local Linear Steering Models with Model Predictive Control for Collision Avoidance Maneuvers. In: *IFAC Symposium on Intelligent Autonomous Vehicles, Leipzig*. 2016.

[84] B. Yi, J. Ferdinand, and H. Wu. Robuste Fahrdynamikregelung zur Kollisionsvermeidung. In: *Automotive meets Electronics, Dortmund* (2015).

[85] B. Yi, S. Gottschling, J. Ferdinand, N. Simm, F. Bonarens, and C. Stiller. Real Time Integrated Vehicle Dynamics Control and Trajectory Planning with MPC for Critical Maneuvers. In: *IEEE Intelligent Vehicles Symposium*. Gothenburg, 2016.

Supervised theses

[18] S. Engel. Regelungstechnische Konzepte zum Umgang mit dem Fahrer in Kollisionsvermeidungssystemen. MA thesis. Technische Universität Darmstadt, 2016.

[27] S. Gottschling. Integrierte Fahrdynamikregelung und Trajektorienplanung zur Kollisionsvermeidung. MA thesis. Technische Universität Darmstadt, 2016.

[57] F. G. Papi. Control Strategies for Collision Avoidance of Ground Vehicles. Bachelor's thesis. Universidade Federal de Santa Catarina, 2015.

[58] C. Pfeiffer. Fahrdynamikanalyse und Entwicklung eines Entscheideralgorithmus für ein Kollisionsvermeidungssystem. Bachelor's thesis. Hochschule Darmstadt, 2014.

[66] F. Schindler. Parameter Study and Robustness Analysis of Control Concepts for Collision Avoidance. Bachelor's thesis. Hochschule Rhein-Main, 2016.

[72] H. Stübing. Entwicklung von Kriterien zur Bewertung von Kollisionsvermeidungssystemen. Bachelor's thesis. Hochschule Darmstadt, 2015.

[80] H. Wu. Fahrdynamikregelung von kombinierten Brems- und Ausweichmanövern. MA thesis. Technische Universität Darmstadt, 2014.

Schriftenreihe
Institut für Mess- und Regelungstechnik
Karlsruher Institut für Technologie
(1613-4214)

Band 001 Hans, Annegret
Entwicklung eines Inline-Viskosimeters auf Basis eines magnetisch-induktiven Durchflussmessers. 2004
ISBN 3-937300-02-3

Band 002 Heizmann, Michael
Auswertung von forensischen Riefenspuren mittels automatischer Sichtprüfung. 2004
ISBN 3-937300-05-8

Band 003 Herbst, Jürgen
Zerstörungsfreie Prüfung von Abwasserkanälen mit Klopfschall. 2004
ISBN 3-937300-23-6

Band 004 Kammel, Sören
Deflektometrische Untersuchung spiegelnd reflektierender Freiformflächen. 2005
ISBN 3-937300-28-7

Band 005 Geistler, Alexander
Bordautonome Ortung von Schienenfahrzeugen mit Wirbelstrom-Sensoren. 2007
ISBN 978-3-86644-123-1

Band 006 Horn, Jan
Zweidimensionale Geschwindigkeitsmessung texturierter Oberflächen mit flächenhaften bildgebenden Sensoren. 2007
ISBN 978-3-86644-076-0

Band 007 Hoffmann, Christian
Fahrzeugdetektion durch Fusion monoskopischer Videomerkmale. 2007
ISBN 978-3-86644-139-2

Band 008 Dang, Thao
Kontinuierliche Selbstkalibrierung von Stereokameras. 2007
ISBN 978-3-86644-164-4

Band 009 Kapp, Andreas
Ein Beitrag zur Verbesserung und Erweiterung der Lidar-Signalverarbeitung für Fahrzeuge. 2007
ISBN 978-3-86644-174-3

Band 010 Horbach, Jan
Verfahren zur optischen 3D-Vermessung spiegelnder Oberflächen. 2008
ISBN 978-3-86644-202-3

Band 011 Böhringer, Frank
Gleisselektive Ortung von Schienenfahrzeugen mit bordautonomer Sensorik. 2008
ISBN 978-3-86644-196-5

Band 012 Xin, Binjian
Auswertung und Charakterisierung dreidimensionaler Messdaten technischer Oberflächen mit Riefentexturen. 2009
ISBN 978-3-86644-326-6

Band 013 Cech, Markus
Fahrspurschätzung aus monokularen Bildfolgen für innerstädtische Fahrerassistenzanwendungen. 2009
ISBN 978-3-86644-351-8

Band 014 Speck, Christoph
Automatisierte Auswertung forensischer Spuren auf Patronenhülsen. 2009
ISBN 978-3-86644-365-5

Band 015 Bachmann, Alexander
Dichte Objektsegmentierung in Stereobildfolgen. 2010
ISBN 978-3-86644-541-3

Band 016 Duchow, Christian
Videobasierte Wahrnehmung markierter Kreuzungen mit lokalem Markierungstest und Bayes'scher Modellierung. 2011
ISBN 978-3-86644-630-4

Band 017 Pink, Oliver
Bildbasierte Selbstlokalisierung von Straßenfahrzeugen. 2011
ISBN 978-3-86644-708-0

Band 018 Hensel, Stefan
Wirbelstromsensorbasierte Lokalisierung von Schienenfahrzeugen in topologischen Karten. 2011
ISBN 978-3-86644-749-3

Band 019 Carsten Hasberg
Simultane Lokalisierung und Kartierung spurgeführter Systeme. 2012
ISBN 978-3-86644-831-5

Band 020 Pitzer, Benjamin
Automatic Reconstruction of Textured 3D Models. 2012
ISBN 978-3-86644-805-6

Band 021 Roser, Martin
Modellbasierte und positionsgenaue Erkennung von Regentropfen in Bildfolgen zur Verbesserung von videobasierten Fahrerassistenzfunktionen. 2012
ISBN 978-3-86644-926-8

Band 022 Loose, Heidi
Dreidimensionale Straßenmodelle für Fahrerassistenzsysteme auf Landstraßen. 2013
ISBN 978-3-86644-942-8

Band 023 Rapp, Holger
Reconstruction of Specular Reflective Surfaces using Auto-Calibrating Deflectometry. 2013
ISBN 978-3-86644-966-4

Band 024 Moosmann, Frank
Interlacing Self-Localization, Moving Object Tracking and Mapping for 3D Range Sensors. 2013
ISBN 978-3-86644-977-0

Band 025 Geiger, Andreas
Probabilistic Models for 3D Urban Scene Understanding from Movable Platforms. 2013
ISBN 978-3-7315-0081-0

Band 026 Hörter, Marko
Entwicklung und vergleichende Bewertung einer bildbasierten Markierungslichtsteuerung für Kraftfahrzeuge. 2013
ISBN 978-3-7315-0091-9

Band 027 Kitt, Bernd
Effiziente Schätzung dichter Bewegungsvektorfelder unter Berücksichtigung der Epipolargeometrie zwischen unterschiedlichen Ansichten einer Szene. 2013
ISBN 978-3-7315-0105-3

Band 028 Lategahn, Henning
Mapping and Localization in Urban Environments Using Cameras. 2013
ISBN 978-3-7315-0135-0

Band 029 Tischler, Karin
Informationsfusion für die kooperative Umfeldwahrnehmung vernetzter Fahrzeuge. 2014
ISBN 978-3-7315-0166-4

Band 030 Schmidt, Christian
Fahrstrategien zur Unfallvermeidung im Straßenverkehr für Einzel- und Mehrobjektszenarien. 2014
ISBN 978-3-7315-0198-5

Band 031 Firl, Jonas
Probabilistic Maneuver Recognition in Traffic Scenarios. 2014
ISBN 978-3-7315-0287-6

Band 032 Schönbein, Miriam
Omnidirectional Stereo Vision for Autonomous Vehicles. 2015
ISBN 978-3-7315-0357-6

Band 033 Nicht erschienen

Band 034 Liebner, Martin
Fahrerabsichtserkennung und Risikobewertung für warnende Fahrerassistenzsysteme. 2016
ISBN 978-3-7315-0508-2

Band 035 Ziegler, Julius
Optimale Trajektorienplanung für Automobile. 2017
ISBN 978-3-7315-0553-2

Band 036 Harms, Hannes
Genauigkeitsuntersuchung von binokularen Normalenvektoren für die Umfeldwahrnehmung. 2017
ISBN 978-3-7315-0628-7

Band 037 Ruhhammer, Christian
Inferenz von Kreuzungsinformationen aus Flottendaten. 2017
ISBN 978-3-7315-0721-5

Band 038 Stein, Denis
Mobile laser scanning based determination of railway network topology and branching direction on turnouts. 2018
ISBN 978-3-7315-0743-7

Band 039 Yi, Boliang
Integrated Planning and Control for Collision Avoidance Systems. 2018
ISBN 978-3-7315-0785-7

Schriftenreihe
INSTITUT FÜR MESS- UND REGELUNGSTECHNIK
KARLSRUHER INSTITUT FÜR TECHNOLOGIE (KIT)

039

Collision avoidance systems like emergency braking assist systems have demonstrated their effectiveness in increasing the safety of vehicle passengers in various studies. To further increase the effectiveness of collision avoidance systems, the exploitation of the lateral free space by evasive maneuvers is being investigated in this book.

This work focuses on methods for integrated trajectory planning and vehicle dynamics control in collision avoidance scenarios by combined evasion and braking. Integrated planning and control allows for consistent model representation for both planning and control functionality and lead to a reduced number of design parameters in the overall system. The proposed nonlinear method based on a model predictive approach plans collision-free trajectories taking into account environmental information of obstacles and the available maneuver space. The concept of terminal collision avoidance, introduced in this work, allows for planning with obstacles detected outside the current prediction horizon. The successive linearization of nonlinear constraints in the optimization problem enables planning on a real time computation platform. The performance and effectiveness of the proposed algorithm is demonstrated in simulation and in a real vehicle, successfully avoiding the collision in characteristic scenarios.

The design concepts investigated in this work are promising to accelerate the realization of future design principles and thereby contribute to the overall development of automated driving technologies.

ISSN 1613-4214
ISBN 978-3-7315-0785-7

Gedruckt auf FSC-zertifiziertem Papier

ISBN 978-3-7315-0785-7
9 783731 507857 >